

CRANFIELD UNIVERSITY

YU LU

VIBRATION ENERGY HARVESTERS FOR WIRELESS SENSOR
NETWORKS FOR AIRCRAFT HEALTH MONITORING

SCHOOL OF AEROSPACE, TRANSPORT AND
MANUFACTURING
Msc By Research

MSc Thesis
Academic Year: 2014 - 2015

Supervisor: Dr. Al Savvaris
October 2015

CRANFIELD UNIVERSITY

SCHOOL OF AEROSPACE, TRANSPORT AND
MANUFACTURING
Msc By Research

MSc Thesis

Academic Year 2014 - 2015

YU LU

Vibration Energy Harvesters for Wireless Sensor Networks for
Aircraft Health Monitoring

Supervisor: Dr. Al Savvaris
October 2015

© Cranfield University 2015. All rights reserved. No part of this
publication may be reproduced without the written permission of the
copyright owner.

Abstract

Traditional power supply for wireless sensor nodes is batteries. However, the application of batteries in WSN has been limited due to their large size, low capacity, limited working life, and replacement cost.

With rapid advancements in microelectronics, power consumption of WSN is getting lower and hence the energy harvested from ambient may be sufficient to power the tiny sensor nodes and eliminate batteries completely.

As vibration is the widespread ambient source that exists in abundance on an aircraft, a WSN node system used for aircraft health monitoring powered by a piezoelectric energy harvester was designed and manufactured.

Furthermore, simulations were performed to validate the design and evaluate the performance.

In addition, the Z-Stack protocol was migrated to run on the system and initial experiments were carried out to analyse the current consumption of the system.

A new approach for power management was reported, the execution of the operations were determined by the amount of the energy stored on the capacitor. A novel power saving interface was also developed to minimise the power consumption during the voltage measurement.

Keywords:

Self-powered; Piezoelectric; WSN; Z-Stack; ZigBee; Power Management

Acknowledgements

First of all, I would like to thank my supervisor Dr. Al Savvaris and professor. Antonios Tsourdos, for having given me the opportunity, for providing all the resources needed in the project, for their guidance, advices, and continuous support during my study and live in Cranfield University. Thanks again, my supervisor.

I appreciate the staffs in Cranfield University for their excellent services. In particular, I would like to express my gratitude to Serena Slattery for her kind help and patience with me.

Then I would like to thank my company, COMAC, for offering me the chance and the financial support to study here. I would like to express my deepest gratitude and thanks to the support from my bosses Mr Qingming Xiao and Mr Shunli Wang in SAMC.

Also, I would to extend my gratitude to my friends and roommates who shared the office and accommodation with me.

Finally and most importantly, I would like to thank my wife who kept giving me motivations, encouraging me and supporting me to accomplish this thesis. Thank my parents for their unconditional love.

Table of Contents

Abstract	i
Acknowledgements	ii
Table of Contents	iii
List of Figures.....	v
List of Tables	viii
List of Equations.....	x
List of Abbreviations	xi
Chapter 1 Introduction	1
1.1 Introduction and background	1
1.2 Aims and objectives	2
1.3 Contribution	3
1.4 Thesis structure	4
Chapter 2 Literature and research review.....	5
2.1 Energy Harvesting Technologies	5
2.1.1 Sources of ambient energy	5
2.1.2 Vibration energy harvesting.....	7
2.1.3 Thermal energy harvesting on aircrafts	9
2.2 Popular wireless network standards comparison.....	12
2.3 Power saving techniques review.....	16
2.4 Main components & modules investigation.....	17
Chapter 3 System overall design.....	19
3.1 Structure of a WSN node powered by vibration energy harvesters.....	19
3.2 An overall design of the WSN system powered by piezoelectric energy harvester.....	23
3.2.1 Energy harvesting unit.....	24
3.2.2 Microcontroller & wireless transceiver unit	29
3.2.3 Sensors unit	31
Chapter 4 Hardware development & simulation	33
4.1 Circuit design and parameter specification	33
4.1.1 Energy harvesting and power management unit.....	33
4.1.2 Microcontroller & wireless transceiver unit	39

4.1.3 Sensors unit	44
4.2 Simulation & results analysis	48
4.2.1 Modelling in LTspice.....	48
4.2.2 Simulation results and analysis	57
4.3 PCB layout & hardware assembly.....	65
4.3.1 PCB layout design.....	65
4.3.2 Assembly.....	68
Chapter 5 Software development & initial experiments	70
5.1 Introduction of the ZigBee network & structure	70
5.2 Configuration of Z-Stack protocol and proposed algorithm for power management.....	74
5.2.1 Z-Stack protocol and OSAL.....	74
5.2.2 Configuration of Z-Stack and proposed algorithm for energy harvesting solution	75
5.3 Initial measurements and results of the algorithm.....	80
5.3.1 Experiment environment setup.....	80
5.3.2 Results & analysis of the proposed algorithm.....	81
Chapter 6 Conclusion and future work.....	88
6.1 Conclusion	88
6.2 Future work.....	89
REFERENCES	91
APPENDICES	97

List of Figures

Figure 2-1 Power requirements of small electronic devices [13]	6
Figure 2-2 Typical electromechanical transducers	7
Figure 2-3 Temperature profiles of an aircraft's skin during typical short-range flights [8]	10
Figure 2-4 The TEG Module used in aircraft [7]	10
Figure 2-5 Different locations on an aircraft used for the simulation of a TEG [11]	11
Figure 3-1 Block chart of a WSN node powered by vibration energy harvesters	19
Figure 3-2 Passive and active power factor correction techniques.....	21
Figure 3-3 Block chart of a typical vibration energy harvesting module.....	21
Figure 3-4 Block chart of a wireless sensor network node	22
Figure 3-5 The distribution of power consumption in a WSN node [35].....	23
Figure 3-6 An overall integrated design of the WSN system	24
Figure 3-7 Dimension of the MIDÉ V25W [36].....	25
Figure 3-8 Relation between tip mass & natural frequency of V25W [36].....	26
Figure 3-9 Power performance of the V25W at different frequencies [36]	26
Figure 3-10 Functional Block Diagram of LTC3588-1 [37].....	27
Figure 3-11 Typical performance characteristics of LTC3588-1 [37].....	29
Figure 3-12 iM222A radio module compared with a one pound coin.....	29
Figure 4-1 Pinout configuration of V25W	34
Figure 4-2 Schematic of the configurations of the V25W harvester and rectifier	35

Figure 4-3 General guidance for the configuration of the system in different levels of amplitude.....	35
Figure 4-4 100mA Piezoelectric Energy Harvesting Power Supply [37]	36
Figure 4-5 Schematic of the output voltage configuration of V25W	36
Figure 4-6 Schematic of the MCU & RF unit and its peripherals	39
Figure 4-7 Schematic of the voltage divider without (a) / with (b) ADC input impedance	41
Figure 4-8 Schematic of the storage capacitor voltage monitor.....	43
Figure 4-9 Schematic of the vibration sensor (ST LIS2DH).....	45
Figure 4-10 Schematic of the pressure sensor (ST LPS25H).....	46
Figure 4-11 Schematic of the temperature and humidity sensor (TI HDC1000).....	47
Figure 4-12 Schematic of the simulation circuit in LTspice IV	48
Figure 4-13 Current consumption and duration of various operations in one cycle	53
Figure 4-14 A typical RC charging circuit	54
Figure 4-15 Time history versus the voltage of the input storage capacitors....	56
Figure 4-16 Start-up time vs. amplitude for different capacitors	57
Figure 4-17 Start-up time vs. different input capacitors (40 Hz and 0.5 g).....	57
Figure 4-18 Output Power & Operating Voltage vs. Time	58
Figure 4-19 Time history of Input Voltage (V_{IN}) and Measured Voltage from the Divider Circuit without the ESI	59
Figure 4-20 Time history of Input Voltage (V_{IN}) and Measured Voltage from the Divider Circuit with the ESI	59
Figure 4-21 Input / output voltage and current consumption of the loads vs. time	61
Figure 4-22 Zoomed detail of the current consumption	62
Figure 4-23 Procedure of the PCB design used in this project	66
Figure 4-24 Trace layout of the WSN system board based on vibration energy harvesting	67
Figure 4-25 PCB board of the WSN system board based on vibration energy harvesting	67
Figure 4-26 PCB board of the sensor board.....	68
Figure 4-27 Procedure of the soldering operation	69

Figure 5-1 Outline of the ZigBee Stack Architecture [27].....	71
Figure 5-2 Comparison of the IEEE 802 wireless standards family[50].....	71
Figure 5-3 ZigBee network topologies.....	73
Figure 5-4 OSAL system operation and task scheduling mechanism in Z-Stack	75
Figure 5-5 Default Z-Stack behaviour of a ZED (a) No network is found at the beginning (b) No network is found after successful joining [54].....	76
Figure 5-6 Proposed Algorithm for the WSN system based on piezoelectric vibration energy harvesting.....	79
Figure 5-7 Measurement Setup.....	80
Figure 5-8 A 50 secs measurement plot of the ZED.....	81
Figure 5-9 Current Consumption Measurement Plot on Operation 1	83
Figure 5-10 Current Consumption Measurement Plot on Operation 2	84
Figure 5-11 Current Consumption Measurement Plot on Operation 3/5	85
Figure 5-12 Current Consumption Measurement Plot on Operation 4	86

List of Tables

Table 1-1 Main objectives of the project	3
Table 2-1 Comparison of most common energy sources and the harvested power available in the ambient [12]	6
Table 2-2 Advantages and disadvantages of different vibrational transducers [14].....	7
Table 2-3 Summary of the literature review of the VEH.....	9
Table 2-4 Simulated results for temperature gradients on different locations of an aircraft [11].....	11
Table 2-5 Comparison of the thermal & vibration energy harvesting on an aircraft.....	12
Table 2-6 Comparison of the popular wireless network standards	15
Table 2-7 Advantages and disadvantages of popular network standards	15
Table 3-1 Specifications of the TI CC2530256 iM222A (TI CC2530256)[38] [39]	30
Table 4-1 Output voltage selection[37].....	38
Table 4-2 Pinout of LIS2DH used in I ² C mode	45
Table 4-3 Pin description of the LPS25H used in I ² C mode	46
Table 4-4 Pin description of the HDC1000	47
Table 4-5 Description of the models used in Figure 4-12	49
Table 4-6 Current consumption and length of time in different operations during a cycle for simulation	52
Table 4-7 Minimum voltage across the storage capacitor to carry out successful operations.....	54
Table 4-8 Average output power and total output energy of the harvester used in the ADC circuit with/without ESI within the first 200S	60

Table 4-9 Average power dissipation and total energy consumption of the ADC circuit with/without ESI within the first 200S.....	60
Table 4-10 Comparison of the loss ratio of the ADC circuit with/without ESI within the first 200S	61
Table 4-11 Specifications and constraints used during the PCB design in EAGLE.....	66
Table 4-12 Instruments and tools used for soldering.....	69
Table 5-1 Arrangement of channels in IEEE 802.15.4 [51].....	72
Table 5-2 Data Rates and Modulation [51]	72
Table 5-3 Configuration of the Z-Stack protocol for energy harvesting solution	77
Table 5-4 Current Consumption Measurement Plot on Operation 1	83
Table 5-5 Current Consumption Measurement Plot on Operation 2.....	84
Table 5-6 Current Consumption Measurement Plot on Operation 3/5.....	85
Table 5-7 Current Consumption Measurement Plot on Operation 4.....	86
Table 5-8 Minimum voltage on the storage capacitor to carry out operation 1, 2, 3/5, and 4.....	87

List of Equations

(4-1).....	38
(4-2).....	40
(4-3).....	41
(4-4).....	42
(4-5).....	42
(4-6).....	42
(4-7).....	43
(4-8).....	50
(4-9).....	50
(4-10).....	51
(4-11).....	51
(4-12).....	51
(4-13).....	53
(4-14).....	54
(4-15).....	55

List of Abbreviations

6LoWPAN	IPv6 over Low-power Wireless Personal Area Networks
AC	Alternating Current
ADC	Analog-to-digital Converter
APS	Application Support Sub-Layer
BOM	Bill of Material
CAM	Computer Aided Manufacturing
CPU	Central Processing Unit
DC	Direct Current
DRC	Design Rule Check
EDA	Electronic design automation
ERC	Electrical Rule Check
ESI	Energy Saving Interface
FIFO	First-In First-Out
GND	Ground
GPIO	General Purpose Input / Output
HAL	Hardware Abstraction Layer
I2C	Inter-Integrated Circuit
IC	Integrated Circuit
IEEE	Institute of Electrical and Electronics Engineers
IoT	Internet of Things
ISA	International Standard Atmosphere (ISA)
ISM	Industrial, Scientific, and Medical
IT	Information Technology
LDO	Low Drop-Out

MCU	Microcontroller Unit
MEMS	Micro-electromechanical System
NV	Non-volatile
NWK	Network Layer
OS	Operating System
OSAL	Operating System Layer
OTA	Over-the-air
PAN	Personal Area Network
PCB	Printed Circuit Board
PEH	Piezoelectric Energy Harvesting
PTH	Plated Through Holes
RF	Radio Frequency
SHM	Structural Health Monitoring
SMD	Surface Mount Device
SoC	System-on-Chip
SPI	Serial Peripheral Interface
SPICE	Simulation Program with Integrated Circuit Emphasis
TEG	Thermoelectric generator
TEH	Thermal Energy harvester
TI	Texas Instruments
UART	Universal Asynchronous Receiver/Transmitter
USB	Universal Serial Bus
UVLO	Under-Voltage Lockout
VEH	Vibration Energy harvester
WLAN	Wireless Local Area Network
WSN	Wireless Sensor Network
ZED	Z-Stack End-device
ZDO	ZigBee Device Objects
ZDP	ZigBee Device Profile
ZNP	ZigBee Network Processor

Chapter 1

Introduction

This chapter gives a general introduction of the research work. It starts with the research background and the motivation, which focus on the wireless sensor network (WSN) system used for aircraft health monitoring and powered by energy harvested from the vibration, and then moves to the aims and objectives, the contribution, and finally ends with outlining the framework of this thesis.

1.1 Introduction and background

Aircraft health management / monitoring (AHM) technologies have recently been extensively used in modern "future-aware" aircrafts to optimize the routine maintenance, for instance, the AHM (Airplane Health Management) designed by Boeing, the AIRMAN (AIRcraft Maintenance ANalysis) developed by Airbus, and the PHM (Prognostics and Health Management) introduced by COMAC. These intelligent techniques integrate remote monitoring, airplane information collection and analysis to determine the status of an aircraft's current and future serviceability.

The increasing interest in AHM has also heightened the need for WSN during the last decades, as the WSN system can reduce the amount of cabling necessary in AHM applications significantly. On the contrary, the wired network

used in AHM reduces overall system reliability and increases overall system weight and cost.

However, the main constraint which limits the further development of WSN is the power source [1], as the WSN applications powered by batteries or rechargeable batteries have shortcomings like large size, low capacity, limited working life, and replacement cost.

With the rapid advancement of microelectronics, ultra-low power sensors and microcontrollers, low power wireless transceivers are available nowadays. Therefore, energy harvesting technology is getting more and more attention to replace the batteries and extend the lifespan of WSNs.

WSN systems powered by energy harvesting technology have been reported in many industrial applications. As abundant vibration sources and thermal gradient exist in the aircraft environment, the possibilities and opportunities for the utilization of energy harvesting in aerospace applications are discussed in [2] and demonstrated in [3]–[11], however, most of the reports employed thermoelectric energy harvesting technology in their applications.

In this study, a preliminary design of a WSN system used for aircraft health monitoring based on vibration energy harvesting is proposed. The design offers a whole solution including the hardware design and a basic software implementation.

1.2 Aims and objectives

The aim of this project is to develop a WSN system which is powered by a vibration energy harvester and used for aircraft health monitoring. However, since the energy acquired from the ambient is very limited, the energy harvesting system should be designed with high efficiency, which collects, converts, and stores the energy to power the WSN node as needed. In addition, the device must also include intelligent power management methods to control the power switching and conserve energy.

The main objectives of the project and the methodology are listed in Table 1-1.

Table 1-1 Main objectives of the project

Methodology	Tasks / Objectives	Output
Literature Review	Review current state of the art regarding energy harvesting devices (incl. component selection, pricing, compatibility etc.)	Report
System Design	Design an architecture of the WSN system based on energy harvesting	Schematic
Simulation	Develop a simulation model to test the proposed architecture	Simulation Results
Hardware Design	PCB layout design and hardware assembly	PCB Hardware
Software development	Software development (incl. an intelligent power management controller)	Code Algorithm
Experiment	Initial experiments to study the power consumption of the system	Results

1.3 Contribution

The main gap between the energy harvester and the WSN system is the mechanisms used for power management, as the energy acquired from the ambient is very limited.

This thesis presents a new power management strategy for the applications using capacitors to store harvested energy.

The proposed mechanism relies on the analysis of how much energy has been stored on capacitor to determine the executions of the operations in the system.

A novel energy saving interface (ESI) is designed to minimise the power consumption during the voltage measurement and an intelligent algorithm is developed to implement the strategy.

1.4 Thesis structure

Chapter 1 introduces the background, aims, objectives, and contribution of this project.

Chapter 2 reviews the approaches used for energy harvesting especially the vibration and thermal energy harvesting, the popular network standards for WSNs, the techniques implemented for power saving, and at last the available products in the market for the later hardware development.

Chapter 3 introduces the structure of a WSN node powered by energy harvester and proposes an overall design of the WSN system powered by piezoelectric energy harvester based on the off-the-shelf products.

Chapter 4 presents the hardware development of the system. The simulation of the system is also carried out to validate the design and the results are analysed and discussed.

Chapter 5 gives a brief introduction of the ZigBee network, the configuration of the Z-Stack protocol used in the system and a proposed algorithm for power management. Initial experiments are also performed to evaluate the algorithm.

Chapter 6 presents the conclusion of this study and introduces the future work.

Chapter 2

Literature and research review

This chapter mainly provides a literature review of the energy harvesting technology and the relative applications. The popular wireless network protocols, the techniques and components used for design are also studied.

This chapter is composed of four sections. The first section reviews the approaches used for energy harvesting especially the vibration and thermal gradient energy on an aircraft. The second section compares the popular network standards used for WSN applications. The third section introduces the considerations and techniques used for power saving across the entire development lifecycle. Finally, the last section studies the available products in the market for the later system design.

2.1 Energy Harvesting Technologies

2.1.1 Sources of ambient energy

The most promising and widely-used energy harvesting approaches for WSN are extract power from the ambient by using for example, light, vibration or motion energy, thermal energy, and radio frequency (RF) radiation. Table 2-1 summarizes the approximate amount of energy that can be harvested from environmental sources.

Table 2-1 Comparison of most common energy sources and the harvested power available in the ambient [12]

Source	Source power	Harvested power
Ambient light		
Indoor	0.1 mW/cm ²	10 μW/cm ²
Outdoor	100 mW/cm ²	10 mW/cm ²
Vibration/motion		
Human	0.5 m @ 1 Hz 1 m/s ² @ 50 Hz	4 μW/cm ²
Industrial	1 m @ 5 Hz 10 m/s ² @ 1 kHz	100 μW/cm ²
Thermal energy		
Human	20 mW/cm ²	30 μW/cm ²
Industrial	100 mW/cm ²	1–10 mW/cm ²
RF		
Cell phone	0.3 μW/cm ²	0.1 μW/cm ²

As shown in Figure 2-1, the power consumed by a WSN system is from tens of μW (sleeping) to tens of mW (transmitting), the same order of magnitude as the energy harvested from the ambient, thus it is possible to power a WSN node with the use of energy harvesting technologies.

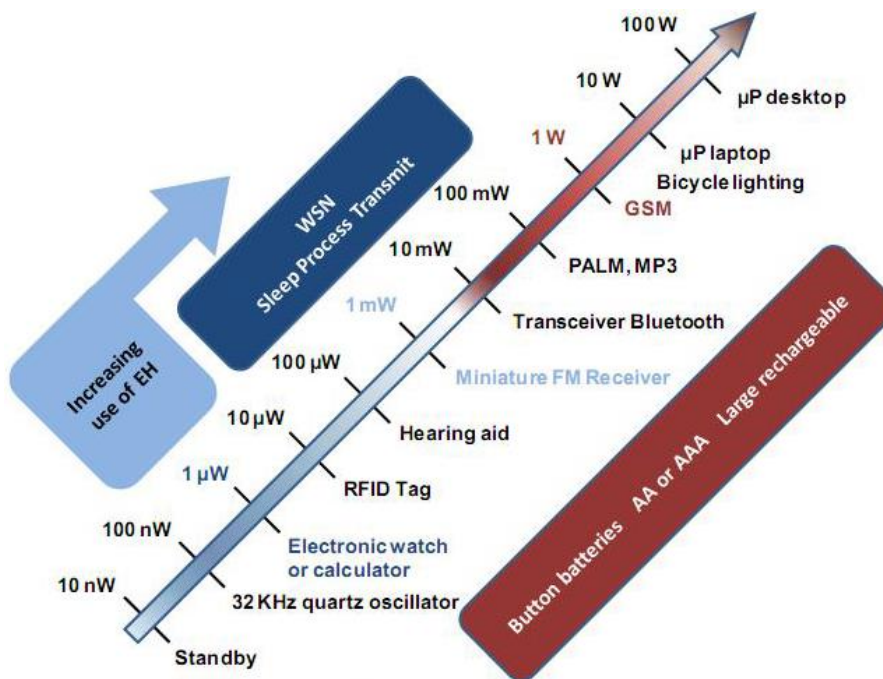


Figure 2-1 Power requirements of small electronic devices [13]

At present, the most mature method is based on solar cells which are used in a wide variety of outdoor applications. However, this method is not useful for sensor nodes that are not accessible to the direct sunlight. As vibration and thermal are the widespread energy harvesting sources that exist in abundance in the aircraft environment[11], applications adopting these harvesting technologies will be reviewed in the next sections.

2.1.2 Vibration energy harvesting

To convert vibration or motion, the typical electromechanical transducers are electromagnetic, electrostatic, piezoelectric or magnetostrictive. A schematic representation of those is shown in Figure 2-2. The advantages and disadvantages of those are compared in Table 2-2.

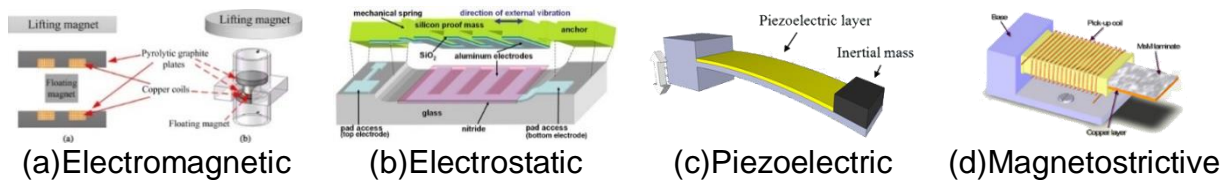


Figure 2-2 Typical electromechanical transducers

Table 2-2 Advantages and disadvantages of different vibrational transducers [14]

Type	Advantages	Disadvantages
Electromagnetic	<ul style="list-style-type: none"> no need of smart material no external voltage source 	<ul style="list-style-type: none"> bulky size: magnets and pick-up coil difficult to integrate with MEMS max voltage of 0.1V
Electrostatic	<ul style="list-style-type: none"> no need of smart material compatible with MEMS voltages of 2~10V 	<ul style="list-style-type: none"> external voltage (or charge) source mechanical constraints needed capacitive
Piezoelectric	<ul style="list-style-type: none"> no external voltage source high voltages of 2~10V compact configuration compatible with MEMS high coupling in single crystals 	<ul style="list-style-type: none"> depolarization brittleness in PZT poor coupling in piezo-film (PVDF) charge leakage high output impedance
Magnetostrictive	<ul style="list-style-type: none"> ultra-high coupling coefficient >0.9 no depolarization problem high flexibility suited to high frequency vibration 	<ul style="list-style-type: none"> non-linear effect pick-up coil may need bias magnets difficult to integrate with MEMS

Piezoelectric energy harvester can convert the kinetic energy from shocks, vibrations or motions into electrical energy by the means of the piezoelectric effect. Currently, this technology is getting more popular and widely used because the performance of piezo transducers has been boosted and ultra-low power ICs like MEMS sensors and MCUs have emerged. Moreover, piezoelectric has many advantages, such as, simple structure, no heat, no electromagnetic pollution, easy to manufacture and integrate, etc. Applications using piezoelectric technology have been studied and reported in many researches recent years.

Researchers from the University of Exeter had successfully developed a high performance energy harvesting powered wireless sensor node demonstrator to harvest aircraft wing strain energy for structural health monitoring applications. The system integrated piezo-fibre composites with carbon fibre laminates to harvest energy from the vibration of air vehicles in an active service and generated 2-12mW at 1-10Hz [15].

In [16], a piezoelectric cantilever device had been shown to harvest 11.4nW power with a load of 12.5M Ohms at the resonant frequency of 35.8 Hz and 0.1g acceleration.

A test rig was developed to evaluate the Quickpack piezoelectric energy harvester from Mide Company. Experimental results showed that a RMS power of 220 μ W and 440 μ W can be generated at 40Hz and 300Hz respectively from vibrations on an aircraft [11].

Mathers et al. presented a piezoelectric energy harvester based on the piezoelectric device (PMN-PT), and the maximum output power obtained under the 1.3 kHz excitation frequency is about 0.3mW [17].

Gu reported a piezoelectric harvester with a low resonance frequency of 20.1Hz can output maximum power up to 1.53mW [18].

A high efficient (72%) piezoelectric energy harvester was presented in [19], the experimental results showed that the system can harvest up to 8.4 mW power at the resonant frequency of 47 Hz and 0.5g acceleration.

Zhu, D. et al. designed a credit card sized piezoelectric energy harvester which generated a maximum of 240 μW output power when excited at vibration with a resonance frequency of 66.2 Hz and acceleration of 0.4 g [20].

A novel piezoelectric energy harvester with an adjustable low-duty ratio produced a maximum RMS output power of 100 μW with the frequency of 30 Hz and acceleration of 0.5 g [21].

Table 2-3 Summary of the literature review of the VEH

No.	Type	Power Output	Acceleration	Frequency	Ref.
1	piezoelectric	2-12mW	N/A	1-10Hz	[15]
2	piezoelectric	11nW	0.1g	35.8Hz	[16]
3	piezoelectric	220 μW 440 μW	N/A	40Hz 300Hz	[11]
4	piezoelectric	0.3 mW	N/A	1.3 kHz	[17]
5	piezoelectric	1.53 mW	N/A	20.1Hz	[18]
6	piezoelectric	8.4 mW	0.5 g	47 Hz	[19]
7	piezoelectric	240 μW	0.4 g	66.2 Hz	[20]
8	piezoelectric	100 μW	0.5 g	30 Hz	[21]

2.1.3 Thermal energy harvesting on aircrafts

Thermal harvesters use the Seebeck effect to collect power energy. The main element of a thermal energy harvester is thermopile which is comprised of thermocouples placed between a cold and a hot plate and connected in parallel. An electric voltage can occur if the thermocouple is subjected to a temperature gradient. Researches [12][14] showed that power levels in the mW range can be generated by thermal electric generators.

Thermoelectric generators (TEGs) are also used to harvest energy on an aircraft from the temperature gradient during a flight. From the experiment results in [8], a temperature profile of an aircraft's skin during a typical short-range flight is shown in Figure 2-3, it comprises of take-off and climbing with

temperature changes from about 20 °C to -22 °C in around 15 minutes, followed by a 25 minutes cruise flying with a stable temperature of -22 °C and then the descent and landing with temperature changes opposite to the take-off stage followed by 10 minutes ground time around 20 °C.

Researchers from EADS Germany and the Vienna Institute of Technology have been able to obtain around 23 joules (20mW for a temperature gradient of 20°C) of energy per flight by a TEG (see Figure 2-4), which is sufficient to power up a WSN node. Some test flights were also carried out on an Airbus aircraft [7].

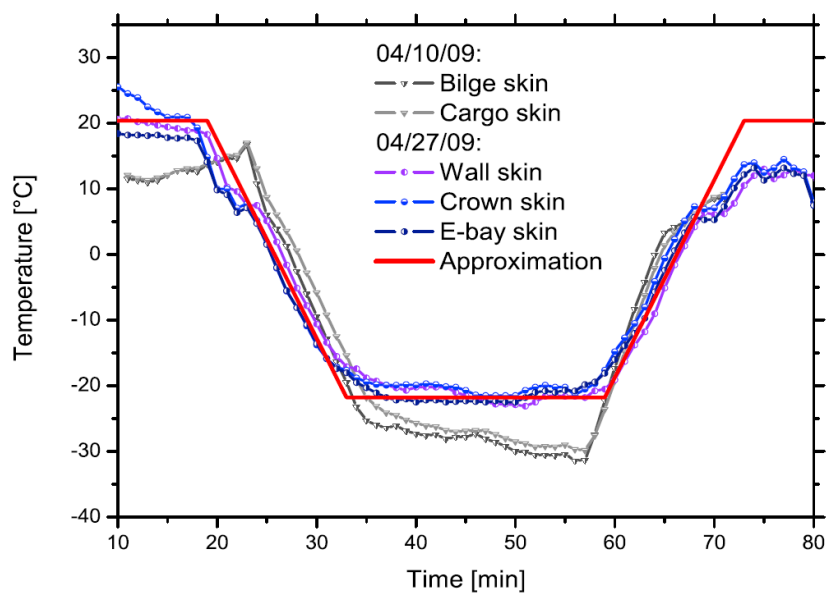


Figure 2-3 Temperature profiles of an aircraft's skin during typical short-range flights [8]



Figure 2-4 The TEG Module used in aircraft [7]

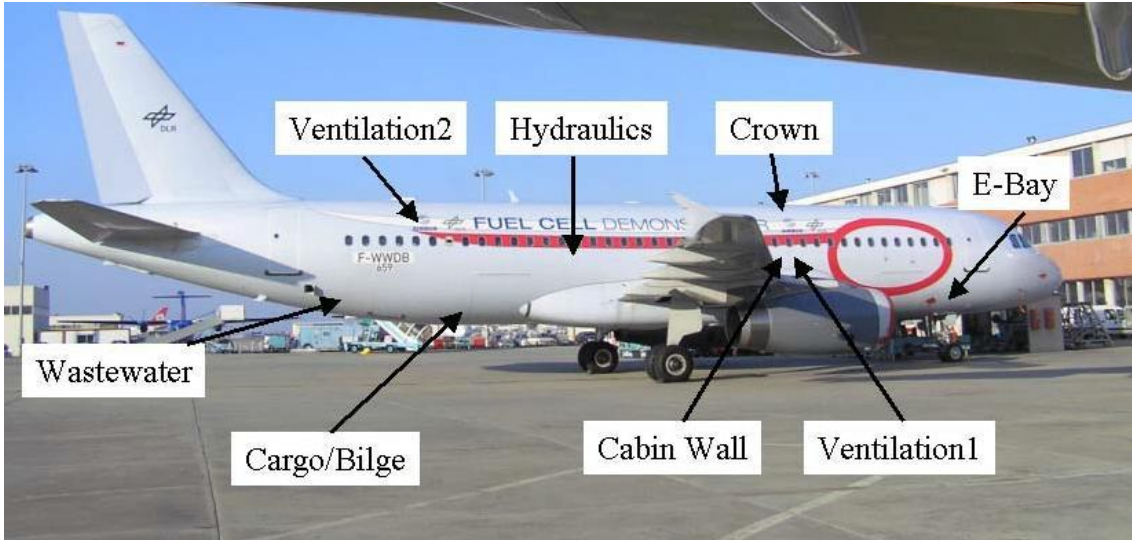


Figure 2-5 Different locations on an aircraft used for the simulation of a TEG [11]

A simulation was undertaken utilising the Mypelt software from Micropelt to analyse the power output for a single TEG (Micropelt MPG-D751) on various locations of an aircraft at Cardiff University. As shown in Figure 2-5, the results revealed that peak power levels ranging from 5.46 to 34.15mW and average power levels 2.99 to 22.58 mW were generated [11].

Table 2-4 Simulated results for temperature gradients on different locations of an aircraft [11]

	Peak temperature differential °C	Peak power mW	Average power mW
Cargo skin	40	34.15	22.58
Cargo primary Insulation			
Hydraulic pipeline 1	20	7.97	3.07
Hydraulic pipeline 2			
Waste water tank	15	5.46	2.99
Waste water ambient			
E-bay fuselage skin	35	18.72	6.42
E-bay primary insulation			
Cabin wall fuselage skin	30	13.36	3.97
Cabin wall primary insulation			
Cabin wall fuselage skin	40	30.06	11.70
Cabin wall secondary insulation			

The above researches show that both piezoelectric and thermal energy harvesting techniques have the real potential to power a WSN system. However in reality these two methods have different performance characteristics and Table 2-5[22] presents the pros and cons between them in an aircraft environment.

Table 2-5 Comparison of the thermal & vibration energy harvesting on an aircraft

Source	Pros	Cons
Thermal	Able to continuously supply DC power	Temperature differentials can be difficult to implement in enclosed environments ⁽¹⁾ .
vibration	Does not need to be manually charged. The aircraft provides plenty of vibrational force.	Each element has to be manually tuned to the aircraft's vibrational frequency.

(1) The best opportunity for temperature differential in an aircraft is between the aircraft “skin” on the inside of the cabin and the internal cabin temperature.

2.2 Popular wireless network standards comparison

The wireless network standards are designed for different applications such as industrial automation, home control and health monitoring. Each application has different requirements on the communication system.

Selecting the right network standard for wireless designs is getting more challenging as there are many standards which are also very similar.

To choose the right standard for this project, an overview of the popular wireless network standards operates in 2.4 GHz ISM (Industrial, Scientific, and Medical) band is studied.

ISM band is the radio bands reserved internationally for the use of radio frequency (RF) energy for industrial, scientific and medical purposes other than telecommunications. It is unlicensed in most countries and offers

communication medium for most wireless technologies like ZigBee, WiFi, Bluetooth and 6LoWPAN.

(1) ZigBee:

ZigBee[23], maintained by ZigBee Alliance, is an IEEE 802.15.4-based specification for remote control, monitoring and sensor network applications. The specification was created to address the need for a cost-effective, standards-based wireless networking solution that supports low-power consumption, low data-rates, reliability, and security. With its support of self-healing mesh networking, ZigBee allows nodes to find new routes throughout the network if one route fails, making it a robust wireless solution.

It can handle up to 65,000 nodes and operates in the unlicensed RF worldwide (868 MHz Europe, 915MHz America or 2.4GHz global) with the raw data rate up to 250kbps and the range up to 100 meters.

(2) WiFi:

WiFi is a local area wireless computer networking technology that used widely in both home appliances and industrial applications. It integrates the protocol designed for exchanging data with Internet access to devices. It is based on the IEEE 802.11 standards and operates in the 2.45 GHz frequency range.

It has many derivations such as 802.11a, 802.11b, 802.11b/g, 802.11g and 802.11n, and the transfer rate goes up to 54 Mbps for 802.11g and up to 300 Mbps for 802.11n [24]. This protocol is a great option where longer range and high speeds are needed in the application.

(3) Bluetooth:

Bluetooth, which is also known as IEEE802.15.1, is invented by Ericsson and managed by the SIG (Bluetooth Special Interest Group). It is a wireless protocol that used to build personal area networks and exchange data over short distances.

It operates in the 2.4 GHz ISM band and uses frequency-hopping. The maximum transfer rate of this protocol is 3 Mbps and the range is up to 100 meters [24].

One notable point to mention is that when a Bluetooth device is in power down mode, it would take about 3 secs to wake up and respond [25].

(4) 6LoWPAN:

6LoWPAN (IPv6 over Low-power Wireless Personal Area Networks) is developed by the 6LoWPAN IETF (Internet Engineering Task Force) that provides a method to transmit internet protocols (IPv4 and IPv6) over low-power wireless sensor networks. Its base specification (RFC4944) permits the implementation of the IoT (Internet of Things) on even the smallest and remote devices [26].

6LoWPAN operates at the frequency of 2.4 GHz with the transfer rate up to 250 kbps and the range is up to 200 meters. The main area of this protocol is applications that need an internet connection, like energy management, home and building automation [24].

The use of a certain protocol is always dependent on the application to be implemented. The major criteria to choose the appropriate protocol are: available electrical power supply, required data rate, and number of network nodes.

From the above discussion, it can be seen that Bluetooth offers a good compromise between data rate and range while WiFi seems to be preferred for higher data rates and ZigBee for lower consumptions and longer battery life. For the applications need an Internet connection with a low rate, 6LoWPAN is the choice.

The four popular network standards for WSNs are compared in Table 2-6 [27][24][25][28] and Table 2-7 [28].

Table 2-6 Comparison of the popular wireless network standards

Protocol Name	ISM Frequency Band (MHz)	Max Tx Data rate (bps)	Modulation Scheme	Number Channels	Spread Spectrum	Nominal Range	Max. Nodes	Power	Star Topology	Tree Topology	Mesh Topology	Network Stack Size	Security	Development Complexity
	868	100K	BPSK, ASK OQPSK	1	DSSS									
ZigBee	916	250K	BPSK, ASK OQPSK	10	DSSS	75m	65536	Very Low	√	√	√	Very High	AES 128	Med-High
	2400	250K	OQPSK	16	DSSS									
WiFi	2400 5000	300M	CCK/QAM64	3	FHSS DSSS	300m	32	High	√	-	-	-	WEP WPA	High
Bluetooth	2400	3M	GFSK	3	FHSS	10m	8	Low	√	-	-	Very Low	AES 128	Low
6LoWPAN	2400	250K	OQPSK	16	DSSS	200m	100	Low	√	√	-	Med	IPsec	High

Table 2-7 Advantages and disadvantages of popular network standards

Name	Advantages	Disadvantages	Applications
ZigBee	<ul style="list-style-type: none"> widely available widely supported low cost interoperable nodes from other vendors 	<ul style="list-style-type: none"> routers are not designed to sleep coordinator is a single point of failure 	<ul style="list-style-type: none"> home automation industrial control embedded sensing medical systems
WiFi	<ul style="list-style-type: none"> very high data rates worldwide infrastructure 	<ul style="list-style-type: none"> complex expensive very high power 	<ul style="list-style-type: none"> high speed internet connectivity applications
Bluetooth	<ul style="list-style-type: none"> high data-rates that can support digitized audio transmission 	<ul style="list-style-type: none"> high power limited battery operation limited range requires a border router to connect to the internet 	<ul style="list-style-type: none"> mobile headsets
6LoWPAN	<ul style="list-style-type: none"> IPv6 compatible 		<ul style="list-style-type: none"> IoT

It is obvious that ZigBee offers the most network options including multiple operational ISM bands, three network topologies, high network scalability, and various modulation schemes. It consumes very low power with a moderate data rate and transfer range. With the ability to build large mesh networks, it widens the using range for sensor monitoring. In consideration of the unit cost, network topology, security and complexity, ZigBee standard is chosen as the wireless protocol in this project.

2.3 Power saving techniques review

For a sensor node fully powered by ambient energy, the generated mean power must be greater than or equal to the mean consumed power. The ideal means to accomplish this is to choose a high output harvester and a low power WSN node. In addition to this, power supply efficiency can be optimized through proper design and implementation.

The following lists a general overview of typical power saving considerations and techniques which are reviewed from [29][30][31][32]. These techniques can be taken into account in both hardware design and software design.

(1) Hardware level

(a) Components Selection

- Effective energy harvester
- High efficiency AC/DC and DC/DC convertor
- Small and efficient energy storage device
- Single-chip low power MCU / wireless transmitter
- Ultra-low-power Sensors

(b) Circuit Design

- Care must be taken not to drive an IO that does not have power.
- Eliminate pull-resistors, if possible, use pull-down resistors instead of pull-up resistors.

- Use high quality surface-mount low series resistance (ESR) capacitors to minimize the lead inductance. The capacitors should have an ESR value as small as possible. Ceramic capacitor should be used where possible.

(c) PCB Design

- Minimize the start-up peak current during the power up period by sequencing devices correctly.
- Place as many bypass capacitors as possible between VDD pins and GND and as close as possible to provide the shortest and lowest inductance path.
- Keep ground leads short; preferably tie individual ground pins directly to the respective ground plane.
- Avoid sharing via holes. Connect each ground pin to the ground plane individually.
- Use of larger diameter via holes to connect the capacitor pads between power and ground planes aid in minimizing the overall inductance.

(2) Software level

- Unused I/O pins should be configured as outputs and driven low to reduce ground bounce in the configuration.
- Avoid of high frequency oscillators during idle/sleep mode.
- Schedule the system in different operation modes (active, idle, and sleeping) intelligently.

2.4 Main components & modules investigation

To make the development rapid and effective, a research about the off-the-shelf products together with these used in the literatures was carried out to investigate and select the suitable components for the system design.

Table A-1 in Appendix A gives the specifications of the vibration harvesting products while Table A-2 presents examples of commercially available low power ZigBee modules (combined with microcontrollers).

The performance of the discrete circuit compared with the integrated circuit used for power management is studied and analysed in [33], results show that the integrated circuit has a much better performance and helps reduce the development time. Therefore, the state of the art commercial power management ICs used for vibration energy harvesting are studied and listed in Table A-3.

Chapter 3

System overall design

This chapter mainly describes the structure of a WSN system powered by piezoelectric energy harvester and proposes an overall design for this project.

This chapter is divided into two sections. In the first section, the structure of a WSN node powered by energy harvester and the operating mechanism is presented. In the last section, an overall design based on the off-the-shelf products is designed and illustrated.

3.1 Structure of a WSN node powered by vibration energy harvesters

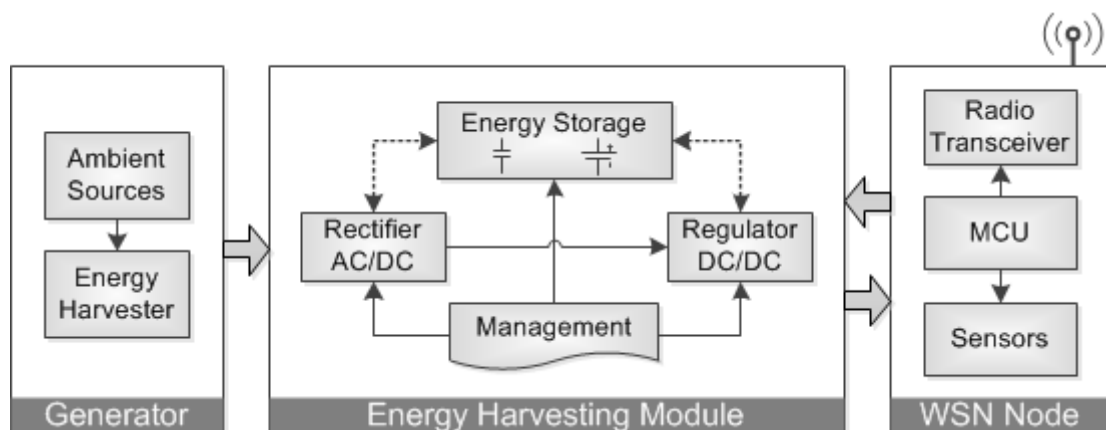


Figure 3-1 Block chart of a WSN node powered by vibration energy harvesters

A normal wireless sensor network system powered by a vibration energy harvester is usually consists of three main units (see Figure 3-1): energy generator, energy harvesting/conditioning circuit, and WSN node.

A generator is a specific material or transducer which used to convert the ambient vibration energy surrounding the system into the useful electrical power. To maximize its power output, the transducer should be designed or tuned to work at resonance with the dominate frequency of the ambient system.

The loads (microcontroller and sensors) in the WSN node are non-linear and need a regulated DC voltage to operate. Unfortunately, the raw output of the piezoelectric energy harvester is an AC waveform whilst the value changes irregularly as the harvester deflects in both directions with different amplitudes. In an AC electrical power system, Power Factor (PF) is used to measure how efficiently the electrical power is being used. PF is the ratio of the real power flowing to the load to the apparent power from the circuit and it is usually less than one as the voltage and current waveforms are not in phase. To improve the power quality and make the AC power supply to operate at its maximum efficiency, a technique named power factor correction (PFC) is widely used [34].

As shown in Figure 3-2 [34], there are two types of PFC techniques: Passive PFC and Active PFC. Passive PFC utilizes a filter at the AC input to reduce the harmonic current, consequently, make the non-linear load look like a linear one. This method is simple and inexpensive, however, as the filter is comprised of capacitors and inductors (hundreds of mH), the passive PFC has heavy weight and bulky size. Another limitation of this means is the range of allowable input voltages is very narrow.

Compared with the passive PFC, active PFC is a lighter, smaller, and more efficient control method. The core component in the active PFC is the PFC control unit between the load and the AC input (See Figure 3-2(b)). This intelligent unit operates at high switching frequencies and presents an in phase voltage and current load to the input, as a result, a better power factor over 95% can be achieved.

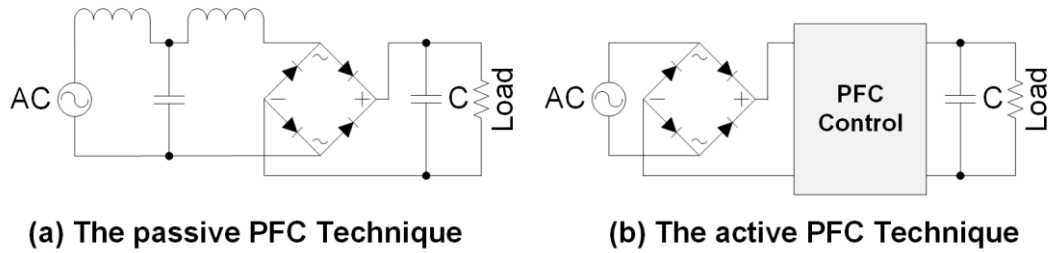


Figure 3-2 Passive and active power factor correction techniques

Another important condition to be considered is the scavenged energy from the harvester is range from μW to mW while the power consumption of a typical WSN node is μW (sleeping) to tens of mW (processing). Namely, the harvester can't power the WSN node in a continuous active mode but only keep the node in a sleep or standby mode. The best method to solve this problem is storing the extra energy in a reservoir (such as tantalum capacitor, super-capacitor, or rechargeable battery). The energy storage works like a buffer, it reserves the energy for a later burst power consumption like the radio transmission, which consumes a high current (tens of mW) with a short duration (few milliseconds).

As shown in Figure 3-3, an energy harvesting or conditioning module is employed to address the abovementioned issues. The module is composed of an AC-to-DC rectifier, a storage unit (capacitor/ battery), a DC-to-DC regulator, and the power control/management unit.

As mentioned before, the frequency of the AC input is changing and determined by the ambient vibration, the active PFC technique is implemented in the power management design as it is capable of a wide range of input voltage.

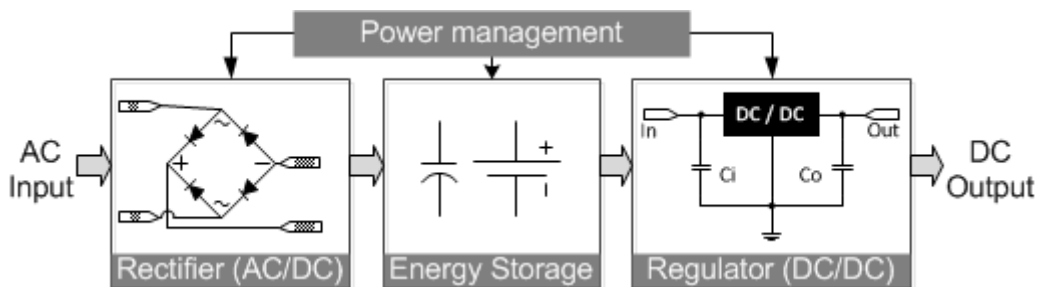


Figure 3-3 Block chart of a typical vibration energy harvesting module

The module rectifies the input AC current power from the energy harvester, charges the storage device, converts and steps down the energy into a well-regulated DC power, and outputs the energy to supply the target components. With the help of the power management unit, the module can convert the energy and supply the system efficiently.

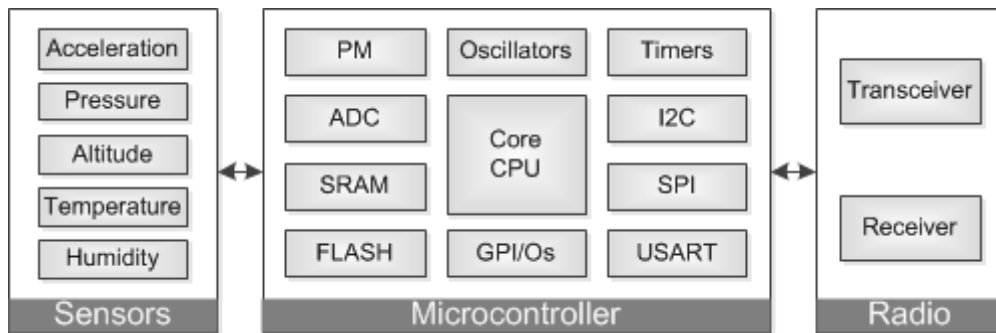


Figure 3-4 Block chart of a wireless sensor network node

The last part of the system is the WSN node (shown above in Figure 3-4), which is typically made up of a microcontroller, a wireless transceiver and different sensors.

The microcontroller/processor is the heart of a WSN system. In the active mode, the microprocessor controls different sensors to sample data, processes and packets the data to the wireless transceiver, and handles the radio communication with other nodes. After that, it turns off the CPU, high-frequency oscillators, RF transceiver and other peripherals to make the system enter a power-saving sleep mode, waiting for an interrupt (external interrupt, sleep timer, and etc.) to wake up the system.

The sensors are implemented in a WSN system to sense/measure the ambient parameters, such as vibration, pressure, altitude, temperature and humidity. These data are processed and sent by the WSN to the central station for further analysis.

A wireless network with different topologies can be established by the radio frequency transceivers to make one node communicate with others. As shown in Figure 3-5, the RF activity of the transceivers is the highest power

consumption in the WSN node, in order to reduce the whole consumption of the system, it is very important to select a low power transceiver with a suitable transmission range.

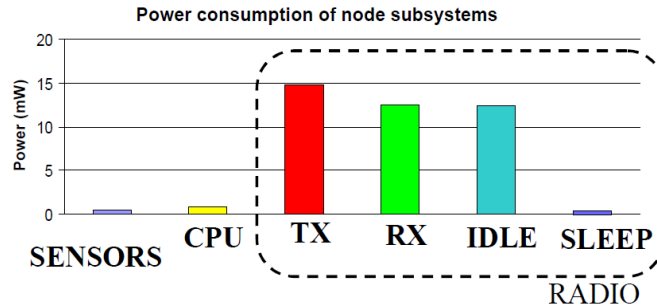


Figure 3-5 The distribution of power consumption in a WSN node [35]

3.2 An overall design of the WSN system powered by piezoelectric energy harvester

In terms of the power consumption, operating voltage, accuracy, and interface support, the main components/modules (Listed in Table B-1 in Appendix B) for the design of the vibration energy harvesting WSN system are selected from the market. In addition, there are also trade-offs between size, weight, package, operating ambient temperature range, and price during the evaluation.

An overall integrated design of the WSN system is finished based on the discussion in section 3.1, shown in Figure 3-6, consists of three main subsystems, energy harvesting unit, microcontroller & wireless transceiver unit, and sensors unit.

The ambient vibration energy is harvested by V25W (Piezoelectric energy harvester, from Midé Technology), rectified and regulated by LTC3588-1 (Nano-power Energy Harvesting Power Supply, from Linear Technology), and then outputted to power iM222A (ZigBee Network Processor module, from IMST GmbH) and three sensors (HDC1000 from TI, LIS2DH and LPS25H from ST) in the system. The extra energy is stored in a capacitor during an inactive mode and consumed for the burst operation in the active mode.

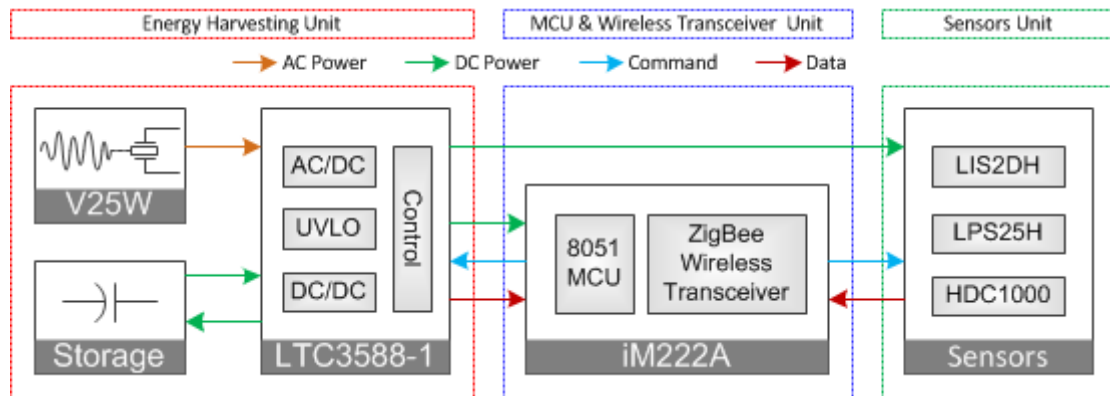


Figure 3-6 An overall integrated design of the WSN system

A general introduction and key specifications of the components/modules used in Figure 3-6 will be described next in this chapter, and the detailed design of each subsystem will be presented in the hardware and simulation development part.

3.2.1 Energy harvesting unit

The left (red dotted border) rectangle in Figure 3-6 shows the energy harvesting unit which includes an energy harvester, an energy storage capacitor and an integrated chip which converts the energy from harvester/capacitor into a useful regulated DC voltage.

Consider of the weight, power output, work frequency, dimension and cost, a piezoelectric energy harvester, Volture™ V25W from Midé Technology, is employed in the system as the transducer. V25W is designed for battery replacement which transduces wasted energy from useless mechanical vibrations into useable electrical power.

Figure 3-7 shows the dimension of the harvester, which is about half the size of a credit card, with a weight of only 6 grams. By using the patented robust packaging technology from Midé Technology, Volture™ V25W harvester is sealed hermetically and can be used in harsh environments.

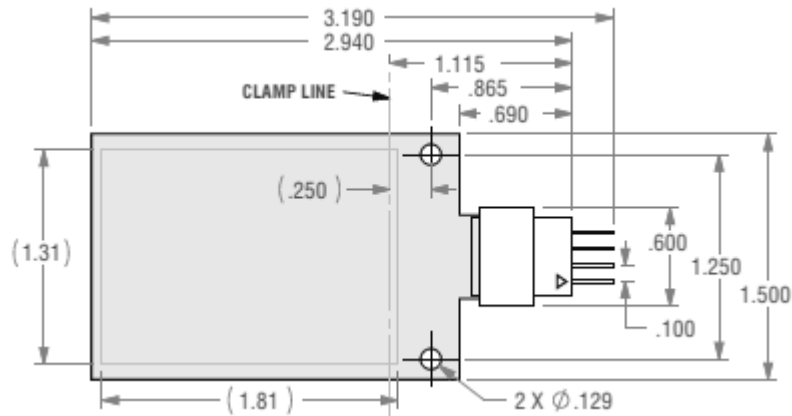


Figure 3-7 Dimension of the MIDÉ V25W [36]

The harvester has a wide work frequency range, from 40 Hz to 120 Hz. As the frequency of the vibration occurs on an aircraft is between 0-300Hz depending on different operations [11], the harvester satisfies the requirement and can be employed in the aircraft environment.

By the use of a tip mass, the harvester can be tuned to match the vibrating structure from which it is harvesting, and thus output the maximum power at the resonant frequency. A tip mass has the effect of driving down the natural frequency of the harvester, increasing the harvested energy and reducing the complete cycle time [36].

Figure 3-8 shows the relation between tip mass and natural frequency while Figure 3-9 illustrates four (tuned to 40Hz, 50Hz, 75Hz, and 120Hz) typical performance power characteristics of the V25W harvester respectively. By the use of the tip mass, V25W can output up to 9.231 mW power, which is power enough for most low power WSN applications.

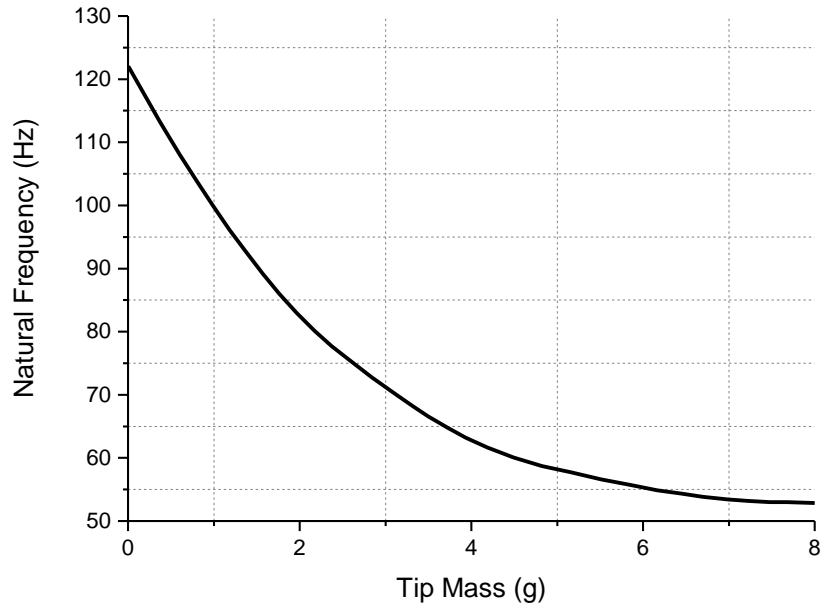


Figure 3-8 Relation between tip mass & natural frequency of V25W [36]

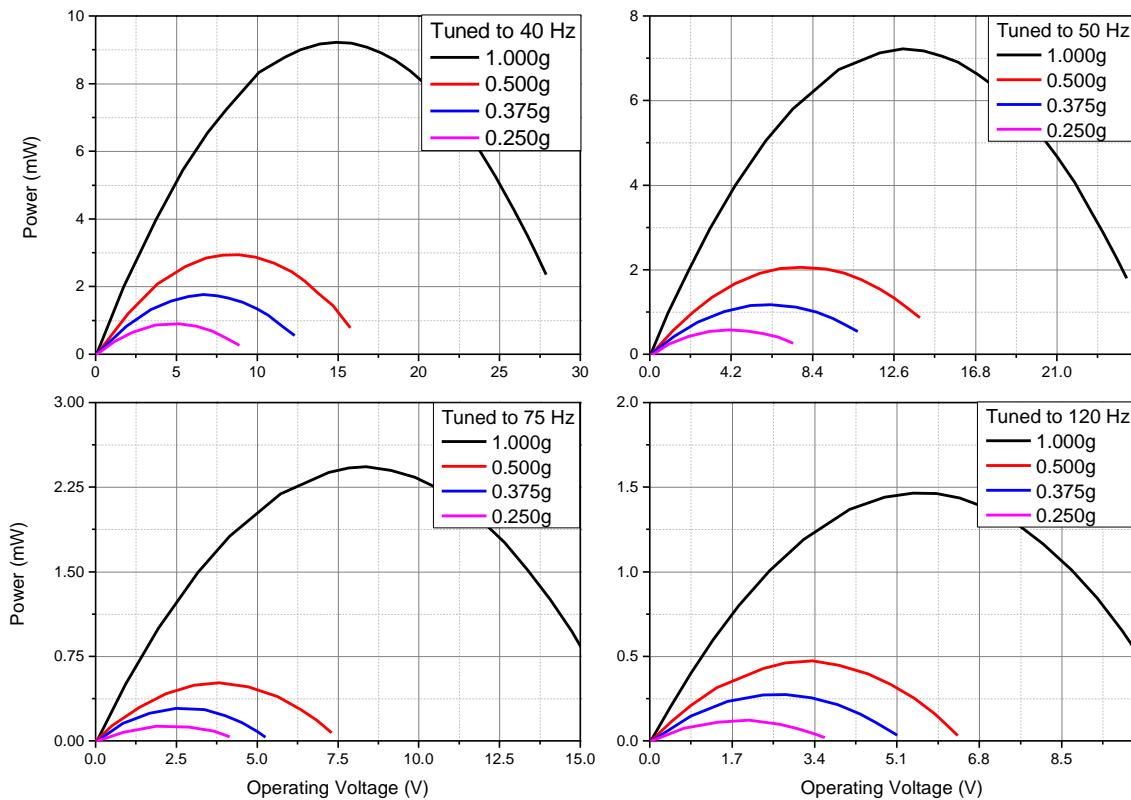


Figure 3-9 Power performance of the V25W at different frequencies [36]

As discussed before, the piezoelectric harvester generates the energy in the form of an AC waveform when it experiences a vibration, and the amount of the

harvested energy is determined by the amplitude and frequency of the vibration. To power the microcontroller and sensors effectively and efficiently, the harvested power should be transformed into a regulated DC power which within the scope of the power consumption demand (e.g., power, current and voltage) in both sleep mode and active mode. An integrated chip LTC3588-1 from Linear Technology is chosen to achieve the above targets based on the investigation in Table A-3.

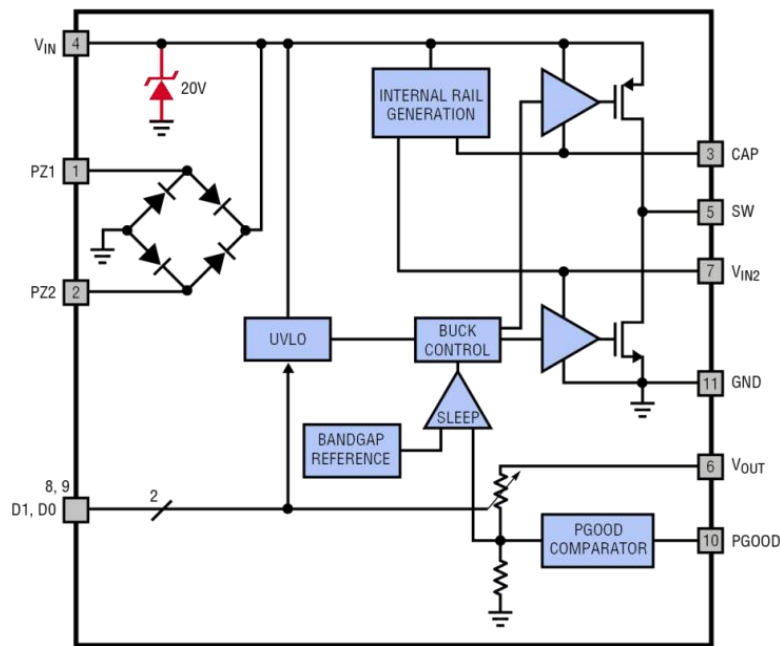


Figure 3-10 Functional Block Diagram of LTC3588-1 [37]

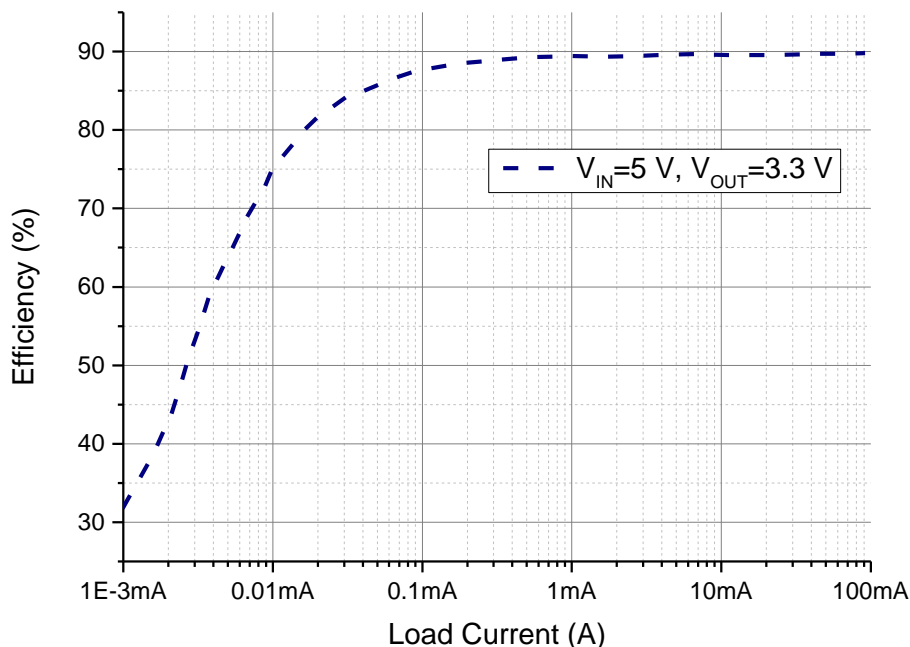
As the functional block diagram shown in Figure 3-10, all the critical components used for the power management are integrated together into one single chip on LTC3588-1, including a full-wave diode bridge rectifier with a total drop of about 400mV loss, an efficient UVLO module with a wide hysteresis window that accumulates/stores the energy on a storage capacitor during the sleeping state and a DC-DC buck converter that outputs a regulated DC voltage. It is worthwhile to mention that the output voltage can be programmed to one of four fixed voltages (1.8 V, 2.5 V, 3.3 V, or 3.6 V) by different set at the input pins (D1 and D0), which provides a wide supply voltage range and meets the need of different WSN applications. The input operating voltage range of this chip is

from 2.7 V to 20 V and an internal input protective shunt is used to support up to 25 mA pull-down when the input voltage exceeds 20 V.

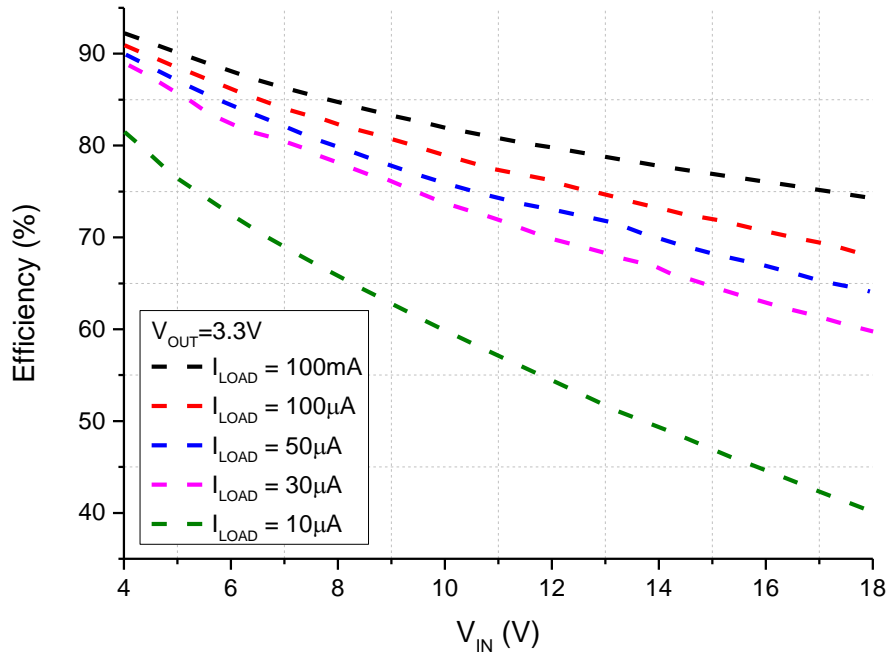
Low quiescent current is necessary in a power management system to maximize the overall efficiency, especially for high output impedance energy sources such as piezoelectric harvester. LTC3588-1 has a quiescent current of only 450 nA during the under voltage lockout (ULVO) mode and 950 nA during the output in regulation (with no load), making it ideal for the piezoelectric energy harvesting based applications.

With just a few external components, LTC3588-1 can output current up to 100mA, making it meet the need of the wireless transmission operation in most WSN systems

Figure 3-11 illustrates the typical efficiency performance (Efficiency vs. I_{LOAD} and V_{IN}) characteristics of the LTC3588-1. It shows a high efficiency of up to 90% can be achieved during a normal operation of the microcontroller in the active mode. It is acceptable that the efficiency is low in the standby mode, as most of the harvested energy is consumed in the input storage capacitor.



(a) Efficiency vs. I_{LOAD} while $V_{IN} = 5\text{V}$ and $L = 10\mu\text{H}$



(b) Efficiency vs. V_{IN} while $V_{OUT} = 3.3\text{V}$ and $L = 10\mu\text{H}$

Figure 3-11 Typical performance characteristics of LTC3588-1 [37]

3.2.2 Microcontroller & wireless transceiver unit

As the energy harvested from the environment tends to be small and intermittent, a successful design needs a low power microcontroller and wireless transceiver with different power-saving features.

An investigation of the popular microcontrollers and wireless transceivers used in low power consumption applications was carried out and a pre-qualified RF module iM222A from IMST GmbH is selected for the microcontroller & wireless transceiver unit according to the results (shown in Table A-2 in Appendix A).

The iM222A is a low power radio module operates in the 2.4 GHz ISM band. It integrates a TI CC2530F256 chip and the relevant external components on a compact SMD board with an internal PCB antenna (see Figure 3-12 below).

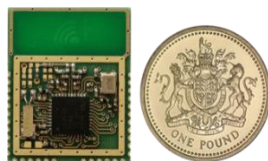


Figure 3-12 iM222A radio module compared with a one pound coin

TI CC2530F256 is a powerful System-on-Chip (SoC) based on the architecture of an enhanced 8051 core MCU. It combines a leading RF transceiver, 256KB In-System-Programmable flash, 8KB RAM and many other powerful features, making it a complete solution for 2.4-GHz IEEE 802.15.4 and ZigBee relevant applications.

One notable point to mention is that the chip is compatible with the ZigBee protocol stack (Z-Stack™) from Texas Instruments, Z-Stack is a complete protocol stack and application development solution that conforms to ZigBee Alliance standards, providing the support for manufacturer-specific or proprietary wireless implementations, and employing the full mesh networking capabilities offered by ZigBee technology.

The summarized specifications of the iM222A (TI CC2530256) are shown in Table 3-1. Additionally, CC2530256 incorporates advanced power-management functionalities that can be used when power consumption is a concern such as the applications based on harvesting energy. These functionalities allow the use of different low-power modes (PM1, PM2, and PM3), range from disabling particular peripherals to placing the device into a hibernation state.

Table 3-1 Specifications of the TI CC2530256 iM222A (TI CC2530256)[38] [39]

Electrical Characteristics		Peripherals	
Supply Voltage	2 V -3.6 V	MCU	256 KB Flash
			8 KB RAM
Current Consumption	16MHz: 3.4 mA 32MHz: 6.5 mA RX: 24 mA TX: 29 mA PM1: 0.2 mA PM2: 1 µA PM3: 0.4 µA	Peripherals	32MHz / 32 kHz crystal oscillator
			16 MHz / 32 kHz RC oscillator
			21 GPIO ports
		RF	12-Bit ADC
			2 USARTs
			MAC/Sleep/Watchdog Timer
			3 General Timers
			DMA
			128-Bit AES Coprocessor
			2.4-GHz IEEE 802.15.4 Compliant
			Mesh-, Tree-, Star-Networks
			Output Power Up to 4.5 dB
			250 kbps data rate
			Up to 500 meters range ⁽¹⁾

Note:

(1) Outdoor (line of sight) with external antenna (0 dB)

In addition to the power saving functions, the built-in ADC (Analog-to-Digital Conversion) function supports 7 bits (30 KHz bandwidth) to 12 bits (4 KHz bandwidth) of resolution and the reference voltage can be either internal (1.15 V) or AVDD (3.3 V in this design), making it possible to monitor the voltage of the storage capacitor in the algorithm design.

3.2.3 Sensors unit

Three MEMS-based sensors are used to monitor airplane performance associated parameters, such as vibration, pressure, and temperature. These data are sent to the central station to provide operators with information that can be used to adjust airplane performance factors, analyse performance issues, alert sudden changes, and make comparisons with other airplanes within the fleet.

The LIS2DH is a three-axis linear accelerometer with high performance and ultra-low power consumption. It is capable of measuring accelerations with output data rates from 1 Hz to 5.3 kHz in user-selectable full scales of $\pm 2g/\pm 4g/\pm 8g/\pm 16g$. It can work between 1.71 V and 3.6 V and the low power mode consumption is down to 2 μA [40].

The LPS25H is an ultra-compact absolute digital pressure sensor from STMicroelectronics. The Supply voltage is 1.7 to 3.6 V and the power consumption is as low as 4 μA in Low resolution mode [41].

The HDC1000 is a digital humidity sensor with integrated temperature sensor that provides excellent measurement accuracy at very low power, only 1.2 μA @ 1 measurement/second, with the supply voltage from 3 V to 5 V [42].

The sensors used in this project all have very short initialisation time and conversion time so as to have low power consumption for data acquisition.

Chapter 4

Hardware development & simulation

This chapter describes the hardware design and assembly of the WSN system powered by piezoelectric energy harvester. The simulations of the system are also performed and discussed.

This chapter is comprised of three sections. The first section describes the detailed design of each unit introduced in section 3.2 and discusses the choice of the main components and parameters. The second section models the system in LTspice IV, carries out simulations in different scenarios and analyses the results to validate the design and evaluate the performance of the system. Finally, the third section presents the PCB layout and the manufacturing work of the system.

4.1 Circuit design and parameter specification

4.1.1 Energy harvesting and power management unit

4.1.1.1 Configuration of the V25W energy harvester

The transducer employed in this design is V25W piezoelectric energy harvester from Midé Technology. As shown in Figure 4-1, there are two isolated piezo wafers in the V25W, and the wafers can be connected either in series or in parallel.

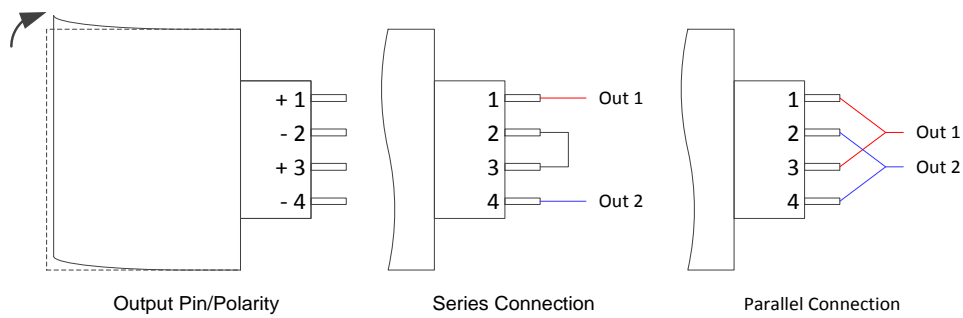


Figure 4-1 Pinout configuration of V25W

Compared with the single wafer, series connection has the double open circuit voltage whilst parallel connection has the double current, and both connections have the same power output. The series connection is more suitable for the vibrations with low levels, as it doubles the voltage which will easily reach the threshold of the power management circuit. Instead, parallel connection is more suitable for the vibrations with high levels and it is recommended for most applications according to the datasheet [36]. However, which connection is chosen depends on the vibration environment of the application.

As shown in Figure 3-10, an internal low-loss full-wave bridge rectifier is integrated in the LTC3588-1, the voltage loss of the rectifier is 0.4 V from the [37], so the output voltage of the rectifier is half the peak-to-peak input voltage minus 0.4 V (two diode drops). This drop can be ignored for the applications where there is a high voltage output (high amplitude). However for the applications with low amplitude, this voltage drop (0.4 V) is not negligible. To address this problem, a "Superseries" connection of the rectifier is used in [43], the voltage drop is only one diode drop, which allows operation from slightly lower minimum input voltages.

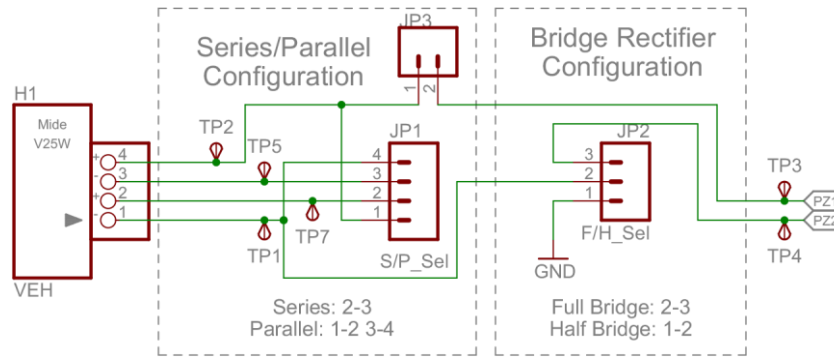


Figure 4-2 Schematic of the configurations of the V25W harvester and rectifier

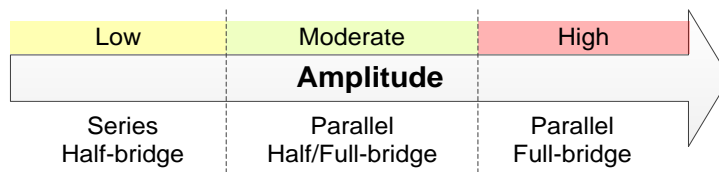


Figure 4-3 General guidance for the configuration of the system in different levels of amplitude

Figure 4-2 illustrates the schematic of the connection between V25W harvester and the diode rectifier in LTC3588-1 while Figure 4-3 gives a general guidance for the configuration in different levels of amplitude respectively. A four header pin JP1 is used to configure the series/parallel connection of the wafers in V25W and a three header pin JP2 is used to determine whether full-bridge mode or half-bridge mode is selected for the rectifier in LTC3588-1. In addition, JP2 can also be used along side with the two header pin JP3 to disconnect the harvester from the power management circuit, namely, support a electrical isolation from the LTC3588-1 power management chip, it is very useful for the measurements of the raw output from the harvester.

4.1.1.2 Design parameter and specification of the power management circuit based on LTC3588-1

The major concerns of designing a successful WSN system based on a piezoelectric harvesting technology is the power management, the reason is that the burst current of the load (like MCU and transceiver) is much higher than the harvester can generate. A complete energy harvesting solution from Liner

Technology, LTC3588-1, which is optimized for the piezoelectric transducer, is used in this design. A general introduction and performance of this chip is given in section 3.2.1, and Figure 4-4 presents its typical application with the power supply capacity of up to 100mA according to [37].

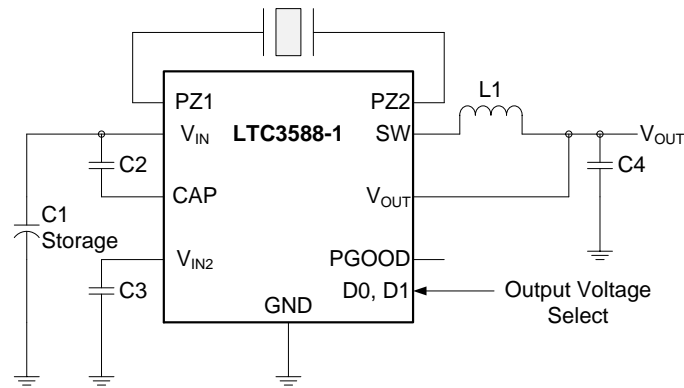


Figure 4-4 100mA Piezoelectric Energy Harvesting Power Supply [37]

As the functional block diagram presented in Figure 3-10, the LTC3588-1 integrates all the critical units needed in a power management circuit, such as full-bridge diode rectifier, UVLO detector, buck regulator and DC/DC converter, providing a low loss and high efficiency solution for the applications based on high-output-impedance piezoelectric harvesters. In addition to those, only five external components are needed, including an input capacitor, two compensating capacitors, an output capacitor and an inductor. Figure 4-5 illustrates the schematic of the power management circuit interfaced with the Midé V25W energy harvester.

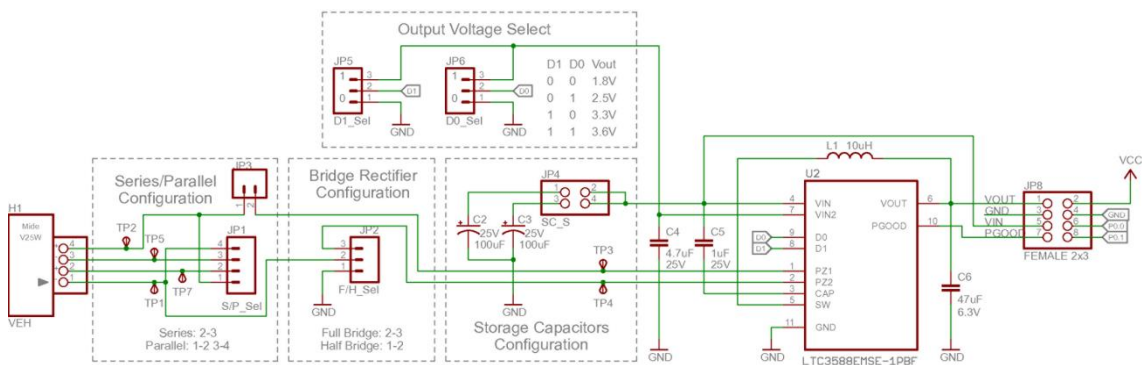


Figure 4-5 Schematic of the output voltage configuration of V25W

Input Capacitor / Storage Capacitor (C1): The energy harvested from the ambient can be accumulated and stored in either input capacitor (C1) or output capacitor (C4) by LTC3588-1 based on the power requirement of the application. According to the datasheet, the buck in the LTC3588-1 can deliver up to 100 mA average current from input storage capacitor to the output load. For the wireless transceiver (TI CC2530) used in this project, the maximum current consumption during the TX mode (4.5-dBm output power) with the 32 MHz XOSC oscillator running is 39.6 mA, plus the consumption from the sensors and other peripherals, the total load current is less than 50 mA, which is far below 100 mA.

Based on the reasons above, the input capacitor is chosen as the storage reservoir, as the wide input range (2.7 V to 20 V) takes advantage of the fact that energy storage on the input capacitor is proportional to the square of the capacitor voltage. Any harvested energy in the sleep mode or excess energy in the active mode will be saved in the storage capacitor with an increase of its voltage.

A Zener limiting diode (Shown in Figure 3-10, marked with red) is used between the V_{IN} and ground, the voltage on the storage capacitor is internally clamped to a maximum of 20 V, namely, the highest voltage ever presents at V_{IN} is 20 V. This diode can also be used to keep the storage capacitors from overcharging if they have a rated voltage (VDC) which is over 20 V.

The value of the storage capacitor is calculated according to the power consumption for certain duration in the output. The charge voltage (V_{IN}) of the capacitor should also be considered. The detailed selection and analysis of the storage capacitor will be discussed in section 4.2.1.

Compensating Capacitors (C2, C3): These two capacitors can compensate the internal rail generation circuits and hold up them during buck. A typical value of 1 μ F and 4.7 μ F is given by [37] to C2 and C3 respectively.

Output Capacitor (C4): For a higher current consumption over 100 mA, the output capacitor can be used as the reservoir to meet the need of a larger load.

The output capacitor also has an impact on the sleep duration of the regulator inside LTC3588-1 alongside with the load current. Equation (4-1) from [37] shows the relationship between these factors:

$$T_{SLEEP} = C_{OUT} \frac{V_H}{I_{LOAD}} \quad (4-1)$$

Here C_{OUT} is the output capacitor, V_H is the value of DC sleep hysteresis window (the value is 24 mV to LTC3588-1 from its datasheet), and I_{LOAD} is the current of the load. The sleep time of the regulator will decrease along with the output capacitor decreases. However, a capacitor less than 10 μ F is not recommended, as the ripple of the output will increase to an undesirable level. A 47 μ F capacitor is used according to the datasheet.

Output Inductor (L1): The buck in the LTC3588-1 is optimized to work with an inductor in the range of 10 μ H to 22 μ H, and 10 μ H is recommended to typical applications. It should be noted that the DC Resistance (DCR) and DC current rating of the inductor should be considered before choosing, as the DCR is a source of loss and DC current rating should above the range of the maximum output current. A 10 μ H inductor with a 0.133 Ω of DCR and 900 mA of saturation current is selected for this design.

Output Voltage Select (D0, D1): The output voltage of the LTC3588-1 can be selected by D0 and D1 from 1.8 V, 2.5 V, 3.3 V and 3.6 V for different applications. Two header pins(JP5, JP6) in Figure 4-5 shows a flexible design for different voltage output according to the Table 4-1 from [37].

Table 4-1 Output voltage selection[37]

D0	D1	V _{OUT} (V)	I _{VOUT} (nA)*
0	0	1.8	44
1	0	2.5	62
0	1	3.3	81
1	1	3.6	89

*: Quiescent current consumes by the internal feedback network

4.1.2 Microcontroller & wireless transceiver unit

4.1.2.1 General design of the MCU & RF unit and its peripherals

To minimize the need for a time consuming RF circuit design, a commercial available RF module iM222A from IMST is used in the microcontroller & wireless transceiver unit. The main component of this module is TI CC2530, which integrates an enhanced 8051 MCU core together with an excellent RF transceiver and supports a whole solution for IEEE 802.15.4/ZigBee. In addition, a free Z-Stack protocol from Texas Instruments which conforms to ZigBee Alliance standards can be used with the CC2530, other profiles like RF4CE and SimpliciTI can also be implemented on it.

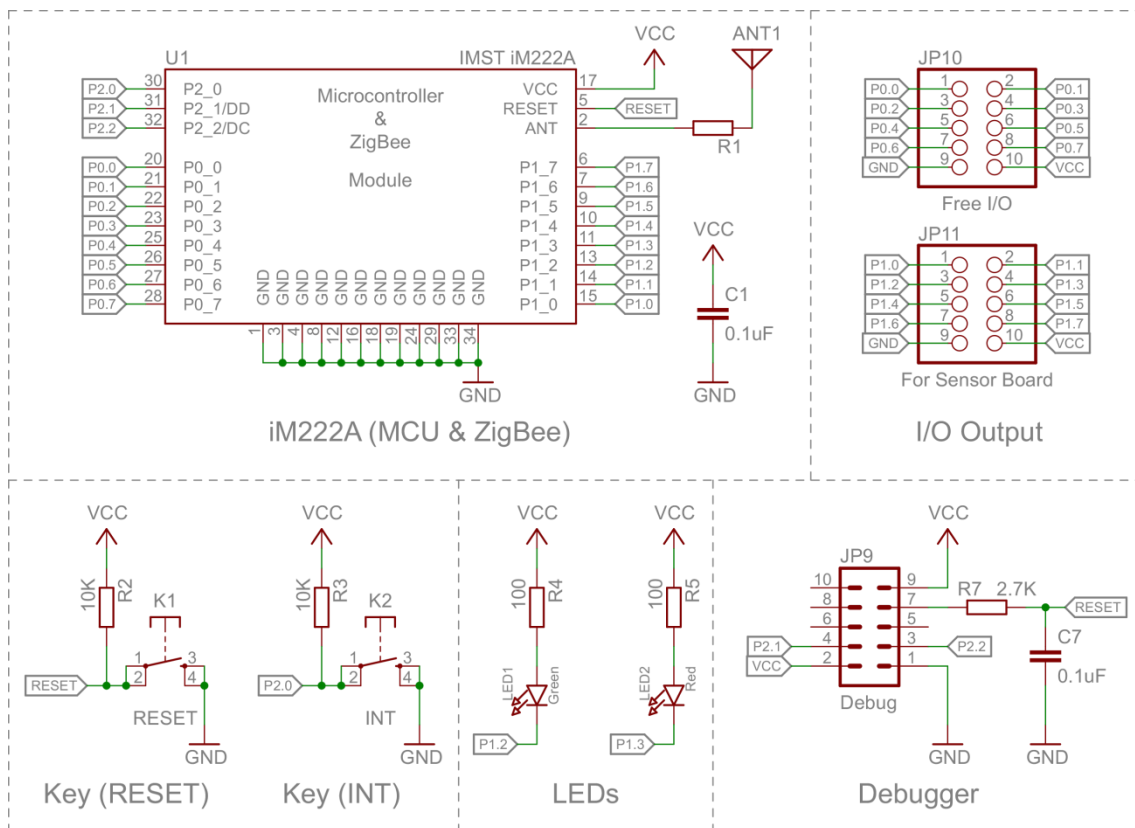


Figure 4-6 Schematic of the MCU & RF unit and its peripherals

Figure 4-6 illustrates the schematic of the MCU&RF unit and its peripherals. All the general-purpose I/O pins in P0 and P1 ports can be accessed from header JP10 and JP11, which provide an interface for the sensor board and voltage

detecting circuit of the storage capacitor. Two LEDs (Green, Red) and two keys (RESET, General-purpose) are designed for status indicating and user interaction.

A debugger interface for programming and debugging is integrated on board according to [44]. A minimum connection is occupied from the device, using only two debug signals Debug Data (DD) and Debug Clock (DC) and the reset signal RESET. The interface can also be used to power the target board by the debugger during testing as the pin 9 is connected to VCC.

4.1.2.2 A novel design of the synchronous voltage monitor circuit for storage capacitor

The MCU & RF unit is the core of the system, managing different units/modules in the system and carry out various operations in different modes. For instance, the microcontroller controls the sensors to collect data like acceleration and pressure, processes and transmits them to the central station through the wireless network by the radio transceiver. Meanwhile, all the tasks need to be handled smartly and the sleep mode is entered timely for power saving. Thus, how much energy has been generated and stored needs to be known for the periodic task scheduling. The energy stored on a capacitor is given by (4-2):

$$E = \frac{1}{2}CV^2 \quad (4-2)$$

Where C is the capacitance in Farads and V is the voltage on the capacitor.

To achieve the above scheduling purpose, the voltage on the storage capacitor needs to be measured by the use of ADC. The ADC integrated in the CC2530 supports eight individual input channels with selectable decimation rates which offer an effective resolution of up to 12 bits. The reference voltage for ADC conversions is selectable as any of an internal voltage, an external single-ended / differential voltage, or the AVDD5 (VDD) pin.

The accuracy of the conversion results depend on the stability and noise properties of the reference voltage. An internally reference voltage provided by CC2530, 1.15 V, with a VDD coefficient of 0.4mV/V, is selected as a stable reference for the ADC operation.

For a successful measurement, the input voltage cannot exceed the reference voltage (1.15V) otherwise an overflow error will be resulted. Meanwhile, the voltage applied to the ADC pins cannot be higher than VDD (3.3V, VDD is voltage on AVDD5 pin) to prevent damage to the chip. However, the voltage on the storage capacitor is range from 2.7 V to 20 V, which is much higher than the reference voltage and VDD. For a correct and safe conversion, a voltage divider circuit is used.

As shown in Figure 4-7(a), the voltage divider is a linear circuit which produces an output voltage (V_{OUT}) a fraction of its input voltage (V_{IN}).

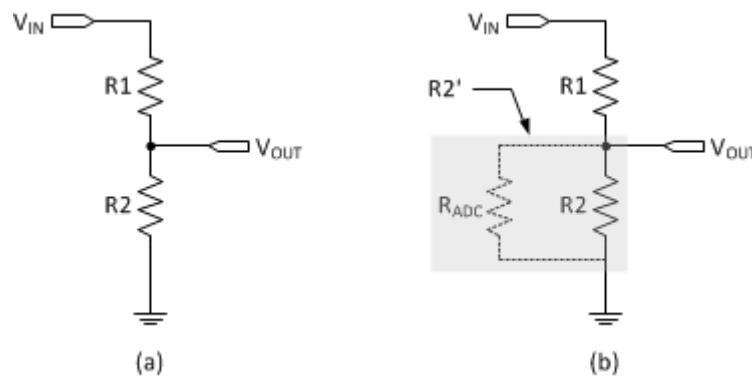


Figure 4-7 Schematic of the voltage divider without (a) / with (b) ADC input impedance

According to the Ohm's Law in equation (4-3), where I (A) is the current through the conductor, U (V) is the potential difference measured across the conductor, and R (Ω) is the resistance of the conductor.

$$I = \frac{U}{R} \tag{4-3}$$

The divided output voltage (V_{OUT}) in Figure 4-7(a) is given by (4-4):

$$V_{OUT} = \frac{R2}{R1 + R2} \times V_{IN} \quad (4-4)$$

Where V_{IN} is the input voltage, $R1$ is the resistor closest to V_{IN} , $R2$ is the resistor closest to ground, and V_{OUT} is the voltage drop across $R2$.

One notable point to mention is that the ADC input is a switched capacitance stage which draws current during the conversion. From [45], the input impedance (R_{ADC}) found in a typical device is 176 K Ω , thus the equivalent divider resistor $R2$ in Figure 4-7(a) during the ADC conversion is the total of $R2$ and R_{ADC} in parallel, which is shown in Figure 4-7(b) as $R2'$. $R2'$ is given by the parallel resistor equation:

$$R2' = \frac{R2 \times R_{ADC}}{R2 + R_{ADC}} \quad (4-5)$$

Therefore, the divided output voltage during the ADC conversion is:

$$V_{OUT} = \frac{R2}{R1 + \frac{R2 \times R_{ADC}}{R2 + R_{ADC}}} \times V_{IN} \quad (4-6)$$

The divider resistors ($R1$, $R2$) consume current all the time, a larger resistor should be chosen for a smaller current consumption as current expresses a reciprocal relationship to resistor in equation (4-3).

Considering of the magnitude of R_{ADC} (176 K Ω), a commercial available resistor 9.6 K Ω for $R2$ is chosen to minimize the effect of the ADC input impedance during the conversion. Thus another commercial available resistor 165 K Ω for $R1$ is selected by the use of equation (4-6).

In accordance with equation (4-3), the current costed by $R1$ and $R2$, for instance, when $V_{IN}=10V$, is 57.4 μA . It is a big consumption compared with the input quiescent current (450nA / 950nA) of LTC3588-1 and the consumption

increases as the voltage increases. As the divider resistors dissipate lots of energy in the input, as a consequence, reducing the power for the following units in the output.

A novel synchronous energy saving interface (ESI) is designed to fill the gap and eliminate the unwanted waste. The energy saving concept is illustrated in Figure 4-8: the ESI (presented in rectangle with red dotted border) establishes a bridge between the voltage divider and the storage capacitor.

Two MOSFETs are used to act like smart switches together with the control signal EN_{ADC} . During the operation of the ADC conversion, a high logic level from the MCU is given on EN_{ADC} , turning on Q2 and then Q1, consequently connecting the voltage divider circuit with V_{IN} on the storage capacitor. As soon as the conversion is completed, a low logic level is given on EN_{ADC} , which turns off Q2 and Q1, accordingly disconnects the voltage divider from the V_{IN} .

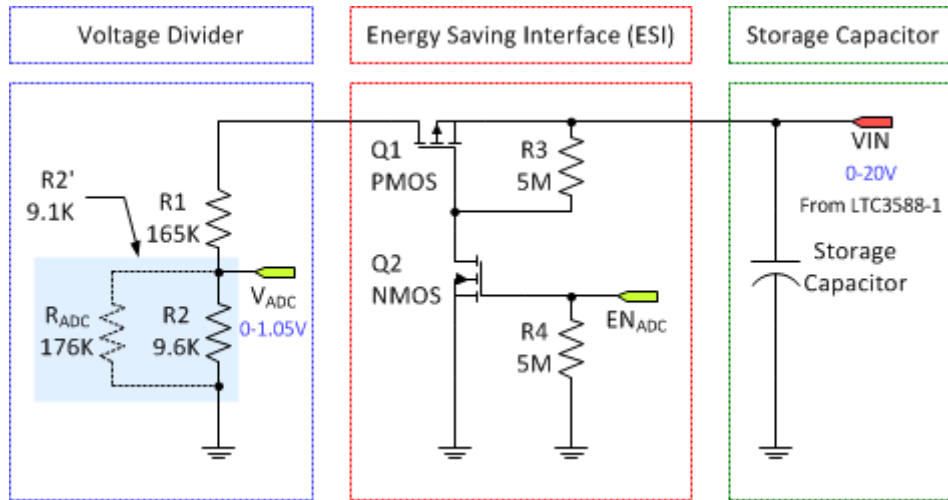


Figure 4-8 Schematic of the storage capacitor voltage monitor

The time of the ADC conversion is given by the equation from [45]:

$$T_{CONV} = (R_{ADC} + 16) \times \frac{1}{F_{ADC}} \quad (4-7)$$

Where R_{ADC} is the selected decimation rate and F_{ADC} is the ADC sampling frequency.

It should be noted that only the 32 MHz external high-frequency oscillator can be used during the ADC as well as no system clock division should be implemented. The actual F_{ADC} for ADC sampling is 4 MHz, internally generated by CC2530. The time T_{CONV} needed to perform an ADC conversion is 132 μ S with a decimation rate of 512 (12 bits ENOB setting) by the formula (4-7).

As a result, the current dissipated on the voltage divider circuit and ESI will only last for T_{CONV} during the conversion. After that, the power consumed on these circuits is quite small and relatively negligible.

An analysis about the performance of voltage monitoring circuit with/without the ESI will be given from the simulation results in section 4.2.2.2.

4.1.3 Sensors unit

A sensor board is developed to collect data from the environment and interface with the microcontroller via the port-1 pins (through JP11) in Figure 4-6.

This unit integrates three ultra-low power MEMS-based sensors, ST LIS2DH ($\pm 2g/\pm 4g/\pm 8g/\pm 16g$ full-scale 3-axis digital accelerometer), ST LPS25H (260-1260 hPa absolute digital barometer / pressure sensor), and TI HDC1000 (high accuracy digital temperature and humidity sensor).

All the sensors are designed to communicate with the microcontroller through the I²C interface to reduce wiring and simplify the circuit design. As there is no I²C hardware module provided in CC2530, the I²C communication will be implemented through two general purpose I/O pins in the software level.

In addition, pull-up resistors are needed to connect SCL and SDA line to VCC, as the pull-up resistors pull the line high when it is not driven low by the open-drain interface.

4.1.3.1 Vibration Sensor (3-axis Accelerometer) Circuit Design

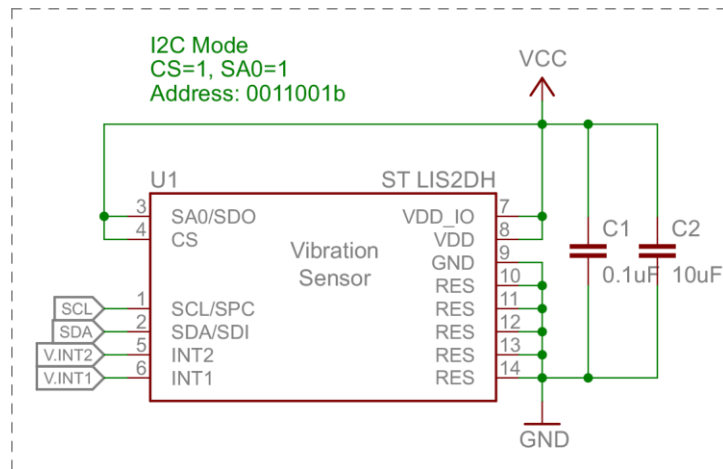


Figure 4-9 Schematic of the vibration sensor (ST LIS2DH)

Figure 4-9 shows the schematic diagram of the vibration sensor based on LIS2DH. By connecting pin4 (CS) to a high logic level, the I²C mode is enabled for LIS2DH. As the slave address associated to the LIS2DH is 001100xb, the less significant bit (LAB) is determined by pin3 (SA0/SDO). Thus the address is set as 0011001b by connecting pin3 to VCC.

Two decoupling capacitors C1 (0.1 µF) and C2 (10 µF) are placed between the VCC and ground to reduce the noise from other circuit elements according to [40]. All the unused pins (pin10 to pin14) are connected to ground.

The description and function of each pin in Figure 4-9 is listed in Table 4-2.

Table 4-2 Pinout of LIS2DH used in I²C mode

Pin	Name	Description / Function
1	SCL	I ² C serial clock
2	SDA	I ² C serial data
3	SA0	I ² C less significant bit of the device address
4	CS	I ² C mode selection: 0 Disabled, 1 Enabled
5	INT2	Interrupt pin 2
6	INT1	Interrupt pin 1
7	VDD_IO	I/O pins Supply Voltage
8	VDD	Supply Voltage
9	GND	Ground
10-14	RES	Reserved pins, connect to Ground

4.1.3.2 Pressure/Altitude Sensor Circuit Design

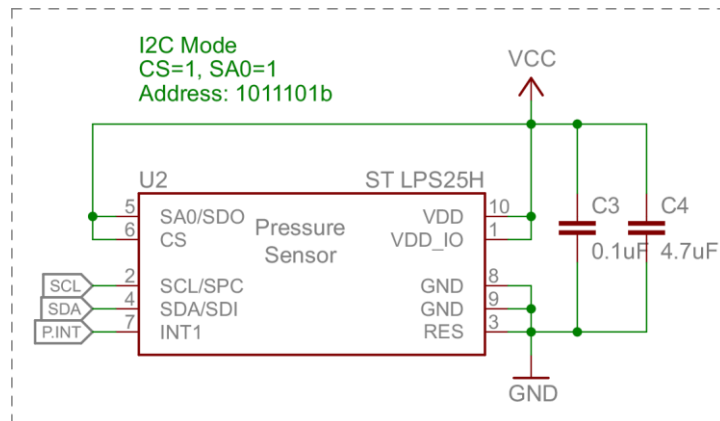


Figure 4-10 Schematic of the pressure sensor (ST LPS25H)

Figure 4-10 depicts the electrical connection of LIS2DH. The routing design is similar to LIS2DH, pin5 (SA0/SDO) and pin6 (CS) are connected to VCC, making LPS25H work in I²C mode with an address of 1011101b. C3 (0.1 μ F) and C4 (4.7 μ F) are worked as decoupling capacitors in accordance with the recommendation in [41]. Pin3 (RES) is connected to ground with pin8 and pin9.

Table 4-3 shows the pin description of LPS25H when it works in I²C mode.

Table 4-3 Pin description of the LPS25H used in I²C mode

Pin	Name	Description / Function
1	VDD_IO	I/O pins Supply Voltage
2	SCL	I ² C serial clock
3	RES	Reserved pin, connect to Ground
4	SDA	I ² C serial data
5	SA0	I ² C less significant bit of the device address
6	CS	I ² C mode selection: 0 Disabled, 1 Enabled
7	INT1	Interrupt 1 (data ready)
8-9	GND	Ground
10	VDD	Supply Voltage

4.1.3.3 Temperature and Humidity Sensor Circuit Design

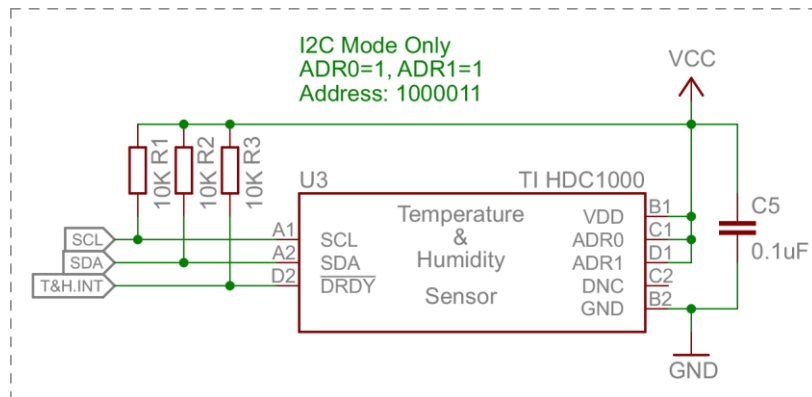


Figure 4-11 Schematic of the temperature and humidity sensor (TI HDC1000)

The schematic for the temperature and humidity sensor HDC1000 is presented in Figure 4-11. All the pins (SCL, SDA, and $\overline{\text{DRDY}}$) for data transmission require a pull-up resistor to VDD to restore the signal to high when no device is asserting it low.

The HDC1000 can only be operated in I²C mode. ADR0 and ADR1 are set to high logic level, as a result, a 7-bit address (1000011) is assigned to HDC1000 for communication from [42]. A bypass capacitor C5 is also connected between VCC and GND.

The pin description for HDC1000 used in Figure 4-11 is given in Table 4-4.

Table 4-4 Pin description of the HDC1000

Pin	Name	Description / Function
A1	SCL	I ² C serial clock
A2	SDA	I ² C serial data
B1	VDD	Supply Voltage
B2	GND	Ground
C1	ADR0	Address select pin
C2	DNC	Reserved pin, connect to Ground
D1	ADR1	Address select pin
D2	$\overline{\text{DRDY}}$	Data ready

4.2 Simulation & results analysis

To validate the hardware design and evaluate the performance of the system, simulations are usually carried out in EDA software before manufacturing. Simulating the circuit with EDA software such as the SPICE is also the industry-standard way to verify circuit design and predict circuit performance before final fabrication, as it computes the full large signal behaviour of the circuit.

A stable, fast, and free SPICE simulator, LTspice IV from Linear Technology, is used as the SPICE implementation in this project. It's a high performance simulator which widely used in analog circuit simulation. It supports unlimited number of nodes and provides a rich library which including the LTC3588-1 power management IC used in this project.

The behaviours of the power management unit and the microcontroller & RF unit are both simulated to study the overall performance of the system.

4.2.1 Modelling in LTspice

As depicted in Figure 4-12, a simulation model is built by the schematic capture in LTspice in terms of the circuit designed in section 4.1.

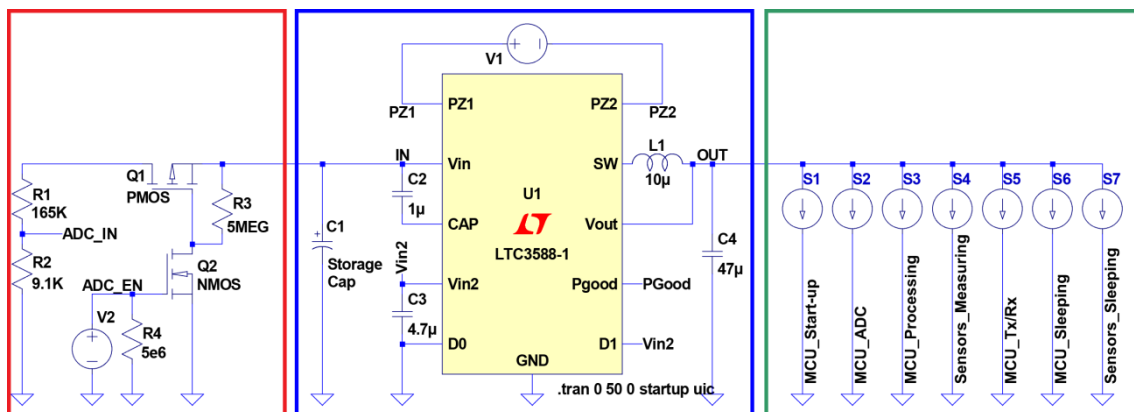


Figure 4-12 Schematic of the simulation circuit in LTspice IV

The circuit in the left red rectangle simulates the voltage measurement circuit for the storage capacitor. The net ADC_IN is the output from the voltage divider

which represents the proportion of the voltage on the storage capacitor, and the net ADC_EN is the command from P0.1 of CC2530 to trigger the ADC conversion only when needed for power saving. The middle circuit in blue rectangle simulates the behaviours of the vibration energy harvesting and power management circuit together with the storage capacitor. The last circuit in green rectangle simulates the operations of the MCU in different scenarios (start-up, normal processing, and sleeping), the wireless transmission of the RF module, and the sensor board.

Table 4-5 lists the main models used in Figure 4-12. An independent voltage source (V1) with a sine wave is used as the vibration energy harvester, and another voltage source (V2) with a pulse wave simulates the behaviour of the control signal from the microcontroller. Seven current sources (S1 to S7) with pulse wave represent the current consumption of the loads (MCU, RF, and Sensors) in various scenarios.

Table 4-5 Description of the models used in Figure 4-12

Name	Component	Function	Behaviour Description
V1	Voltage Source	Sine wave	Piezoelectric energy harvester
V2	Voltage Source	Pulse	Control signal of the ADC enable command
U1	LTC3588-1	Power Supply	Piezoelectric Energy Harvesting Power Supply
S1	Current Source	Pulse	Operations of the MCU during start-up
S2	Current Source	Pulse	Operations of the MCU during ADC conversion
S3	Current Source	Pulse	Operations of the MCU during normal processing
S4	Current Source	Pulse	Operations of the sensors during measuring
S5	Current Source	Pulse	Operations of the RF unit during Tx/Rx
S6	Current Source	Pulse	Operations of the MCU during sleeping
S7	Current Source	Pulse	Operations of the sensors during sleeping

As mentioned in section 3.1 before, the energy scavenged from the environment by the harvester can't power the WSN node continuously, a

compromised solution is to use a storage capacitor as a buffer, and any extra energy from the harvester is reserved in the buffer.

The energy stored on a capacitor is determined by both the capacitance of the capacitor and the voltage across the capacitor according to the aforementioned formula described in (4-2), thus a larger capacitor or a higher charge voltage (V_{IN}) is needed to get more power for the loads.

To carry out a successful operation, the energy stored in the capacitor (E_{Store}) should meet the power requirements (P_{LOAD}) of the output for the desired duration (T_{LOAD}). And consider the losses in the LTC3588-1 during conversion, the equation (4-2) can be transformed to equation (4-8) after the efficiency (η) of the power management circuit was taken into account.

$$E_{Store} = P_{LOAD} T_{LOAD} = \frac{1}{2} \eta C_{StorageCap} (V_{StorageCap}^2 - V_{UVLOFALLING}^2) \quad (4-8)$$

Where η is the efficiency of the buck converter in LTC3588-1, $V_{StorageCap}$ is the voltage across the storage capacitor before reserved energy delivered to the load, $V_{UVLOFALLING}$ is UVLO (under-voltage lockout) falling threshold voltage for a select regulated output, and as a shunt diode ($V_{SHUNT}=20\text{ V}$) is used in LTC3588-1 to clamp the input voltage, the $V_{StorageCap}$ should meet the requirements in (4-9):

$$V_{UVLOFALLING} \leq V_{StorageCap} \leq V_{SHUNT} \quad (4-9)$$

As a $10\ \mu\text{H}$ inductor is used in Figure 4-5 and the output voltage (V_{Out}) is set to be 3.3V by configuring $D1=1/D0=0$ to supply the components like the MCU and sensors, the efficiency η in (4-8) is approximate 80% according to Figure 3-11 and a typical $V_{UVLOFALLING}$ is 3.67V following the guidelines of the LTC3588-1 datasheet [37].

To size the input storage capacitor by use of the equation (4-8), how much power needed on the load (P_{LOAD}) and the length of time (T_{LOAD}) should be studied. As discussed before, all the load components enter a sleeping mode during the charging of the storage capacitor for power saving, namely, a typical cycle in this application consists of two modes, active mode and sleeping mode. Thus the energy stored on the storage capacitor should equal or exceed the sum of the demands from all the electrical components in the loads like MCU and sensors at different stages of a cycle.

During the active mode, the main power consumption includes the operations like MCU controlling, ADC converting, sensors measuring, data processing, and RF transmitting. The total current consumption in active mode ($I_{ActiveMode}$) is:

$$I_{ActiveMode} = I_{MCUProcessing} + I_{MCUADC} + I_{MCUTx/RX} + I_{SensorsMeasuring} \quad (4-10)$$

And the energy needed in the sleeping mode ($I_{SleepingMode}$) is the energy consumed to make all the components in the WSN node on standby with the lowest current consumption:

$$I_{SleepingMode} = I_{MCUSleeping} + I_{SensorsSleeping} \quad (4-11)$$

Accordingly, the total power consumption of the load during one cycle is the sum of the energy consumed in both sleeping mode and active mode with different operations:

$$I_{Load} = I_{ActiveMode} + I_{SleepingMode} \quad (4-12)$$

In addition, attention should be paid to the initialization at start-up as this operation repeats only once but lasts a long time with a moderate current consumption.

An approximate estimation of the current consumption and the duration in different operations is summarized in Table 4-6 in terms of the electrical characteristics described in [39][40][41][42][45], and seven pulse loads (S1 to S7) are used to simulate the behaviours of the MCU and sensors in different modes.

Table 4-6 Current consumption and length of time in different operations during a cycle for simulation

Operation	Current Consumption	Duration	LTspice Model
MCU Start-up	9 mA	400 ms	S1
MCU ADC	1.2 mA	140 μ s ⁽¹⁾	S2
MCU Processing	9 mA	6 ms	S3
Sensors Measuring	33 μ A ⁽²⁾	4 ms	S4
MCU Tx/Rx	35 mA ⁽³⁾	4 ms ⁽⁴⁾	S5
MCU Sleeping	2 μ A ⁽⁵⁾	990 ms	S6
Sensors Sleeping	1.5 μ A	990 ms	S7

(1) 512 decimation rate (12 bits ENOB setting) is set for ADC.

(2) LIS2DH @ ODR 50 Hz and low-power mode. LPS25H @ ODR 1 Hz and highest resolution. HDC1000 @ 1sps, 11 bit RH and Temperature Measurement

(3) $I_{TX}=33.5$ mA (4.5-dBm output power) and $I_{RX}=25$ mA (-100-dBm input power), 35 mA is used for conservative estimation.

(4) 20 bytes of data are transmitted for the estimation.

(5) MCU working in PM2, only 32.768 kHz XOSC and sleep timer are active.

Based on the parameters in Table 4-6, the detailed composition of the current consumption and the corresponding duration in a typical cycle, for instance, one second is illustrated in Figure 4-13. It is obvious that the wireless transmission consumes significantly high energy in one cycle.

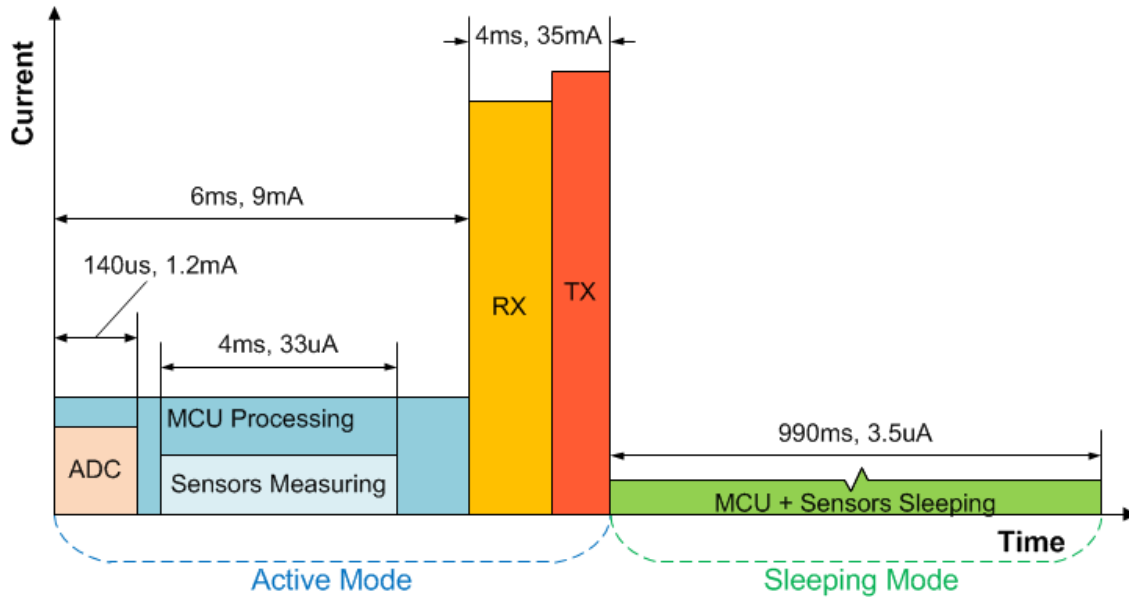


Figure 4-13 Current consumption and duration of various operations in one cycle

For the start-up operation, the energy ($E_{\text{Start-up}}$) needed is:

$$E_{\text{Start-up}} = P_{\text{Start-up}} * T_{\text{Start-up}} = V_{\text{Out}} * I_{\text{Start-up}} * T_{\text{Start-up}} = 11.88 \text{ mJ}$$

For the operations in a cycle, the energy (E_{OneCycle}) needed is the sum of the energy consumed in all the operations in Figure 4-13:

$$E_{\text{OneCycle}} = P_{\text{ActiveMode}} * T_{\text{ActiveMode}} + P_{\text{SleepingMode}} * T_{\text{SleepingMode}} = 0.6526 \text{ mJ}$$

The maximum voltage ($V_{\text{StorageCapMax}}$) on the input storage capacitor is 18V from the datasheet, and choose $E_{\text{Start-up}}$ to get the minimum limit for the storage capacitor which is defined by (4-13) according to equation (4-8):

$$C_{\text{StorageCapMin}} = \frac{P_{\text{LOAD}} T_{\text{LOAD}}}{\frac{1}{2} \eta (V_{\text{StorageCapMax}}^2 - V_{\text{UVLOFALLING}}^2)} = 95.6 \text{ } \mu\text{F} \quad (4-13)$$

Thus, the value of the input storage capacitor should be greater than 95.6 μF to fulfil a successful operation. The commercially available capacitor with a rated voltage (VDC) which can withstand the highest voltage (20 V) ever present at V_{IN} is a 100 μF tantalum capacitor with the VDC of 25 V. As the capacitors can be connected in parallel to double the capacitance, five values are used for simulation to get the best selection of capacitor. Table 4-7 lists the results of the

minimum voltage across the storage capacitor to carry out successful operations. For convenience, the harvester is simulated to work at the frequency of 40Hz with amplitude of 0.5g for this calculation.

Table 4-7 Minimum voltage across the storage capacitor to carry out successful operations

Capacity (μF)	Minimum Voltage for Start-up (V)	Minimum Voltage for one cycle (V)
100	16.53	5.45
200	11.98	4.65
300	10.01	4.35
400	8.86	4.19
500	8.09	4.09

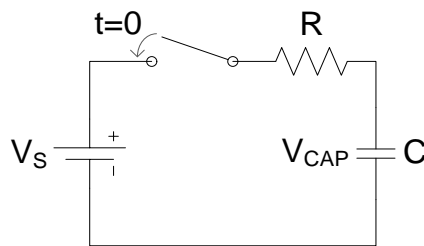


Figure 4-14 A typical RC charging circuit

Another important thing need to be considered is the charging time. The above Figure 4-14 shows a typical RC charge circuit, when a power supply (V_S) is connected to a series resistor(R) and capacitor(C), current begins to flow into the capacitor after the switch is closed at $t = 0$. As the capacitor charges up, the voltage (V_{CAP}) across the capacitor keeps increasing from zero, and its value will be equal to:

$$V_{CAP} = V_S \times (1 - e^{-t/RC}) \quad (4-14)$$

Where V_{CAP} is the voltage across the capacitor, V_S is the supply voltage, t is the time elapsed, and RC is the time constant of the RC charging circuit in Figure 4-14.

Solving for charging time (t):

$$t = RC \ln \frac{V_S}{V_S - V_{CAP}} \quad (4-15)$$

For a larger capacitor, it takes more time to reach the same V_{CAP} from the above equation.

Initially there is no energy reserved in the input storage capacitor and the voltage (V_{IN}) across it is zero. At the same time, the buck converter in the power management unit will not be enabled to transfer the energy from the input capacitor to the output until the voltage on V_{IN} rises above the UVLO rising threshold. As discussed above, a larger capacitor takes longer charging time, it is necessary to measure how long it would take for the storage capacitor to reach the threshold while charging.

A simulation of the circuit in blue rectangle in Figure 4-12 is carried out and Figure 4-15 shows the time history versus the voltage of five different storage capacitors (100 μ F, 200 μ F, 300 μ F, 400 μ F, and 500 μ F). These capacitors are charged by the piezoelectric harvester V25W (work at the frequency of 40 Hz with amplitude of 0.5 g) and managed by LTC3588-1, in addition, no loads are connected in the output.

The curves in Figure 4-15 indicate an exponential relationship between the time and the voltage across the storage capacitor. As the harvester starts to generate energy from the environment, the storage capacitor begins to reserve the energy and the voltage across it increases. As the voltage reaches the rising threshold of V_{UVLO} , the converter in LTC3588-1 is triggered and a selected DC voltage is outputted to the loads, the voltage on the storage capacitor also suffers a small drop at the same time. After that, the voltage keeps increasing to the maximum value of V_S as described in equation (4-14).

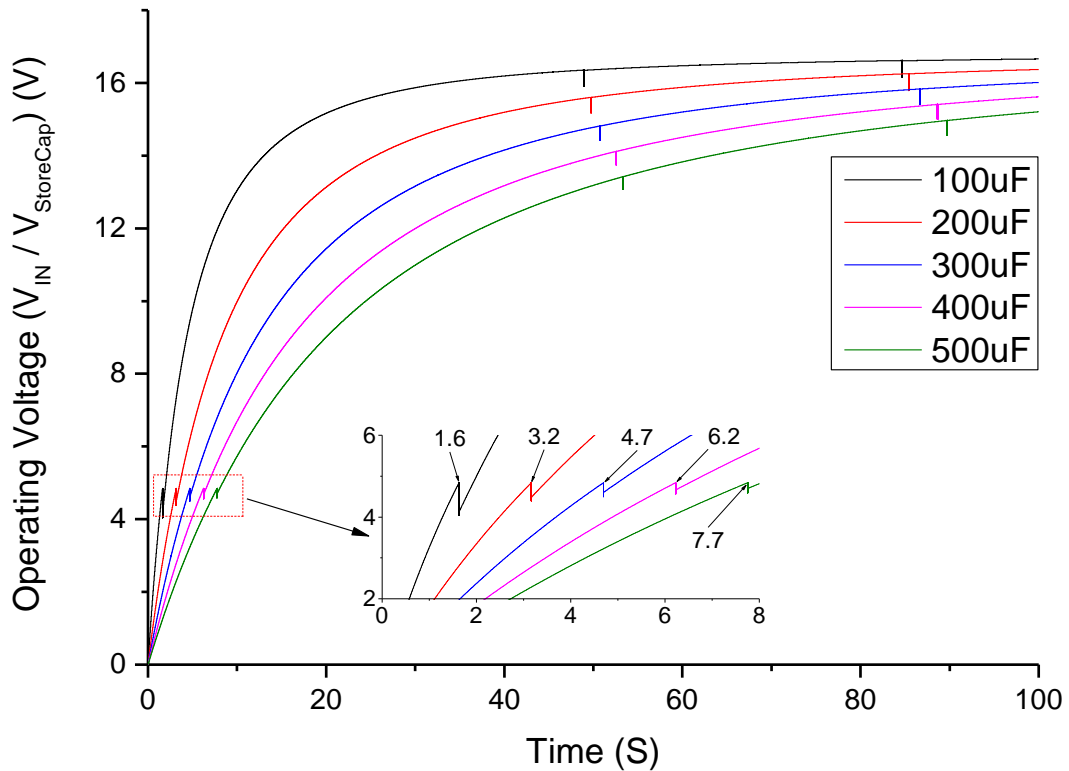


Figure 4-15 Time history versus the voltage of the input storage capacitors

The zoomed detail in Figure 4-15 shows the start-up time for different capacitors. As the charging time presents a proportional relationship to capacitance in equation (4-15), a larger capacitor will take a longer time to reach the same threshold. As presented in Figure 3-9, the harvester outputs a larger power at the same frequency with higher amplitude. For this reason, the charging time will increase as the amplitude decreases.

Figure 4-16 and Figure 4-17 illustrate the relationship of the start-up time between different levels of amplitude, different working frequencies, and different values of the input storage capacitor. As shown in Figure 4-17, a 2mF capacitor takes about 5 mins to provide a working voltage for the load while a 200uF one takes only 3 secs. 5 mins is quite a long time compared with the smaller ones although a 2mF capacitor can store much more energy.

Based on the discussion above, the input storage capacitor is chosen to be 200 μ F (two 100 μ F in parallel) for this application.

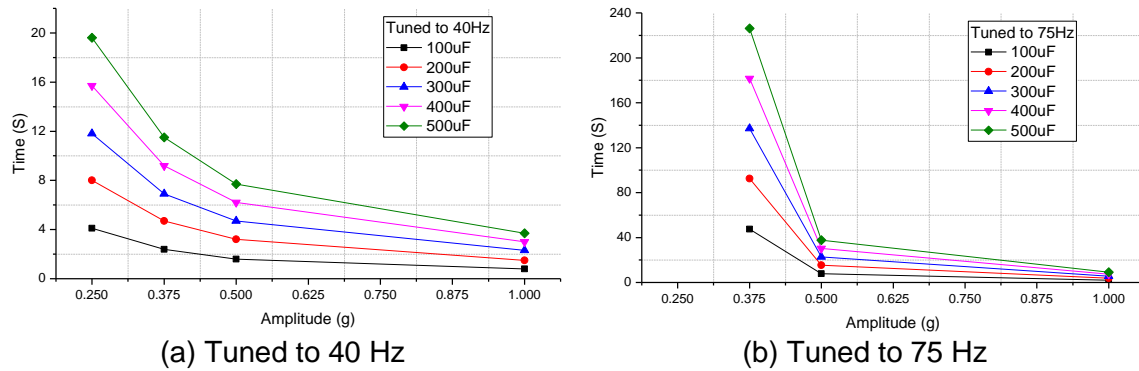


Figure 4-16 Start-up time vs. amplitude for different capacitors

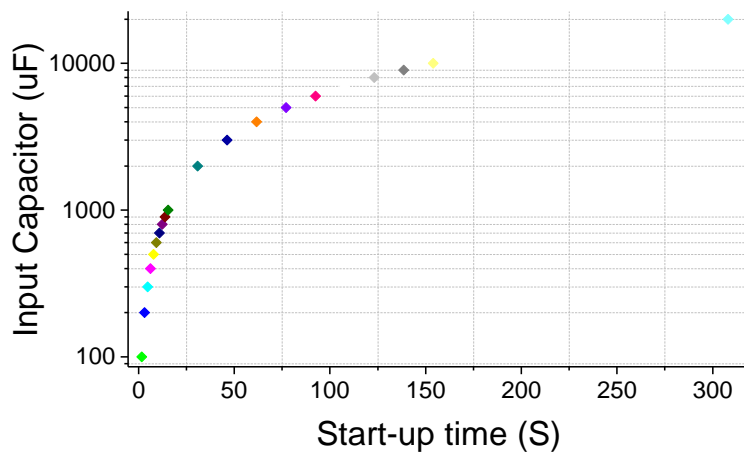


Figure 4-17 Start-up time vs. different input capacitors (40 Hz and 0.5 g)

4.2.2 Simulation results and analysis

To study the performance of the circuit designed in 4.1, the model in Figure 4-12 is simulated with the behaviours of both the power management unit and the microcontroller & RF unit. In a realistic situation, the frequency of the dominant vibration depends on the operating parameters of the equipment causing the vibration, and the harvester will output different power and voltage as the vibration changes. As the peak output power of the harvester is about 9.2 mW according to [36], for convenience here, it is set to work at the resonant frequency of 40 Hz with the amplitude of 0.5 g and output a maximum power of 2.94 mW in the simulation.

4.2.2.1 Output power vs. Operating voltage

A simulation of the circuit in blue rectangle in Figure 4-12 is carried out and Figure 4-18 below shows the instantaneous output power from the harvester and the voltage across the input store capacitor (V_{IN}) versus time for a representative vibration level and frequency mentioned above.

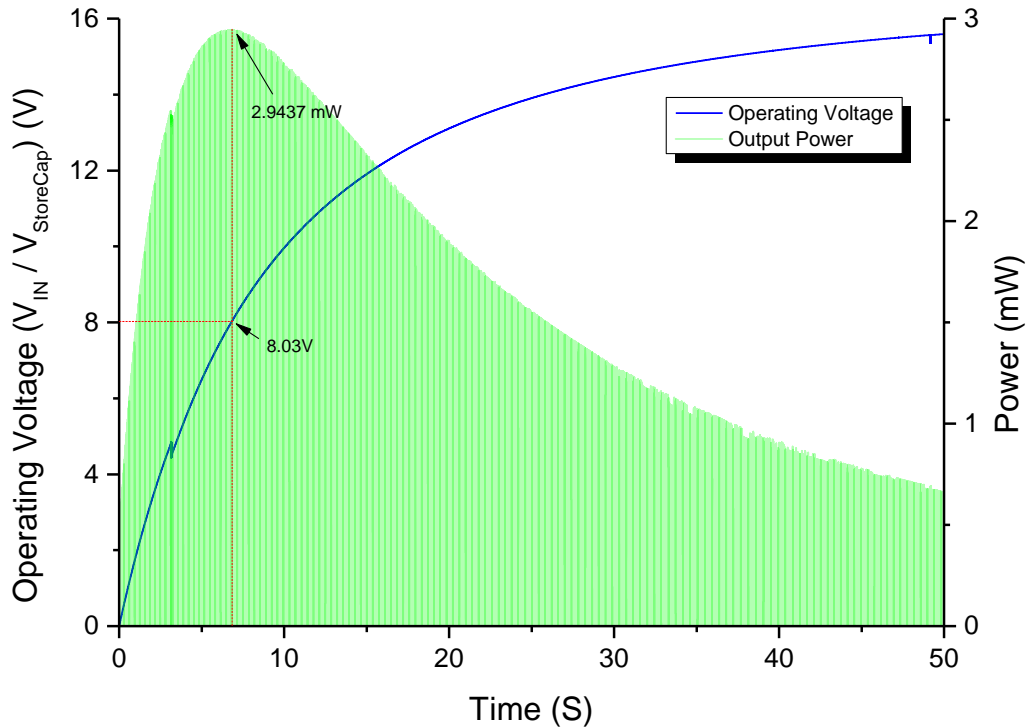


Figure 4-18 Output Power & Operating Voltage vs. Time

The shadowed area illustrates that the output power keeps a sharp increase at the beginning, peaks at about 2.94 mW, from then on, there is a gradual reduction in the power while the voltage increases steadily.

The operating voltage (V_{IN}) is approximate 8V while the power reaches the top point, as the total drop of the internal bridge rectifier is around 800 mV (with a 300 μ A piezo generated current) from the datasheet, the operating voltage of the harvester V25W is about 8.8V, which is about half the open circuit value, demonstrating that to get a maximum output power, the harvester should be set to work at half of its open circuit voltage.

4.2.2.2 Performance of the voltage monitor circuit for storage capacitor

As mentioned in 4.1.2.2, a novel energy saving interface (ESI) is designed to connect the voltage divider circuit with the storage capacitor in Figure 4-8. To evaluate the performance of the design, two circuits are simulated for comparison. Figure 4-19 and Figure 4-20 illustrate the time history of the voltage across the storage capacitor and the voltage measured by the divider circuit without and with the ESI respectively.

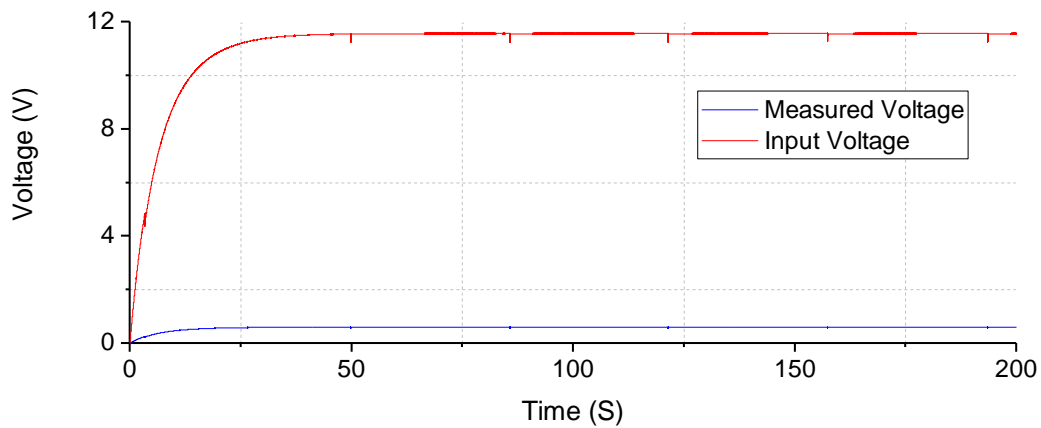


Figure 4-19 Time history of Input Voltage (V_{IN}) and Measured Voltage from the Divider Circuit without the ESI

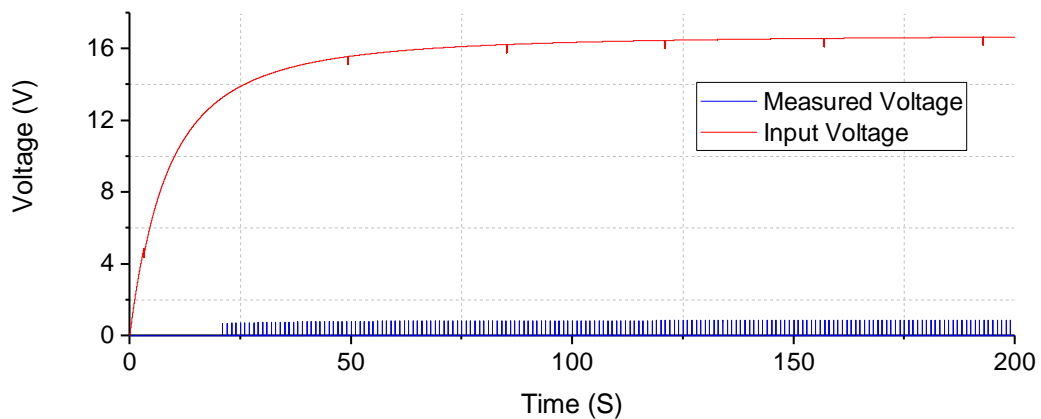


Figure 4-20 Time history of Input Voltage (V_{IN}) and Measured Voltage from the Divider Circuit with the ESI

As can be seen from the Figure 4-19, the input voltage sharply went up to 10 V at the beginning, but the rate of the growth slowed down subsequently until it reached 11.5 V. Finally, it stopped growing and remained stable. The reason

behind this is that the circuit without the ESI measures the input voltage all the time, the dissipation on the divider resistors keeps increasing as the input voltage grows. When the input voltage reaches 11.5 V, the dissipation is almost equal to the output power of the harvester. Consequently, no energy will be stored on the input capacitor and the voltage across it stops rising.

One major drawback of the circuit without ESI is the input voltage will never reach the minimum value (in Table 4-7) to implement the initialization of the system. On the contrary, with the use of ESI, the dissipation on the measurement circuit only exists during the ADC conversion with duration of 140 μ S in a one cycle. Accordingly, the input voltage can keep increasing and energy is reserved on the capacitor for later delivery.

Table 4-8 provides the average power and total energy outputted by the harvester in different circuits in a 200 secs simulation and Table 4-9 gives the corresponding consumption on the components used in the voltage measurement circuits.

Table 4-8 Average output power and total output energy of the harvester used in the ADC circuit with/without ESI within the first 200S

Without ESI		With ESI	
Average Output Power	Total Output Energy	Average Output Power	Total Output Energy
826.14 μ W	165.23mJ	149.39 μ W	29.877mJ

Table 4-9 Average power dissipation and total energy consumption of the ADC circuit with/without ESI within the first 200S

Without ESI			With ESI		
Component	Average Power	Energy Consumption	Component	Average Power	Energy Consumption
R1	689.78 μ W	137.96mJ	R1	173.19nW	34.639 μ J
R2	38.042 μ W	7.6085mJ	R2	9.5519nW	1.9104 μ J
			R3	6.5511nW	1.3102 μ J

			R4	274.2pW	54.841nJ
			Q1	3.9408nW	788.15nJ
			Q2	512.87pW	102.57nJ
Total	727.82μW	145.57mJ		194.02nW	38.81μJ

A comparison of the loss ratio between the voltage measurement circuits with/without ESI is presented in Table 4-10. The ADC circuit without ESI consumes a large portion (88%) of the energy generated by the harvester while the consumption on the circuit with ESI is relatively negligible.

Table 4-10 Comparison of the loss ratio of the ADC circuit with/without ESI within the first 200S

Without ESI	With ESI
Loss ratio	Loss ratio
88.1%	0.13%

4.2.2.3 Input voltage (voltage across the store capacitor), output voltage, current consumption of the loads vs. Time

Figure 4-21 depicts the different behaviours of both the power management unit and the loads in the first 50 secs after the harvester starts working.

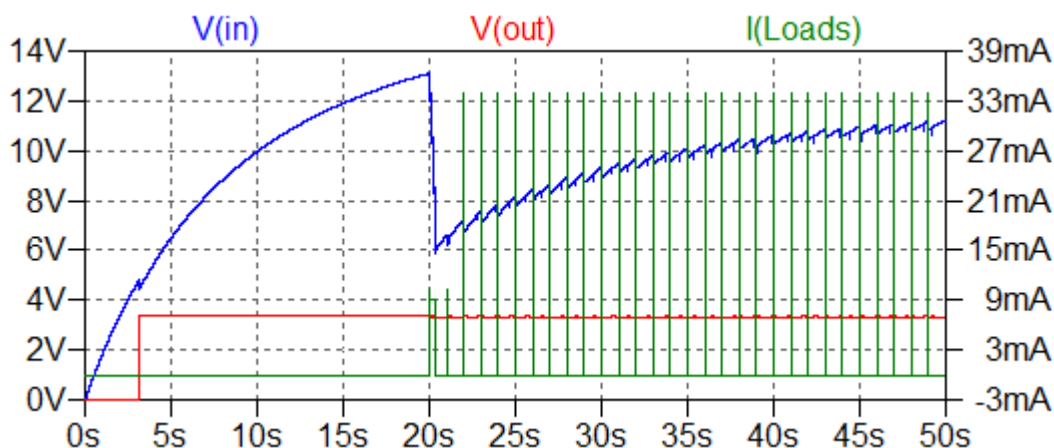


Figure 4-21 Input / output voltage and current consumption of the loads vs. time

The blue curve describes the trend of the input voltage V_{IN} (voltage across the store capacitor) while the red line shows the corresponding output voltage respectively. Another green curve presents the representative current consumption of the loads in different operations.

As is shown in the picture, the input voltage keeps rising steadily until it reaches the rising threshold of the V_{UVLO} (4.8 V) after 3.2 secs from the start, then it suffers a slight drop as the converter is triggered to output a DC voltage of around 3.3 V at the same time. From this time onwards, the input voltage remains growing to 13.1 V after about 17 secs while the output voltage maintains a constant value of 3.3 V for the loads.

The initialization of the system is performed after 20 secs from the beginning when the voltage on the capacitor exceeds the threshold (11.98 V in Table 4-7). Lots of energy stored in the capacitor will be transferred to this burst operation, therefore the input voltage experiences a considerable decrease from 13.1 V to 5.9 V during the operation which lasts 400 msecs.

After completion of the initialization, the input voltage restores itself to a steady upward trend and undergoes small fluctuations in every cycle.

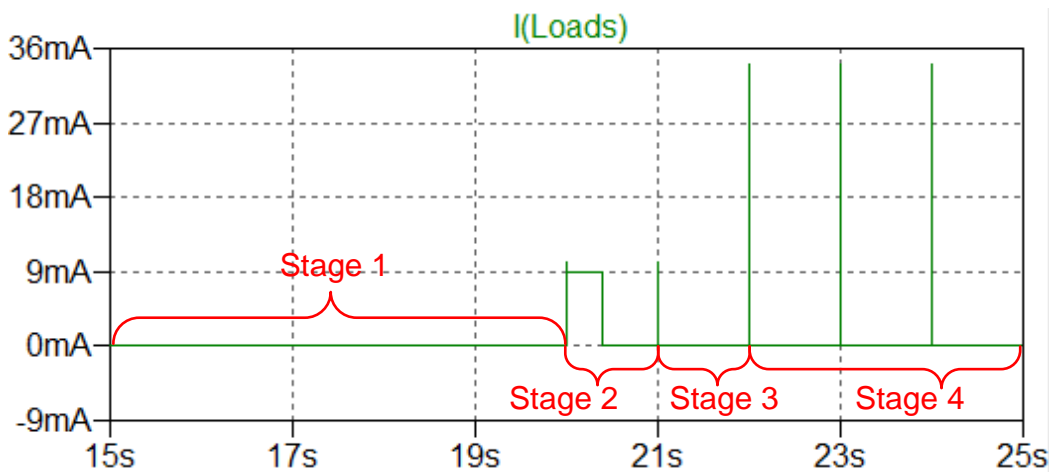


Figure 4-22 Zoomed detail of the current consumption

Figure 4-22 illustrates the zoomed detail of the current consumption in Figure 4-21, exhibiting the behaviours of the loads. Based on the analysis in 4.2.1, all

the items can be classified into four stages: deep sleep, initialization, one-cycle stage without RF transmission, and one-cycle stage with RF transmission.

Deep sleep (Stage 1): As soon as the power management unit starts to output a regulated DC voltage, the loads (MCU and sensors) are powered on but forced to enter a sleep mode at once as there is not enough energy to implement the initialize tasks.

Initialization (Stage 2): As there is enough energy to carry out the initial operations, the MCU performs initialization and other setup tasks for both the operating system and the hardware, after that, it enters the sleep mode right away to accumulate more energy for the next cycle.

One-cycle stage without RF transmission (Stage 3): In this stage, the MCU triggers the ADC conversion to measure the voltage on the capacitor after wake-up. As the results do not meet the requirement to fulfil the wireless transmission after comparison, the system resumes sleeping for the next cycle.

One-cycle stage with RF transmission (Stage 4): In contrast, the input voltage exceeds the threshold, indicating that there is enough energy reserved for the burst RF transmitting operation. The MCU controls the sensors to acquire data and transmits them to the base station after processing. After all the tasks have been completed, all the loads fall asleep immediately for power saving.

4.2.2.4 Conclusion of the simulation

The curve presented in Figure 4-18 reveals that the harvester used in this project outputs the maximum power when it operates at half the open circuit voltage. Measures can be taken in the software design to remain the harvester work around this value to achieve the best performance.

It is apparent from the figures and tables in 4.2.2.2 that the dissipation on the voltage measurement circuit is reduced to the lowest levels by the use of the ESI, making it possible for the power management unit to reserve more energy on the storage capacitor for the loads.

Most of the behaviours in an energy harvesting WSN system are simulated and as can be seen from the results in Figure 4-21 and Figure 4-22, with an excitation of 40 Hz frequency and 0.5 g acceleration on the harvester, the power management unit takes about 3 secs to power the system with a selected voltage (3.3 V) and another 17 secs to perform the initialization operations of the system. After the initialization, data are measured and transmitted wirelessly with a total energy consumption of 0.65 mJ in one cycle every 1 sec.

In brief, the results from the simulation demonstrate that the proposed system design in section 3.2 and section 4.1 is feasible and effective.

4.3 PCB layout & hardware assembly

To perform measurements in a lab environment and validate the simulation, prototypes are fabricated and assembled for the experimental tests. In this section, the design of the PCB layout and the assembly will be briefly introduced.

4.3.1 PCB layout design

The PCB design tool used for the prototype is EAGLE developed by CadSoft Computer. It is a worldwide EDA application with schematic capture editor, PCB layout editor, auto-router and CAM and BOM tools, offering a variety of product combinations and allowing every user to choose the configuration that meets their individual requirements.

The version of the software used is a light edition (freeware), the limitations are that only two signal layers (Top and Bottom) can be used and the maximum size of the PCB board is 100 x 80 mm. For the boards designed in this project, the light edition is sufficient.

A few considerations for PCB layout are reviewed in [46][47][48][49] to improve the reliability of the design.

Generally, all the components are placed properly on the top side and routed manually. The top layer is used for horizontal signal traces while the bottom layer used for vertical ones. The decoupling capacitors are placed as close as possible to the ICs. Polygons connected to GND are placed on both the top and bottom layer, these ground planes fill blank space on a PCB with copper, making routing easier and reducing electrical noise on the board. All the rules and constraints used in this design are listed in Table 4-11, and the procedure in Figure 4-23 is followed during the PCB layout design.

Table 4-11 Specifications and constraints used during the PCB design in EAGLE

Sizes		Clearance	
Trace width for normal signals	12 mil	Between different signals	6 mil
Trace width for power signals from the harvester	24 mil	Between drill holes	6 mil
Trace width for power supply signals for the loads	30 mil	To the edge of the board	15 mil
Minimum annular ring	7 mil		
Minimum drill / via	13 mil		

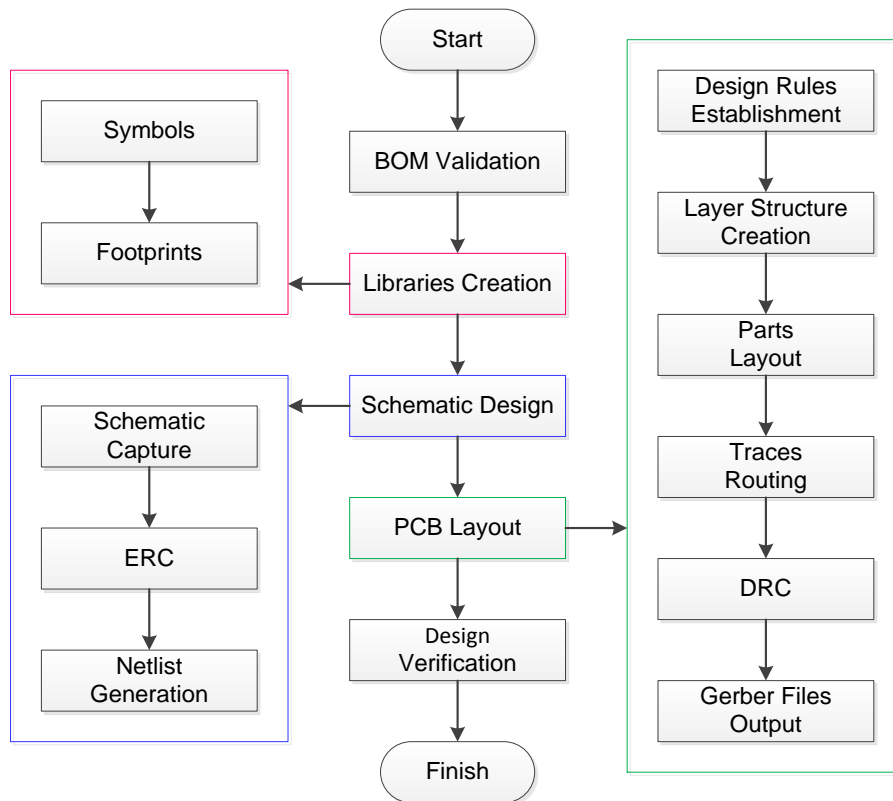


Figure 4-23 Procedure of the PCB design used in this project

Figure 4-24 presents the trace layout of the WSN system board designed in EAGLE 7.2, and the arrows indicate the direction of the signal current flow on the board is left-to-right.

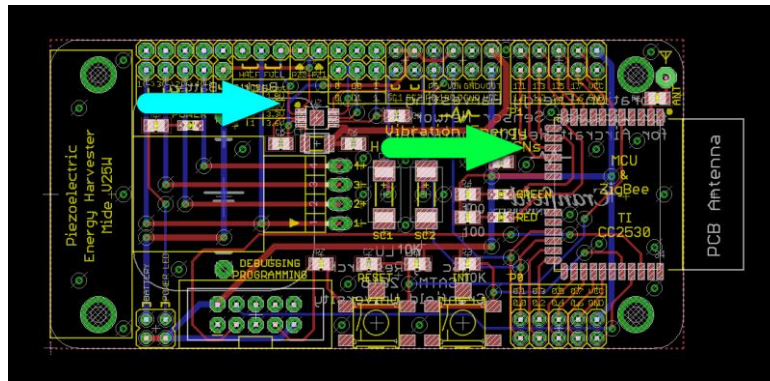


Figure 4-24 Trace layout of the WSN system board based on vibration energy harvesting

First of all, the current is generated by the harvester and input to the system from the left side. Next, as the turquoise blue arrow shows, the current flows to the power management unit for rectification and regulation. After that, it is delivered to the loads along the direction as the yellow green arrow indicates.

As the prototype board is used for experiments, all the signals like the raw output of the harvester, input and output signals of the power management unit, and GPIO pins of the MCU are accessible through header pins on the board for testing purposes. All the traces are hand routed and Figure 4-25 presents both sides of the final WSN system board. The dimension of this PCB board is 83.8 x 40.9 mm.

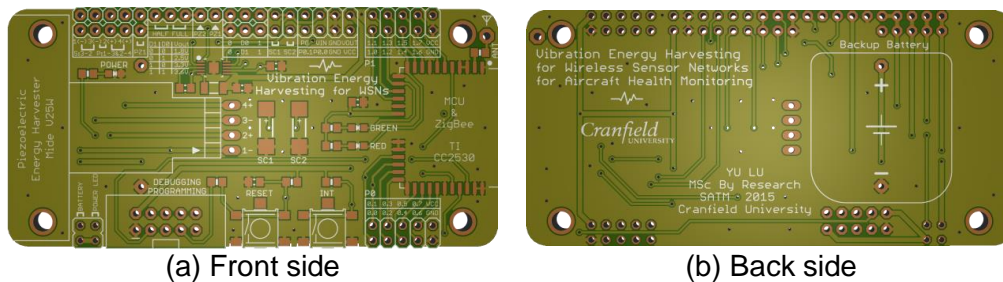


Figure 4-25 PCB board of the WSN system board based on vibration energy harvesting

To keep all the Port 0/Port 1 pins of the CC2530 out and accessible for future development, a standalone sensor board shown in Figure 4-26 is designed.

The sensor board integrates the accelerometer, barometer, and temperature & humidity sensor together. In addition, another 1.27mm pitch connector is

reserved to be compliant with the TE-CORE/RF (Thermo-Harvesting Wireless Sensor System) in our lab for further integration and future studying.

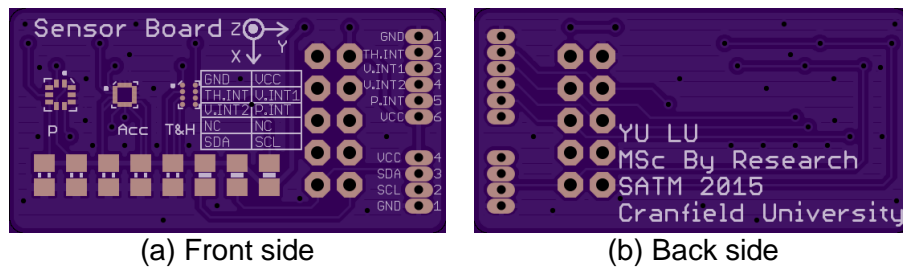


Figure 4-26 PCB board of the sensor board

Figure E-2 in Appendix E shows the PCB board of the voltage divider circuit with the ESI designed in Figure 4-8. The components used on this board are PTH ones for easy assembly and testing.

Figure F-1 in Appendix G presents different shapes of the clamps designed to mount the piezoelectric in a cantilevered configuration, taking advantage of resonant beam harvesting. As mentioned in [36], straight clamp is adequate for most of the applications and the performance of the harvester is slightly increased with the use of the curved one.

After the PCB layout work is finished, the DRC (Design Rules Check) is run to ensure no electrical and mechanical mistakes are made and Gerber files are generated for manufacturing.

Figure G-1 in Appendix G shows the 2D view (front side) of the assembled WSN node system integrated with the vibration energy harvester.

4.3.2 Assembly

After the prototyping boards were received from the PCB manufacturer, the assemble work was carried out. The WSN system board and the sensor board were soldered by hand in the lab with the use of the tools listed in Table 4-12. As different footprints of components are used, the procedure in Figure 4-27 is followed during the soldering operation. The sensor boards were sent out to the professional company for assembly as the size of the ICs used is too small for manual soldering.

Table 4-12 Instruments and tools used for soldering

Soldering	Cleaning	Inspection
Soldering station	Brass sponge	Multi-meter
Soldering iron	Solder vacuum	Magnifier
Hot air gun	Solder wick	
Flux pen	Tweezer	
Solder wire / paste		

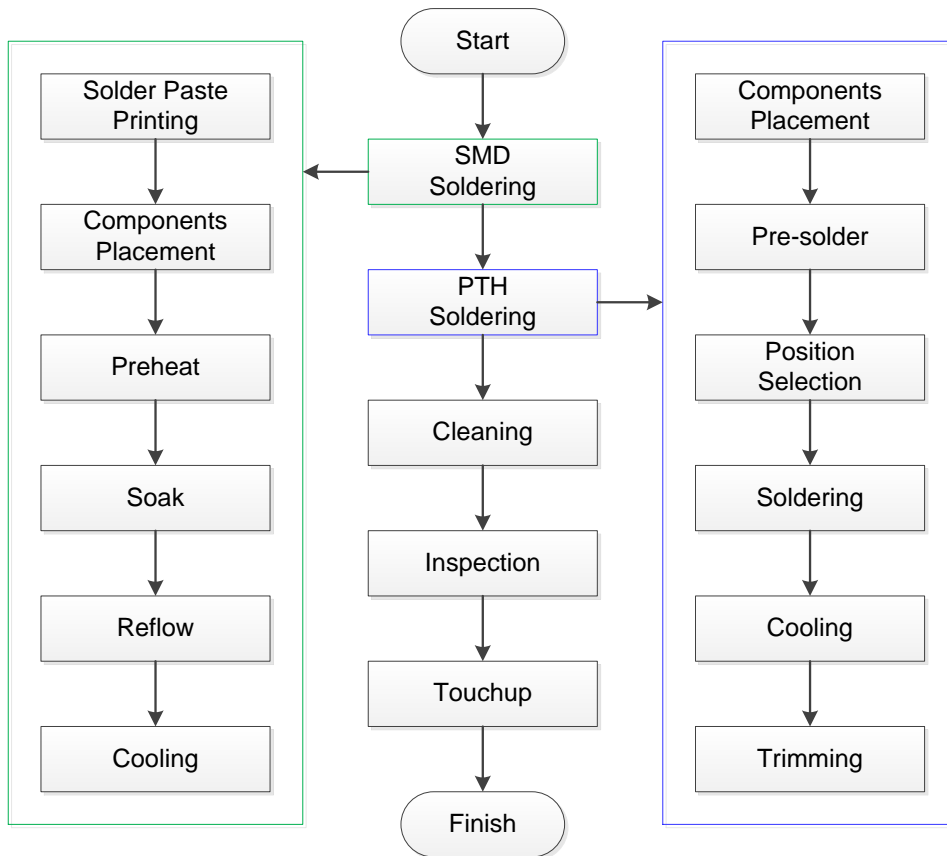


Figure 4-27 Procedure of the soldering operation

Figure H-1 in Appendix G shows the final assembled WSN system integrated with the piezoelectric energy harvester, the dimensions of the integrated system are 138 mm long, 41 mm wide, and 23 mm high while the weight is 40 grams without the tip mass.

Chapter 5

Software development & initial experiments

This chapter is made up of three sections.

The first section gives an introduction to the basics of the ZigBee network. The second section presents the configuration and adaption of the Z-Stack protocol from TI runs on the hardware, a novel power management strategy for the applications using capacitors to store harvested energy is also presented. Lastly, the third section shows the experiment setup and the analysis of the results to evaluate the proposed algorithm.

5.1 Introduction of the ZigBee network & structure

ZigBee is an IEEE 802.15.4-based specification which is specifically designed for low power consumption, low data rate, and low complexity applications.

As shown in Figure 5-1, ZigBee protocol defines the upper layers from network to application while 802.15.4 defines the lower physical and MAC layers [27].

ZigBee operates within IEEE 802 wireless standards family (Shown in Figure 5-2), however, compared with other personal area networks such as Wi-Fi or Bluetooth, ZigBee is defined for the applications which require short-range and low-rate wireless data transfer.

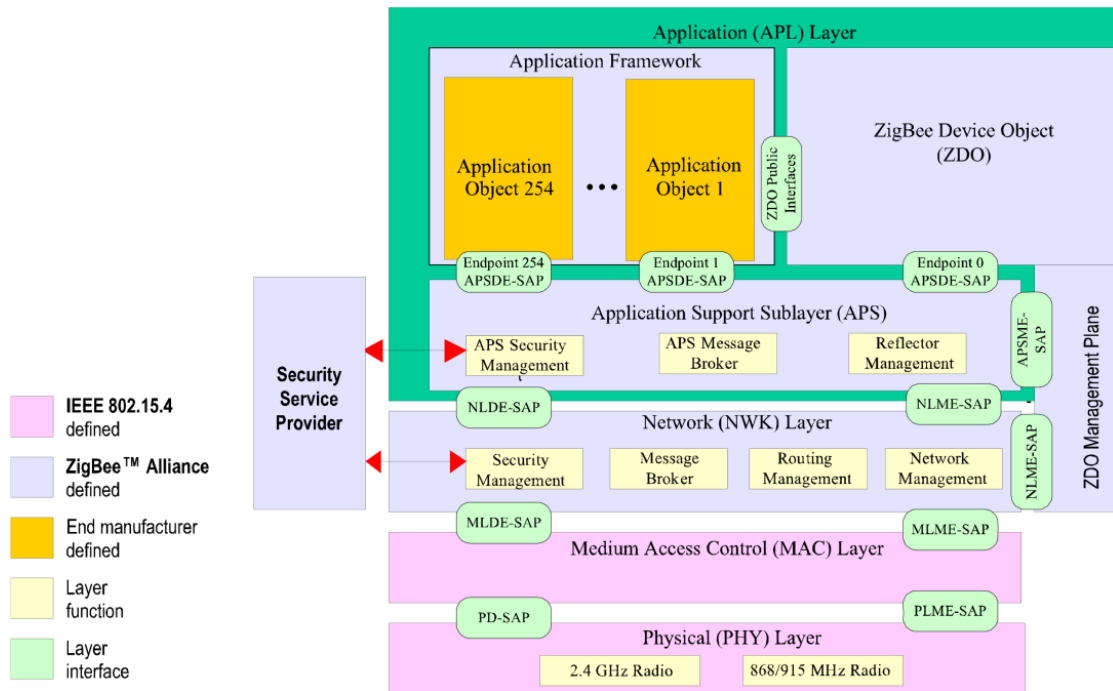


Figure 5-1 Outline of the ZigBee Stack Architecture [27]

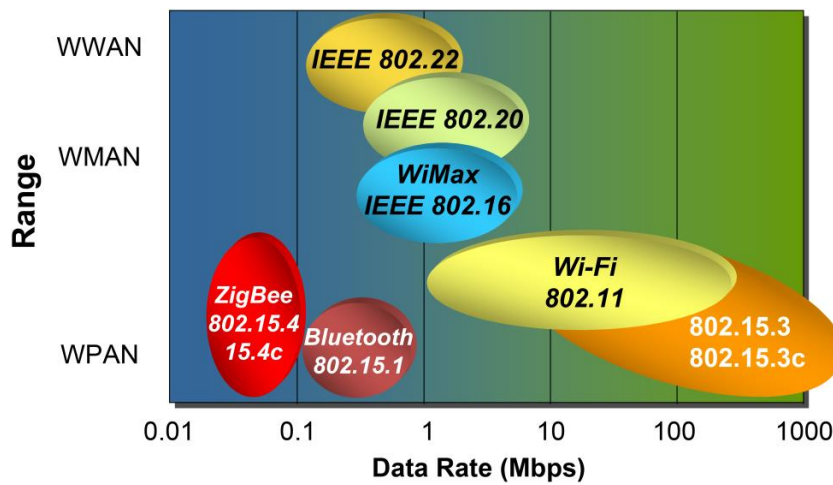


Figure 5-2 Comparison of the IEEE 802 wireless standards family[50]

Based on IEEE 802.15.4, ZigBee can be operated on three unlicensed ISM bands with 27 radio channels, the arrangement of channels is listed in Table 5-1[51].

Table 5-1 Arrangement of channels in IEEE 802.15.4 [51]

Channel Number	Centre Frequency Range	Channel Width
0	868.3 MHz	600 kHz
1 to 10	906 to 924 MHz	2 MHz
11 to 26	2405 to 2480 MHz	5 MHz

The corresponding modulation types and data rates for each of the bands are shown in Table 5-2[51]. A maximum OTA (over-the-air) data rate of 250 Kbps is achieved on the worldwide used 2.4 GHz band, best suited for intermittent data transmissions from a sensor in WSNs.

Table 5-2 Data Rates and Modulation [51]

PHY (MHz)	Frequency Band (MHz)	Spreading Parameters		Data Parameters		
		Chip Rate (kcps)	Modulation	Bit Rate (kbps)	Symbol Rate (Ksps)	Symbols
868	868- 868.6	300	BPSK	20	20	Binary
915	902- 928	600	BPSK	40	40	Binary
2450	2400-2483.5	2000	Offset-QPSK	250	62.5	16-ary Orthogonal

According to different complexities, two types of node are defined in the ZigBee network: a full function device (FFD) and a reduced function device (RFD). FFD has the ability to implement the full protocol set and can act as the Co-ordinator which is in charge of the whole network. In contrast, RFDs are used for the devices which require only minimum functionality, thus reducing the cost and the power consumption. RFD can never act as a coordinator and can only communicate with the FFD.

As shown in Figure 5-3, ZigBee fully implements three network topologies: star, tree, and mesh. Also, there are three general types of device that can exist in a ZigBee network: Co-ordinator, Router, and the End-device. However, the device types don't restrict the type of application that may run on the particular device, they are just roles exist at the network level instead of the application level.

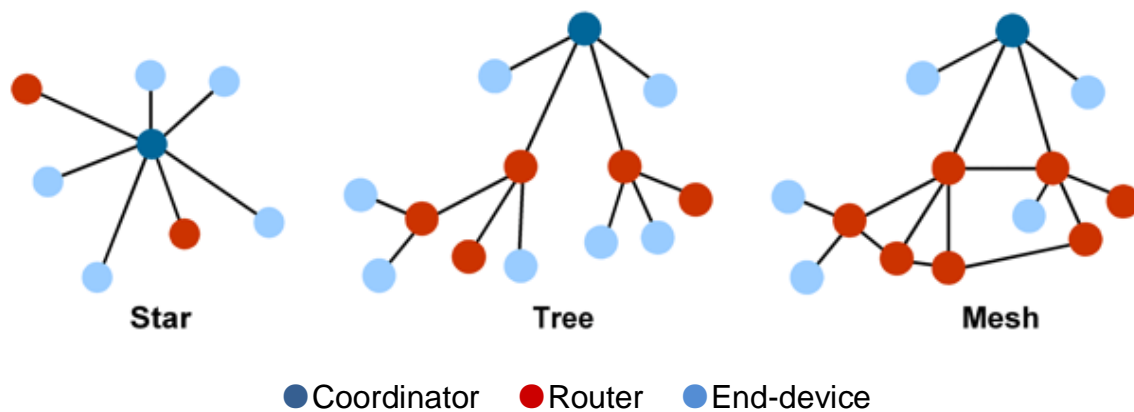


Figure 5-3 ZigBee network topologies

Star: It is the most common structure with a central node. All other nodes in the network are linked to the central node and all messages are passed through it.

Tree: This topology is a good method to gather multiple star networks into one larger network. To reach its destination, a message travels up the tree (as far as necessary) and then down the tree.

Mesh: It is a tree-like topology but some nodes are directly linked. It provides alternate route flexibility and the capability for the network to heal itself when intermediate nodes are removed or RF paths change. Messages can travel across the tree, when a suitable route is available.

Co-ordinator: A ZigBee network must and can only have one Co-ordinator. It is the device that establishes a network and performs the initialisation tasks including (1) scanning and selecting the frequency channel to be used (2) starts a ZigBee network with an identifier (also called PAN ID) and configuring the network (3) allowing child nodes to join the network through it. Once the network is created, the network can operate normally even without the Co-ordinator because of the distributed nature of the ZigBee network[52][53].

Router: At least one or more Routers exist in the ZigBee network. A Router must be available all the time and cannot sleep as it executes essential functions for the ZigBee network, such as (1) multi-hop routing, passing messages from one node to another (2) allowing a child node to join the network through it [53].

End-device: This device has no capabilities of routing and can only communicate directly with its parent. It sends and receives messages in the network and will turn off its receiver when idle. Therefore, only this type of device can be powered by the harvested energy as it can sleep and wake up as it chooses.

5.2 Configuration of Z-Stack protocol and proposed algorithm for power management

5.2.1 Z-Stack protocol and OSAL

The Z-Stack protocol from Texas Instruments runs on CC2530 SoC provides a complete solution for ZigBee application. It is a powerful implementation tool for wireless embedded system, acting like a board support package which consists of a hardware abstraction layer (HAL) and an operating system layer (OSAL). HAL providing interfaces and drivers for the hardware while OSAL offering a mechanism for tasks scheduling and resources allocation, as every operation in OSAL performs like a task and different tasks can communicate with each other by the use of the message queue.

The OSAL system operation and task scheduling mechanism in Z-Stack is shown in Figure 5-4. After start of the system, the OSAL performs the initialization operations before enters the main loop. In the main loop, the OSAL polls the task list and carries out active tasks. The whole system will not enter the sleep mode until all the tasks are finished. User applications can be added in APP task array and run on tasks.

The Z-Stack protocol provides a large number of compile options and run-time settings for users to implement it easily. The IAR Embedded Workbench IDE from IAR Systems is used to develop, manage, debug and compile the application code and Z-Stack code. After the code is compiled, the CC Debugger from Texas Instruments is used for flash programming and debugging software running on CC2530 in this project.

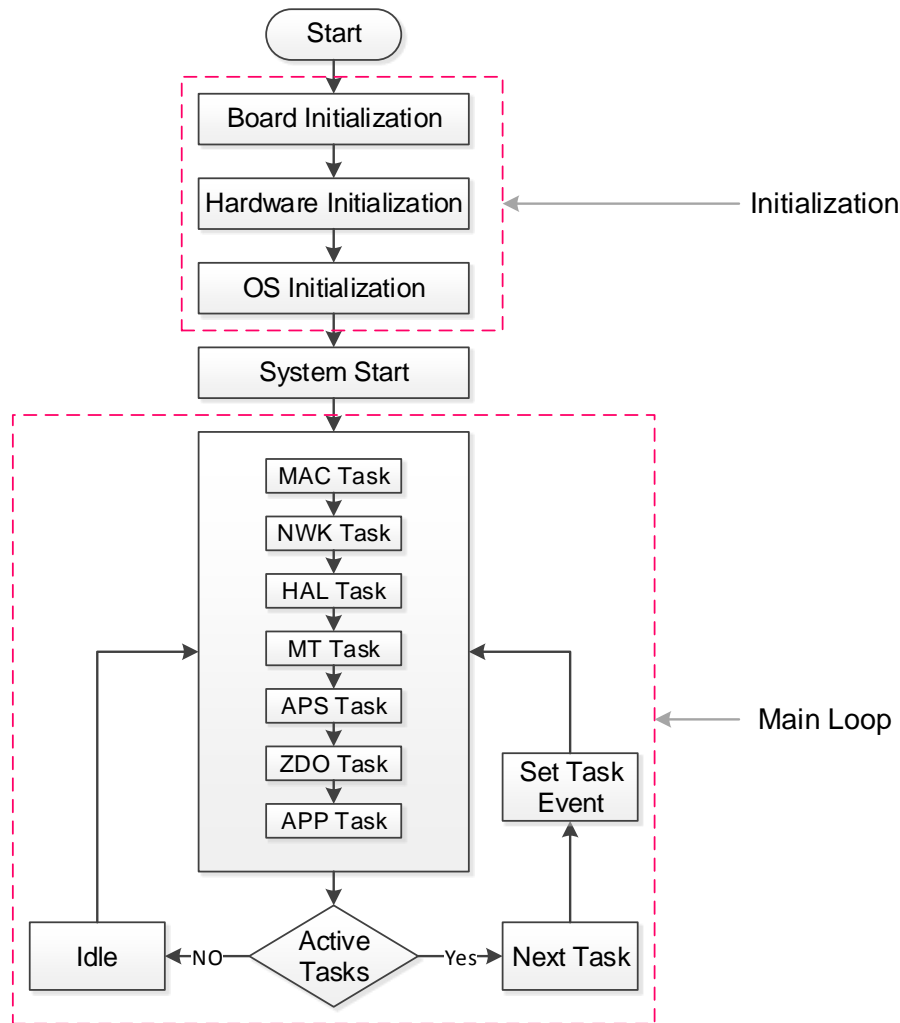


Figure 5-4 OSAL system operation and task scheduling mechanism in Z-Stack

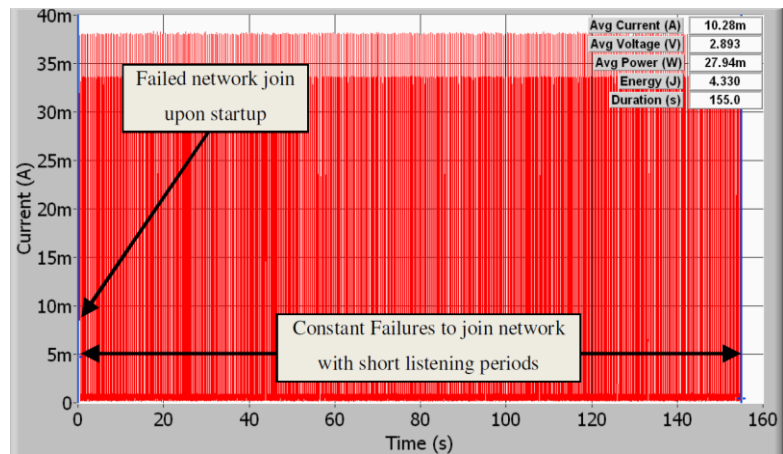
5.2.2 Configuration of Z-Stack and proposed algorithm for energy harvesting solution

According to [52], the Z-Stack protocol provides a strong support for nodes operated on batteries instead of harvested energy.

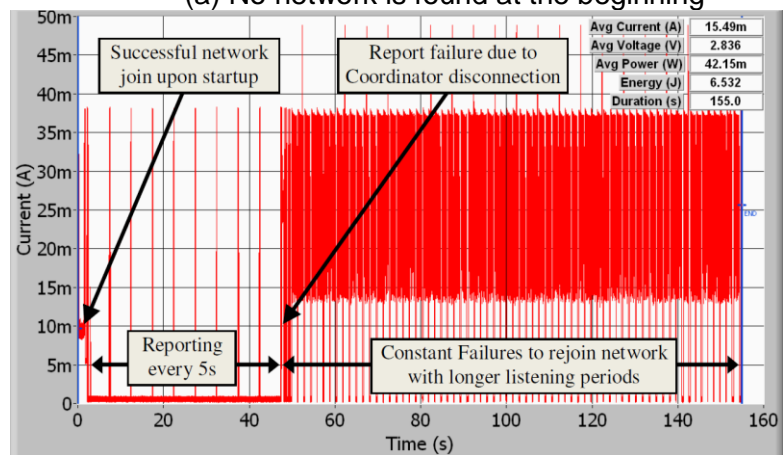
As shown in Figure 5-4, the original implementation of the OSAL initializes the hardware and operating system once the microcontroller is powered on. The duration of this initialization is hundreds of milliseconds to seconds, this short term energy exhaustion is not an issue for the battery powered devices but a huge problem for the energy harvesting devices. In the main loop, the OSAL

polls the task list and only makes the processor in idle mode instead of low power sleep mode when no task is active.

The default behaviour of a Z-Stack End-Device (ZED) is studied in [54] and Figure 5-5 shows the results, this is a natural behaviour for battery operated nodes but impossible for the energy harvesting devices.



(a) No network is found at the beginning



(b) No network is found after successful joining

Figure 5-5 Default Z-Stack behaviour of a ZED (a) No network is found at the beginning (b) No network is found after successful joining [54]

To operate the Z-Stack protocol on the devices based on energy harvesting, meaningful changes must be made in node behaviours to prevent the system power down. Nodes running on harvested energy may be programmed so that their energy constraints are short term while battery operated nodes have strong long term energy limitations.

Based on the study and analysis of the Z-Stack protocol, the most important approaches to migrate the original protocol to the devices powered by harvested energy are the power saving and network preserving configuration.

As the energy stored on the capacitor is limited, prolonged normal operation is impossible, therefore, the system needs to enter a low power mode after processing as soon as possible to prevent unexpected power down. The power management is enabled and used to minimize power consumption by making the system enter a sleep mode when no task is active.

Every time when the system wakes up from the sleep mode, the device needs to perform the network joining process again which consumes lots of energy. The best means to reduce the consumption is enable the network preserving function, so that the configuration items like PAN ID and network settings will be saved in non-volatile (NV) memory and the device will not need to repeat the initial setup after each power cycle.

The configuration of the power saving, network preserving and other alteration for the ZED powered by harvesting energy are listed in Table 5-3.

Table 5-3 Configuration of the Z-Stack protocol for energy harvesting solution

Parameter	Location	Description
POWER_SAVING	Compile Option	Enable power saving functions for battery-powered devices
POLL_RATE=0	f8wConfig.cfg	number of milliseconds to wait between data request polls to its parent
QUEUED_POLL_RATE=0	f8wConfig.cfg	This is used after receiving a data indication to poll immediately for queued messages (in milliseconds)
REJOIN_POLL_RATE=0	f8wConfig.cfg	This is used as an alternate response poll rate only for rejoin request. This rate is determined by the response time of the parent that the device is trying to join
RESPONSE_POLL_RATE=0	f8wConfig.cfg	This is used after receiving a data confirmation to poll immediately for response messages (in milliseconds)
NV_INIT	Compile Option	Enable loading of "basic" NV items at device reset
NV_RESTORE	Compile Option	Enables device to save/restore network state information to/from NV

NWK_AUTO_POLL	Compile Option	Enable End Device to poll from the parents automatically
HAL_BOARD_VEH_END	Compile Option	Set the device type as End-device for compiling
HAL_BOARD_VEH_COR	Compile Option	Set the device type as Coordinator for compiling

According to the hardware design in Chapter 4, the maximum voltage across the storage capacitor is 18V, thus the energy stored on the capacitor can support a maximum 160 msec RF transmission or a maximum 550 msec MCU normal processing operation following the formula in (4-8) in this project.

As shown in Figure 5-6, an initial algorithm is developed based on the modified Z-Stack protocol to manage the power and prevent unexpected shutdowns. The proposed algorithm relies on the analysis of how much energy has been stored on capacitor to determine the executions of the operations in the system. This can be accomplished by using of the voltage monitor circuit designed in Figure 4-8. The running mechanism of the algorithm is described as follows.

After the MCU is power on, the system enters into the low power sleep mode immediately as the initialization operations consume a lot of energy. About 6 secs later, the system wakes up and measure the voltage (V_{SC}) across the store capacitor, if enough energy is accumulated ($V_{SC} > 13$ V), the OSAL executes the initialization tasks, starts the system and enters the main loop.

In the main loop, the system measures V_{SC} every one second after wakes up from the low power mode. If $V_{SC} > 5$ V, the OSAL triggers measurement of the sensors and processes the data from them. Next, if $V_{SC} > 6$ V, the data will be sent to the coordinator wirelessly before entering the sleep mode. Otherwise, if the operation is not possible to perform, the OSAL will place the system in low power mode again and energy is harvested and accumulated for the next cycle.

It is important to point out that the actual implementation of the strategy proposed above depends on which type of MCU chip and what kind of the wireless network protocol is used in the design. The 32.768 kHz crystal oscillator is used for the sleep timer in TI CC2530 to provide a stable clock signal and the Start-up time is 0.4 second according to [39], [45]. Thus the

voltage across the store capacitor should be over 13 V to perform the system initialization in OSAL. The 13 V chosen here is for the specific chip used in this design, on the other hand, for a different chip or protocol, the threshold of the start voltage will be different.

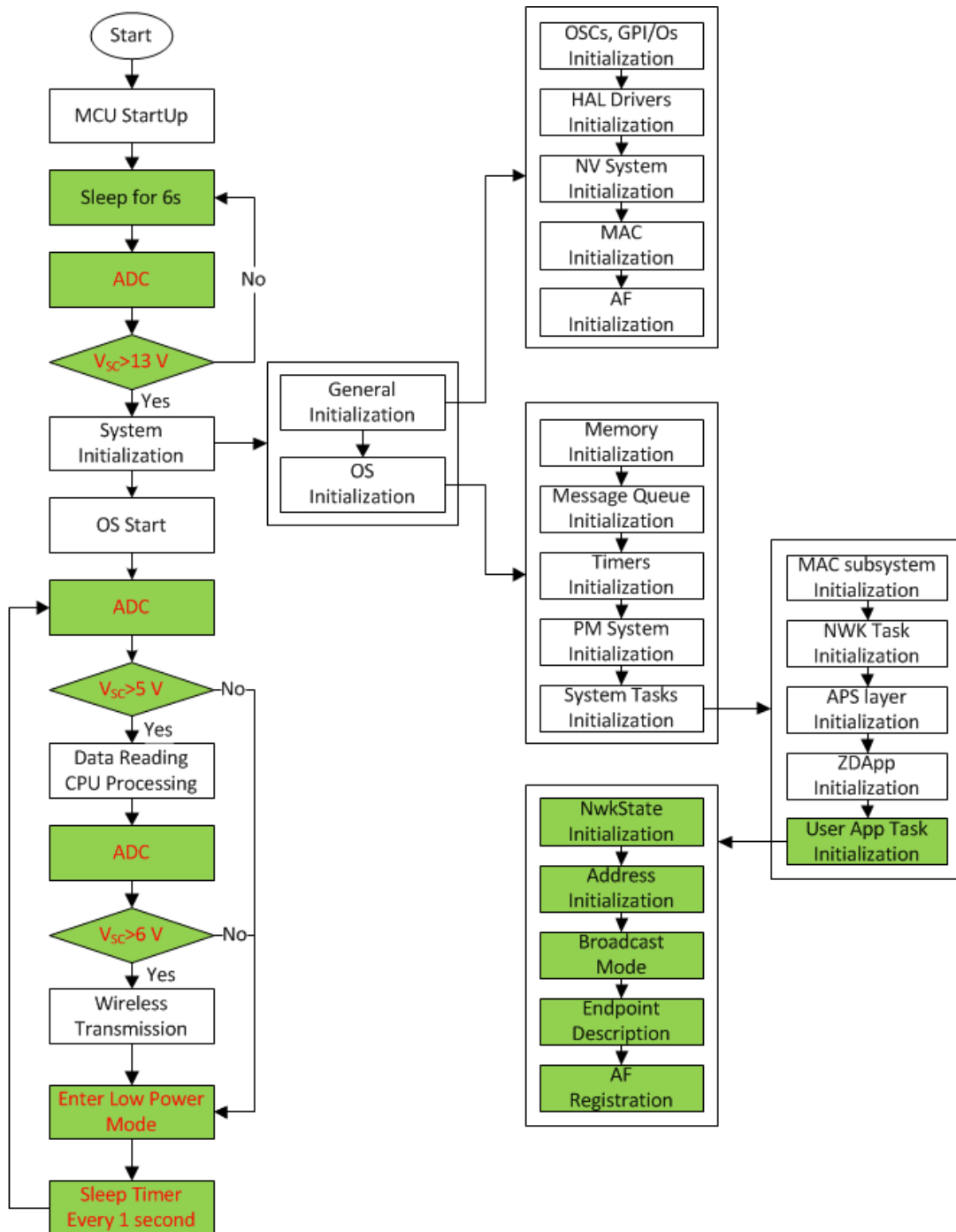


Figure 5-6 Proposed Algorithm for the WSN system based on piezoelectric vibration energy harvesting

5.3 Initial measurements and results of the algorithm

To evaluate the performance of the adapted Z-Stack protocol and the proposed algorithm for future integration with the vibration energy harvester, initial experiments were carried out.

5.3.1 Experiment environment setup

As shown in Figure 5-7, a measurement setup is performed in a lab environment in order to measure power consumption.

As the oscilloscope provides a graphical representation of the voltage and there is a linear relationship between voltage and current according to Ohm's Law, the general idea of the current consumption measurement is to visualize the current profile on an oscilloscope by measuring the voltage drop over a fixed resistor[55].

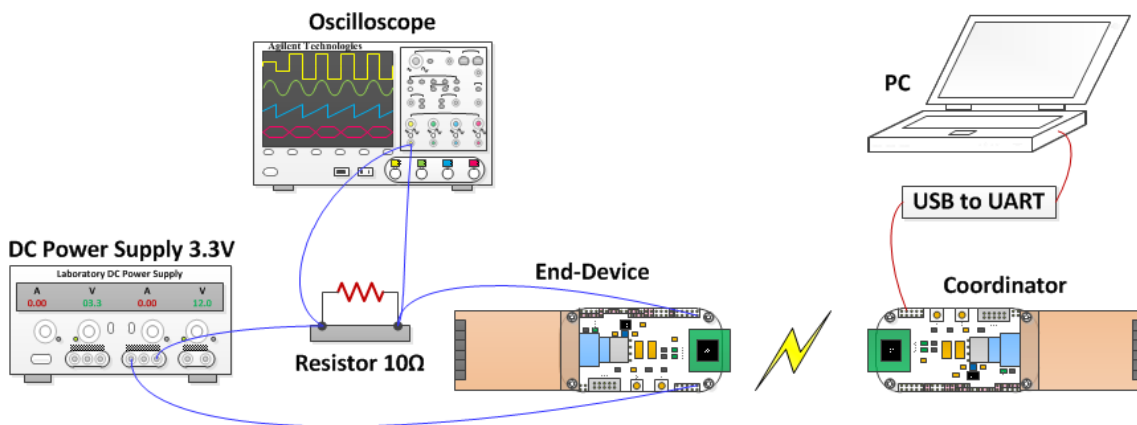


Figure 5-7 Measurement Setup

A ZigBee network is formed before the measurement by one ZigBee Coordinator (ZC) and one ZigBee end device (ZED) using the abovementioned adapted TI Z-Stack 2.5.1a. As network restore function is enabled, the ZED will rejoin the network effectively after power-up with no OTA traffic when the ZC is power on.

The ZED is powered by a constant voltage of 3.3V and in series with a 10Ω resistor while the ZC is powered and communicated with the computer by a USB-UART adapter. The ZED is programmed to rejoin the network and send measured data to ZC periodically, and ZC is programmed to receive data and communicate with PC through serial communication port.

In addition, the current consumption during the low power sleep mode is in the magnitude of μA which is too small and cannot be observed from the oscilloscope. The current is measured and reported to be the same as the value in datasheet in [55]. The error and the voltage drop introduced by the resistor are acceptable and thus they are omitted.

5.3.2 Results & analysis of the proposed algorithm

Figure 5-8 shows the 50 secs measurement plot of the ZED after power on.

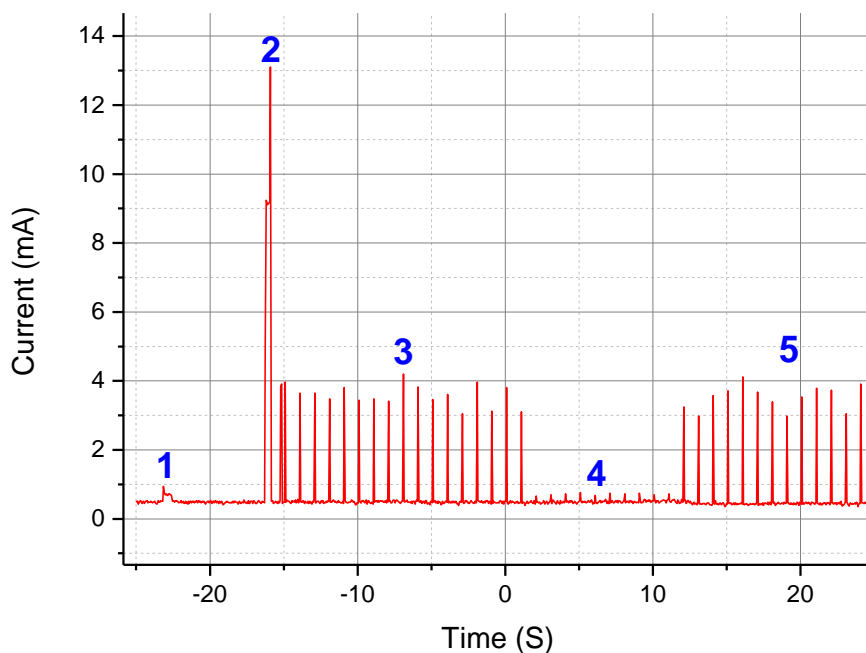


Figure 5-8 A 50 secs measurement plot of the ZED

There are five operations during this measurement in Figure 5-8 according to the algorithm in Figure 5-6.

Operation 1: After the MCU is power on, the system enters into the low power sleep mode (PM2) immediately for about 6 secs. The purpose of this operation is to accumulate more energy on the energy for the next operation.

Operation 2: If the voltage across the store capacitor is over 13 V, the OSAL performs the initialization of the system.

Operation 3/5: In this operation, the system controls the sensors to measure data, packets the data and sends them to the ZC. After that, it enters the low power mode for power saving. The time interval of this operation is one second.

Operation 4: The premise of operation 3/5 is that there is enough energy stored on the capacitor, on the contrary, in this operation, the system resume to sleep again without the execution of the measurement or RF communication.

Figure 5-9, Figure 5-10, Figure 5-11, and Figure 5-12 present the current consumption measurement plots of the operation 1, operation 2, operation 3/5, and operation 4 respectively while the Table 5-4, Table 5-5, Table 5-6, and Table 5-7 give the detail and calculation of the measured data.

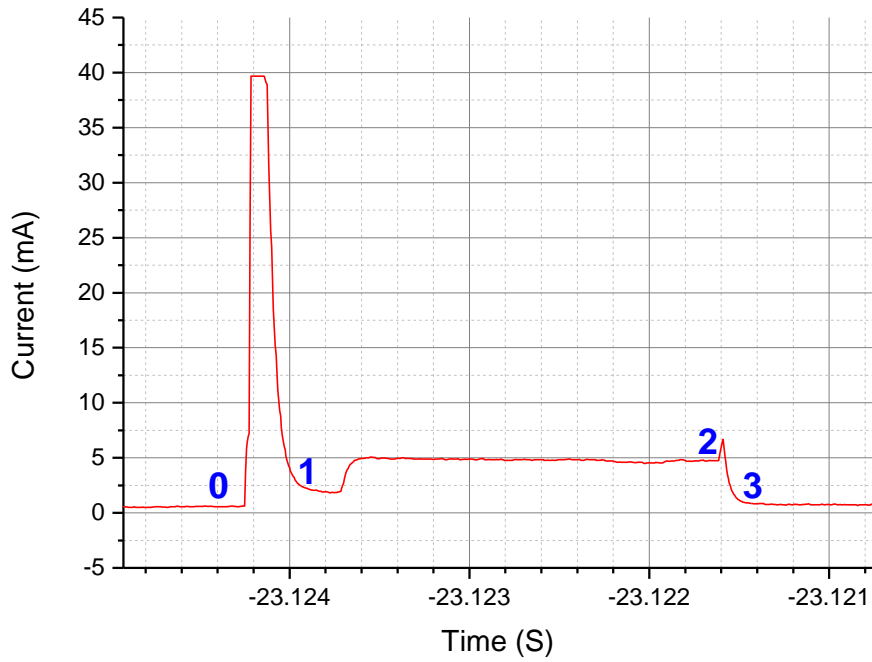


Figure 5-9 Current Consumption Measurement Plot on Operation 1

Table 5-4 Current Consumption Measurement Plot on Operation 1

Section	Operation	Current (mA)	Time (ms)	Consumption (mA*ms)
Before 0	Sleep Mode (PM2)	0.001		
0 to 1	Start-up, PM2 → Active mode (16MHz clock)	40	0.1	4
1 to 2	Active mode (16MHz clock)	6	2.5	15
After 3	Sleep Mode (PM2)	0.001		
			2.6	19

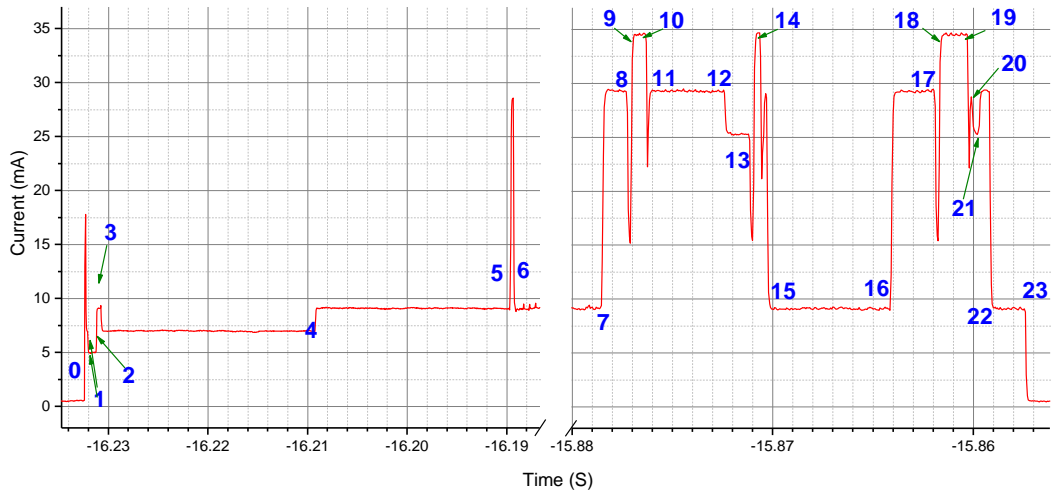


Figure 5-10 Current Consumption Measurement Plot on Operation 2

Table 5-5 Current Consumption Measurement Plot on Operation 2

Section	Operation	Current (mA)	Time (ms)	Consumption (mA*ms)
Before 0	Sleep Mode (PM2)	0.001		
0 to 1	Start-up, PM2 → Active mode (16MHz clock)	26	0.13	3.38
1 to 2	OSAL Initialization 1	5	1.04	5.2
2 to 3	OSAL Initialization 2	9	0.6	5.4
3 to 4	OSAL Initialization 3	7	21.38	149.66
4 to 5	OSAL Initialization 4	9	19.57	176.13
5 to 6	OSAL Initialization 5	28.5	0.43	12.255
6 to 7	Processing, MCU running on 32-MHz clock	9.2	310.7	2858.44
7 to 8	RX mode: CSMA/CA algorithm.	29.4	1.27	37.338
8 to 9	RX to TX	15.3	0.31	4.743
9 to 10	TX mode: Transmitting MAC data request	34.5	0.65	22.425
10 to 11	TX to RX, Receiving MAC ACK from ZC	26	0.1	2.6
11 to 12	RX mode	29.4	3.8	111.72
12 to 13	Receiving command	25.1	1.25	31.375
13 to 14	RX to TX	20.5	0.31	6.355
14 to 15	Transmitting, Radio in TX mode	25	0.7	17.5
15 to 16	MCU Processing	9	6	54
16 to 17	CSMA/CA, Radio in RX mode	29.4	2.23	65.562
17 to 18	RX to TX	25	0.3	7.5
18 to 19	TX mode: Transmitting	34.5	1.33	45.885
19 to 20	TX to RX	29	0.19	5.51
20 to 21	Receiving MAC ACK from ZC	27.5	0.45	12.375
21 to 22	RX mode: processing the MAC ACK	29.4	0.66	19.404
22 to 23	MCU Processing, shut down	9	1.75	15.75
After 23	Sleep Mode (PM2)	0.001		
		375.15	3670.507	

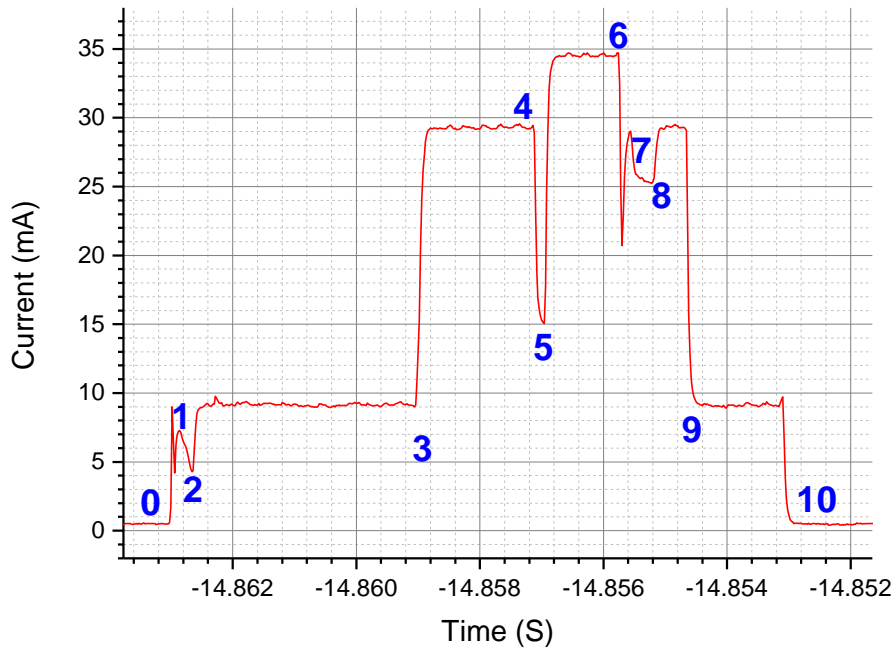


Figure 5-11 Current Consumption Measurement Plot on Operation 3/5

Table 5-6 Current Consumption Measurement Plot on Operation 3/5

Section	Operation	Current (mA)	Time (ms)	Consumption (mA*ms)
Before 0	Sleep Mode (PM2)	0.001		
0 to 1	Start-up, PM2 → Active mode (16MHz clock)	22	0.1	2.2
1 to 2	Active mode (16MHz clock)	6	0.33	1.98
2 to 3	Active mode (32MHz clock)	9.2	3.5	32.2
3 to 4	RX mode: CSMA/CA	29.4	0.95	27.93
4 to 5	RX to TX	15.4	0.17	2.618
5 to 6	TX mode: Transmitting	35	1.205	42.175
6 to 7	TX to RX	29	0.206	5.974
7 to 8	Receiving MAC ACK from ZC	25.5	0.374	9.537
8 to 9	RX mode: processing the MAC ACK	29.4	0.66	19.404
9 to 10	MCU Processing, shut down	9.3	1.725	16.0425
After 10	Sleep Mode (PM2)	0.001		
			9.22	160.0605

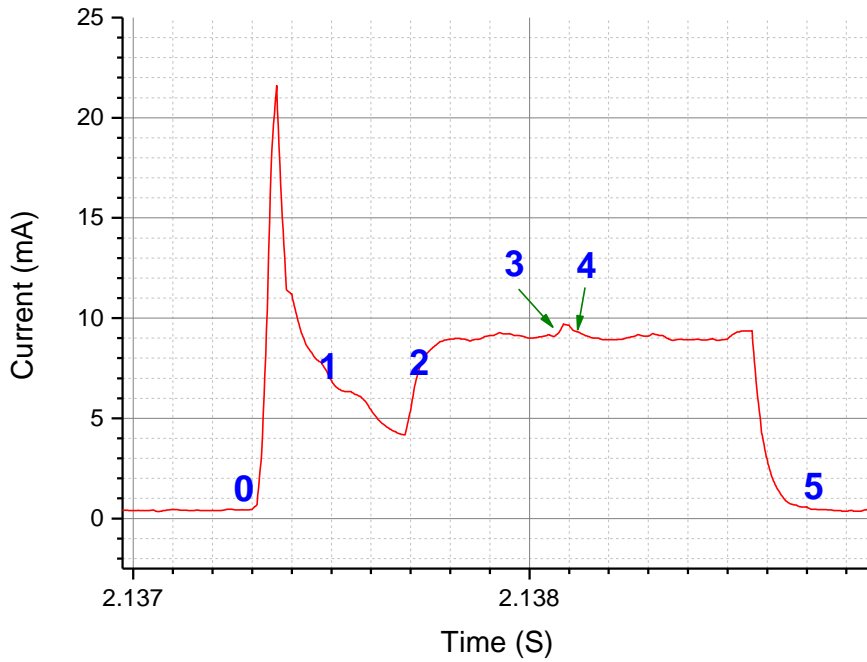


Figure 5-12 Current Consumption Measurement Plot on Operation 4

Table 5-7 Current Consumption Measurement Plot on Operation 4

Section	Operation	Current (mA)	Time (ms)	Consumption (mA*ms)
Before 0	Sleep Mode (PM2)	0.001		
0 to 1	Start-up, PM2 → Active mode (16MHz clock)	22.5	0.2	4.5
1 to 2	Active mode (16MHz clock)	7	0.22	1.54
2 to 3	Active mode (32MHz clock)	9.2	0.35	3.22
3 to 4	Active mode (32MHz clock), ADC	10	0.076	0.76
4 to 5	Processing and shut down	9.2	0.6	5.52
After 5	Sleep Mode (PM2)	0.001		
			1.446	15.54

Based on the above measurement and according to the formula in (4-8), the minimum voltage on the storage capacitor to carry out different operations is listed in Table 5-8. The results show that the adapted Z-Stack and the proposed algorithm can be implemented on the system designed in Chapter 4.

Table 5-8 Minimum voltage on the storage capacitor to carry out operation 1, 2, 3/5, and 4

Mode	Minimum Voltage
Operation 1	3.78 V
Operation 2	12.85 V
Operation 3 / Operation 5	4.48 V
Operation 4	3.76 V

Chapter 6

Conclusion and future work

This chapter presents the conclusion of this study and introduces the work for further integration and improvement. It consists of two sections: conclusion and future work.

6.1 Conclusion

This study presents a preliminary solution for the wireless sensor networks for aircraft health monitoring based on vibration energy harvesting.

Relevant literature and research was reviewed and the selection criteria of energy harvesting technologies on different aircrafts were proposed.

the popular network standards for WSNs, the techniques implemented for power saving, and at last the available products in the market for the later hardware development.

A complete system was designed and the prototypes were fabricated, including the energy harvester, the power management circuit, the microcontroller, the RF, and the sensors unit.

To evaluate the performance, most behaviours of the system were simulated in LTspice. Results showed that with an excitation of 40 Hz frequency and 0.5 g acceleration on the harvester, the power management unit takes about 3 secs

to power the system with a selected voltage and another 17 secs to perform the initialization operations of the system. After the initialization, data are measured and transmitted wirelessly with a total energy consumption of 0.65 mJ in one cycle every one second.

Furthermore, Z-Stack protocol was migrated to run on the system and initial experiments were carried out to analyse the current consumption of the system.

As the acquired energy is very limited and influenced by the ambient, the main gap between the energy harvester and the WSN system is the mechanisms used for power management. A new power management strategy for the applications using capacitors to store harvested energy was proposed. The mechanism relies on the analysis of how much energy has been stored on capacitor to determine the executions of the operations in the system.

A novel energy saving interface (ESI) was designed to minimise the power consumption during the voltage measurement and an intelligent algorithm was developed to implement the strategy.

The analysis of the calculated results from the initial experiments shows that the proposed algorithm works well with the vibration energy harvesting WSN system designed in this project.

6.2 Future work

As the preliminary solution includes the hardware design and basic software implementation, further work should be done to validate the whole system and improve it, which including:

(1) Integration of the sensor board

A resistor was used as the sensors during the simulation and initial experiments. However, a sensor board which integrates three MEMS-based sensors had been developed and assembled at the end of the project.

The next work is integrating the sensor board with the energy harvesting system to collect data from the environment.

(2) Experiment and analysis

As time is limited, no further experiments have been carried out with a shaker for further analysis. The next work is deploying the hardware and software in an experimental environment with the use of a shaker.

Results from different configurations with regards to different frequency, variable-frequency, different acceleration, variable- acceleration, different tip mass will be compared and analysed.

(3) Optimization of the strategy for power management

The current strategy for power management is measure the data when the voltage across the store capacitor is higher than 5 V and transmit them (20 bytes of data) when the voltage over 6 V. Otherwise, the system enters the low power mode for power saving.

A different option, for example, is that the system keeps reading the data when the voltage over 5 V but below 6 V instead of sleeping. Different strategies can be studied and analyzed for future optimization.

(4) Implementation

After the optimization of both the circuits and the software including the algorithm, implement the system on an aircraft in a real application environment to evaluate its performance.

REFERENCES

- [1] I. F. Akyildiz, T. Melodia, and K. R. Chowdhury, "A survey on wireless multimedia sensor networks," *Comput. Networks*, vol. 51, no. 4, pp. 921–960, 2007.
- [2] L. Janak and V. Singule, "Energy harvesting for aerospace: Application possibilities," *Mechatronics - Mechatronika (ME), 2014 16th Int. Conf.*, pp. 183–187, 2014.
- [3] K. Thangaraj, A. Elefsiniots, T. Becker, U. Schmid, J. Lees, C. a. Featherston, and R. Pullin, "Energy storage options for wireless sensors powered by aircraft specific thermoelectric energy harvester," *Microsyst. Technol.*, vol. 20, no. 4–5, pp. 701–707, 2014.
- [4] O. Sosnicki, N. Lhermet, and F. Claeysen, "Vibration energy harvesting in aircraft using piezoelectric actuators," in *Proc Actuator*, 2006, pp. 968–971.
- [5] D. Samson, T. Otterpohl, M. Kluge, U. Schmid, and T. Becker, "Aircraft-specific thermoelectric generator module," *J. Electron. Mater.*, vol. 39, no. 9, pp. 2092–2095, Nov. 2010.
- [6] D. Samson, M. Kluge, T. Fuss, U. Schmid, and T. Becker, "Flight test results of a thermoelectric energy harvester for aircraft," *J. Electron. Mater.*, vol. 41, no. 6, pp. 1134–1137, Feb. 2012.
- [7] D. Samson, M. Kluge, T. Becker, and U. Schmid, "Wireless sensor node powered by aircraft specific thermoelectric energy harvesting," *Sensors Actuators, A Phys.*, vol. 172, no. 1, pp. 240–244, Dec. 2011.
- [8] D. Samson, M. Kluge, T. Becker, and U. Schmid, "Energy harvesting for autonomous wireless sensor nodes in aircraft," *Procedia Eng.*, vol. 5, pp. 1160–1163, 2010.
- [9] V. Giurgiutiu, A. Zagrai, and J. Jing Bao, "Piezoelectric Wafer Embedded Active Sensors for Aging Aircraft Structural Health Monitoring," *Struct. Heal. Monit.*, vol. 1, no. 1, pp. 41–61, 2002.
- [10] C. a. Featherston, K. M. Holford, and G. Waring, "Thermoelectric Energy Harvesting for Wireless Sensor Systems in Aircraft," *Key Eng. Mater.*, vol. 413–414, no. 2009, pp. 487–494, Jun. 2009.
- [11] M. R. Pearson, M. J. Eaton, R. Pullin, C. a Featherston, and K. M. Holford, "Energy Harvesting for Aerospace Structural Health Monitoring Systems," *J. Phys. Conf. Ser.*, vol. 382, p. 012025, Aug. 2012.

- [12] R. J. M. Vullers, R. van Schaijk, I. Doms, C. Van Hoof, and R. Mertens, "Micropower energy harvesting," *Solid. State. Electron.*, vol. 53, no. 7, pp. 684–693, 2009.
- [13] P. Harrop, "Energy harvesting and storage for electronic devices 2009-2019." 2009.
- [14] L. Wang and F. G. Yuan, "Energy harvesting by magnetostrictive material (MsM) for powering wireless sensors in SHM," in *The 14th International Symposium on: Smart Structures and Materials & Nondestructive Evaluation and Health Monitoring*, 2007, pp. 18–22.
- [15] University of Exeter, "Energy harvesting projects." [Online]. Available: <http://emps.exeter.ac.uk/engineering/research/structures-dynamics/energyharvesting/projects/>. [Accessed: 06-Apr-2015].
- [16] H. Liu, C. Quan, C. J. Tay, T. Kobayashi, and C. Lee, "A MEMS-based piezoelectric cantilever patterned with PZT thin film array for harvesting energy from low frequency vibrations," *Phys. Procedia*, vol. 19, pp. 129–133, 2011.
- [17] A. Mathers, K. S. Moon, and J. Yi, "A Vibration-Based PMN-PT Energy Harvester," *Sensors Journal, IEEE*, vol. 9, no. 7, pp. 731–739, 2009.
- [18] L. Gu, "Low-frequency piezoelectric energy harvesting prototype suitable for the MEMS implementation," *Microelectronics J.*, vol. 42, no. 2, pp. 277–282, 2011.
- [19] N. Kong and D. S. Ha, "Low-power design of a self-powered piezoelectric energy harvesting system with maximum power point tracking," *IEEE Trans. Power Electron.*, vol. 27, no. 5, pp. 2298–2308, 2012.
- [20] D. Zhu, S. P. Beeby, M. J. Tudor, and N. R. Harris, "A credit card sized self powered smart sensor node," *Sensors Actuators, A Phys.*, vol. 169, no. 2, pp. 317–325, 2011.
- [21] B. Jiang, K. Cao, L. Chen, H. Chen, H. Zhang, and Q. Wang, "Low-Power Design of a Self-powered Piezoelectric Energy Harvesting System," in *Control Conference (CCC), 2014 33rd Chinese*, 2014, pp. 6937–6940.
- [22] T. Armstrong, "Aircraft structures take advantage of energy harvesting implementations," *Electron. World*, vol. 118, no. 1916, pp. 28–31, 2012.
- [23] Texas Instruments, "Zigbee Wireless Networking Overview (Rev. D)." 2013.
- [24] K. Gravogl, J. Haase, and C. Grimm, "Choosing the best wireless protocol for typical applications," *24th Int. Conf. Archit. Comput. Syst. (ARCS)*, p. 6, 2011.
- [25] "Bluetooth Specification (Rev. 4.2)." <https://www.bluetooth.org/en-us/specification/adopted-specifications> [Accessed: 10 March 2015], 2014.

- [26] G. Mulligan, "The 6LoWPAN architecture," *Proc. 4th Work. Embed. networked sensors - EmNets '07*, p. 78, 2007.
- [27] Z. Alliance, "ZigBee Specification (Rev.r20)." <http://www.zigbee.org/non-menu-pages/zigbee-pro-download/> [Accessed: 25 July 2015], 2012.
- [28] A. El Kouche, "WIRELESS SENSOR NETWORK PLATFORM FOR HARSH by," 2013.
- [29] Analog Devices, "Hardware Design Techniques." <http://www.analog.com/library/analogDialogue/archives/39-06/Chapter%209%20Hardware%20Design%20Techniques%20F.pdf> [Accessed: 15 February 2015], p. 2005, 2005.
- [30] Texas Instruments, "Hardware Design Guide for KeyStone I Devices (Rev. SPRABI2C)." <http://www.ti.com/lit/an/sprabi2c/sprabi2c.pdf> [Accessed: 03 February 2015], 2013.
- [31] M. K. Stojčev, M. R. Kosanovic, and L. R. Golubovic, "Power management and energy harvesting techniques for wireless sensor nodes," *Proc. 9th Int. Conf. Telecommun. Mod. Satell. Cable, Broadcast. Serv. 2009 (TELSIKS '09)*, pp. 65–72, 2009.
- [32] S. Rhee, D. Seetharam, and S. Liu, "Techniques for minimizing power consumption in low data-rate wireless sensor networks," *2004 IEEE Wirel. Commun. Netw. Conf. (IEEE Cat. No.04TH8733)*, vol. 3, 2004.
- [33] A. Kurude and M. Bhole, "Analysis of Discrete & Integrated Circuits for Piezoelectric Energy Harvesting," *Int. J. Innov. Res. Electr. Electron. Instrum. Control Eng.*, vol. 1, no. 5, pp. 194–198, 2013.
- [34] Z. Yang and P. Sen, "Recent developments in high power factor switch-mode converters," *Electr. Comput. Eng. 1998.*, pp. 477–480, 1998.
- [35] D. Estrin, "Wireless sensor networks tutorial part IV: sensor network protocols," *Mobicom, Westin Peachtree Plaza, Atlanta, Georg. USA*, pp. 23–28, 2002.
- [36] Mide Technology, "Vulture v25w Datasheet (Rev. 2)." <http://www.mide.com/products/vulture/piezoelectric-vibration-energy-harvesters.php> [Accessed: 06 April 2015].
- [37] Linear Technology, "LTC3588-1 Datasheet (Rev. B)." <http://www.linear.com/product/LTC3588-1> [Accessed: 06 April 2015].
- [38] IMST GmbH, "iM222A Datasheet (Rev. 2.2)." <http://www.wireless-solutions.de/products/radiomodules/im222a-zigbee-network-processor> [Accessed: 06 April 2015].
- [39] Texas Instruments, "CC2530 Datasheet (Rev. B)." <http://www.ti.com/product/cc2530> [Accessed: 06 April 2015].

- [40] STMicroelectronics, "LIS2DH Datasheet (Rev. 1)." http://www.st.com/web/en/catalog/sense_power/FM89/SC444/PF252928 [Accessed: 06 April 2015].
- [41] STMicroelectronics, "LPS25H Datasheet (Rev. 3)." http://www.st.com/web/catalog/sense_power/FM89/SC1316/PF255230 [Accessed: 06 April 2015].
- [42] Texas Instruments, "HDC1000 Datasheet (Rev. A)." <http://www.ti.com/product/hdc1000> [Accessed: 06 April 2015].
- [43] Mide Technology, "EHE004 Datasheet (Rev. 2)." www.mide.com/pdfs/vulture_EHE004_Datasheet.pdf [Accessed: 15 February 2015].
- [44] Texas Instruments, "CC Debugger User's Guide (Revised April 2014)." www.ti.com/lit/ug/swru197h/swru197h.pdf [Accessed: 27 May 2015].
- [45] Texas Instruments, "CC253x/4x User's Guide (Rev. F)." <http://www.ti.com/lit/ug/swru191f/swru191f.pdf> [Accessed: 16 June 2015].
- [46] Atmel Corporation, "AVR40: EMC Design Considerations (Rev. 1619D-AVR-06/06)." www.atmel.com/Images/doc1619.pdf [Accessed: 20 May 2015].
- [47] Cypress Semiconductor Corp., "Top 10 EMC Design Considerations," no. 2011. <http://www.cypress.com/file/106951/download> [Accessed: 20 May 2015].
- [48] Texas Instruments, "Considerations for PCB Layout and Impedance Matching Design in Optical Modules." <http://www.ti.com/lit/an/slla311/slla311.pdf> [Accessed: 21 May 2015], 2011.
- [49] Fairchild semiconductor Corporation, "Considerations in Designing the Printed Circuit Boards of Embedded Switching Power Supplies (Rev. A)." <https://www.fairchildsemi.com/application-notes/AN/AN-1031.pdf> [Accessed: 22 May 2015], 1999.
- [50] Z. Alliance, "ZigBee Overview." <https://docs.zigbee.org/zigbee-docs/dcn/07/docs-07-5482-01-0mwg-zigbee-alliance-overview.pdf> [Accessed: 22 July 2015], 2009.
- [51] P. Chandra, D. M. Dobkin, D. Bensky, R. Olexa, D. Lide, and F. Dowla, *Wireless Networking: Know It All*. Newnes, 2007.
- [52] Texas Instruments, "Z-Stack Developer's Guide (Rev. 1.10)." <http://www.ti.com> [Accessed: 26 July 2015], 2011.
- [53] NXP Laboratories UK, "ZigBee PRO Stack User Guide (Rev. 2.5)," no. December. www.nxp.com/documents/user_manual/JN-UG-3048.pdf [Accessed: 30 July 2015], p. 418, 2012.




- [54] A. El Kouche, a. M. Rashwan, and H. Hassanein, "Energy consumption measurements and reduction of Zigbee based wireless sensor networks," *GLOBECOM - IEEE Glob. Telecommun. Conf.*, pp. 557–562, 2013.
- [55] Texas Instruments, "Measuring Power Consumption of CC2530 With Z-Stack." <http://www.ti.com/litv/pdf/swra292> [Accessed: 02 September 2015].
- [56] Texas Instruments, "BQ25505 Datasheet (Rev. C)." <http://www.ti.com/product/bq25505> [Accessed: 20 December 2014].
- [57] Texas Instruments, "BQ25504 Datasheet (Rev. B)." <http://www.ti.com/product/bq25504> [Accessed: 20 December 2014].
- [58] Cypress Semiconductor, "MB39C811 Datasheet (Rev. 3.0)." http://www.spansion.com/fjdocuments/fj/Datasheet/e-ds/MB39C811_DS405-00013.pdf [Accessed: 19 December 2014].
- [59] Maxim Integrated, "MAX17710 Datasheet (Rev. 2)." <https://www.maximintegrated.com/en/products/power/battery-management/MAX17710.html> [Accessed: 19 December 2014].
- [60] L. Technology, "LTC3588-2 Datasheet (Rev. B)." <http://www.linear.com/product/LTC3588-2> [Accessed: 17 December 2014].
- [61] L. Technology, "LTC3331 Datasheet (Rev. B)." <http://www.linear.com/product/LTC3331> [Accessed: 17 December 2014].
- [62] L. Technology, "LTC3330 Datasheet (Rev. B)." <http://www.linear.com/product/LTC3330> [Accessed: 17 December 2014].






APPENDICES

Appendix A Comparison of the components

A.1 Comparison of vibration energy harvesters


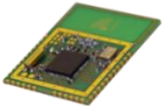


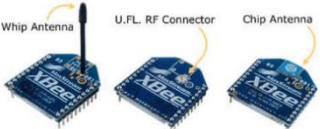
Table A-1 Comparison of Vibration Energy harvesters

No.	Mfr.	Type	Harvested frequency	Max Power Output	Dimensions Unit: mm	Weight	Price	Appearance
1	Midé	Volture v25w	120 Hz 75 Hz 50 Hz 40 Hz	1.000g 1.468 mW 1.000g 2.431 mW 1.000g 7.220 mW 1.000g 9.231 mW	50x38x0.5	5-21g	\$87.5	
2	Piezo Systems, Inc.	Quick Mounted Bending Harvesters	275 Hz 275 Hz 275 Hz 68 Hz	1.1 mW 2.3 mW 4.5 mW 4.7 mW	28.6x3.2x2.5 28.6x6.3x2.5 28.6x12.7x2.5 28.6x31.8x2.5	0.9g 1.4g 2.3g 9.5g	\$197 \$175 \$197 \$241	
3	MicroGen Systems, Inc.	BOLT™ Power Cells	100 HZ 120 Hz 600 Hz	200 μW 200 μW 400 μW	48.5x26.5x17.5	25g	N/A	

No.	Mfr.	Type	Harvested frequency	Max Power Output	Dimensions Unit: mm	Weight	Price	Appearance
4	Perpetuum	PMG17	100-120 Hz	0.015g 0.7 mW 0.025g 1.2 mW 0.100g 5.5 mW 1.000g 50 mW	Diameter 55 Height 55	655 g	N/A	
5	Ferro	VEH-460	60 Hz	0.025g 0.3 mW 0.050g 1.3 mW 0.100g 5.2 mW	Diameter 60 Height 68	430 g	N/A	
6	CEDRAT TECHNOLOGIES	APA400M-MD	110 Hz	95 mW	50x32x22	270 g	N/A	
7	MicroStrain	PVEH™	1000 Hz	1.500g 32 mW	Diameter 45 Height 43	185 g	N/A	
8	MicroStrain	MVEH™	20 Hz	0.200g 4 mW	Diameter 57 Height 64.5	216 g	N/A	

A.2 Comparison of ZigBee modules (With Antenna and MCU, Low power consumption)

Table A-2 Comparison of ZigBee modules (With Antenna and MCU, Low power consumption)

No.	Mfr.	Module Name	SoC Chip	Antenna	TX Current	TX Power	Dimension	Price	Appearance
1	NXP (Jennic)	JN5168-001-M03	JN5168	U.FL connector	15.3mA	+2.5dBm 1.78mW	16mmx31mm	£10.7	
2	IMST GmbH	iM222A	CC2530	PCB antenna	28.5mA	+2.5dBm 1.78mW	25mmx20mm	£14.3	
3	Anaren	A2530R24C	CC2530	U.FL connector	33mA	+4dBm 2.5mW	11mmx19mm	£15	
4	Atmel	ATZB-24-A2	ATmega1281 AT86RF230	balanced dual chip antenna	20.8mA	+3dBm 2mW	13.5mmx24mm	£17	
5	Digi	XBee® ZB	Silicon Labs EM250	U.FL, RPSMA	35mA	+1dBm 1.26mW	24mmx27mm	£18	

A.3 Popular power management ICs used for vibration energy harvesting

Table A-3 Comparison of the popular power management ICs used for vibration input sources [56]–[62]

Part Number	Description	Input Voltage (V)	Min Quiescent Current	Output Voltage (V)	Max Output Current
Linear Technology LTC3330	Nano-power Buck-Boost DC/DC with Energy Harvesting Battery Life Extender	3 -19	750 nA	1.8 2.5 2.8 3.0 3.3 3.6 4.5 5.0	50 mA
Linear Technology LTC3331	Nano-power Buck-Boost DC/DC with Energy Harvesting Battery Charger	3 -19	950 nA	1.8 2.5 2.8 3.0 3.3 3.6 4.5 5.0	50 mA
Spansion® MB39C811	Ultra-low power buck power management IC for solar and vibrations energy harvesting	2.3 - 26	550 nA	1.5 1.8 2.5 3.3 3.6 4.1 4.5 5.0	100 mA
Maxim Integrated MAX17710	Ultra-Low Power Buck Power Management IC for Solar/Vibrations Energy Harvesting	0.75 - 5.3	625 nA	1.8 2.3 3.3	100 mA
Linear Technology LTC3588-1	Piezoelectric energy harvesting power supply	2.7 - 20	450 nA	1.8 2.5 3.3 3.6	100 mA
Linear Technology LTC3588-2	Piezoelectric energy harvesting power supply with 14V Minimum VIN	14 - 20	450 nA	3.45 4.1 4.5 5.0	100 mA
Texas Instruments BQ25504	Ultra-low power boost converter with battery management	0.13 - 3	330 nA	1.8 – 5.5	N/A
Texas Instruments BQ25505	Ultra-low power boost converter with battery management and autonomous power path multiplexing	0.1 – 5.1	325 nA	1.8 -5.5	N/A

Appendix B List of the main components/modules used in this project

Table B-1 List of the main components/modules used in this project

Unit	Device	Current consumption	Voltage Output/Input	Interface	
Energy harvester	Piezoelectric Energy harvester	Mide	120 Hz 1.000g 1.468 m	3.2V to 36.6V	N/A
		Vulture v25w	75 Hz 1.000g 2.431 mW 50 Hz 1.000g 7.220 mW 40 Hz 1.000g 9.231 mW		
Sensors	3-Axis Accelerometer	ST LIS2DHTR	1Hz ODR 2µA Sleep Mode 0.5µA	1.71V to 3.6V	I ² C, SPI
	Temperature & Humidity Sensor	TI HDC1000YPAT	1Hz ODR 1.2µA Sleep Mode 0.11µA	2.7V to 5.5V	I ² C
	Pressure Sensor	ST LPS25HTR	1Hz ODR 4µA Sleep Mode 0.5µA	1.7V to 3.6V	I ² C, SPI
MCU & RF	ZigBee Module With MCU	IMST GmbH iM222A-ZNP	TX current 28.5mA RX current 24.3mA CPU Normal 3.4mA CPU Sleep 0.4-1µA	2V to 3.6V	I ² C, SPI, UART

Appendix C WSN system powered by vibration energy harvester

C.1 Schematic of the WSN system powered by vibration energy harvester

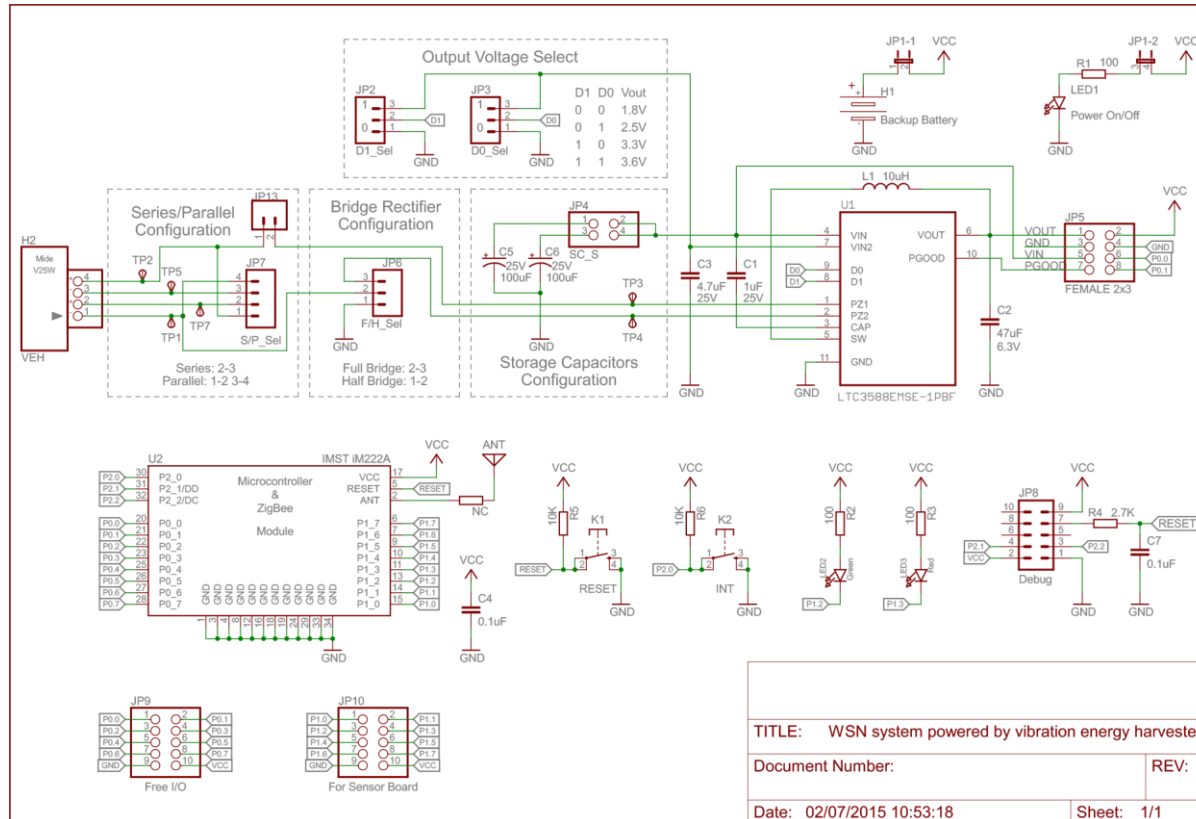
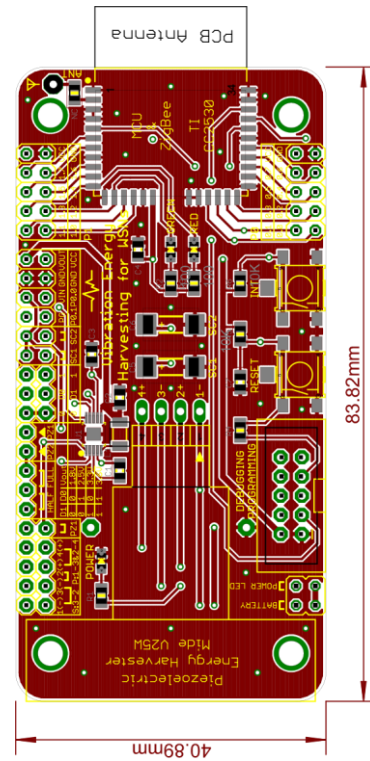
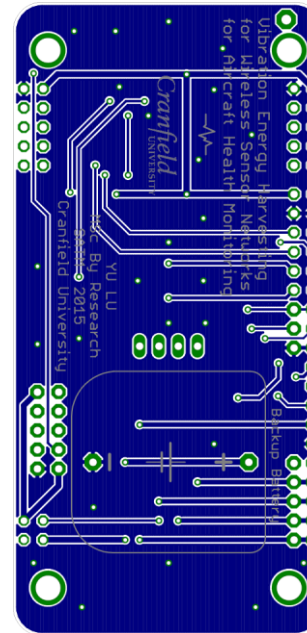


Figure C-1 Schematic of the WSN system powered by vibration energy harvester

C.2 PCB Layout of the WSN system powered by vibration energy harvester



(a) Front view, 1x



(b) Back view, 1x

Figure C-2 PCB layout of the WSN system powered by vibration energy harvester

Appendix D Sensor board

D.1 Schematic of the sensor board

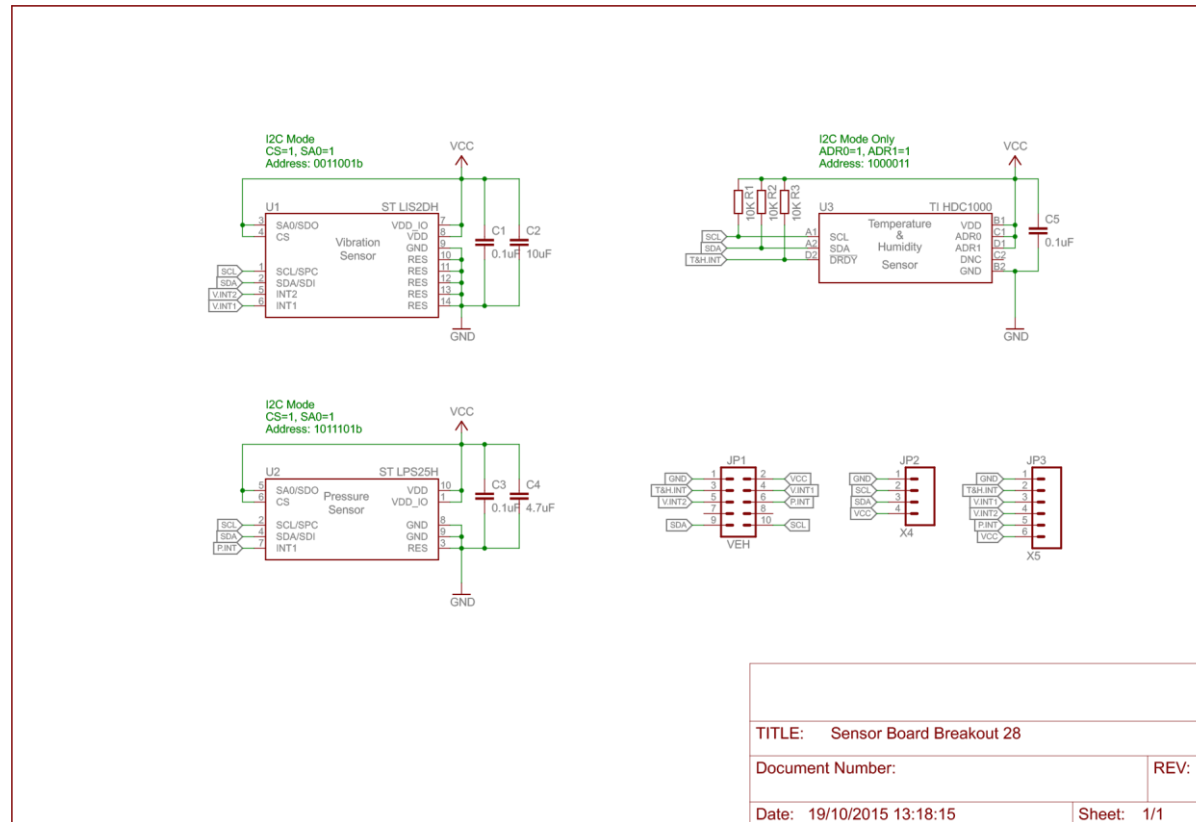


Figure D-1 Schematic of the sensor board

D.2 PCB layout of the sensor board

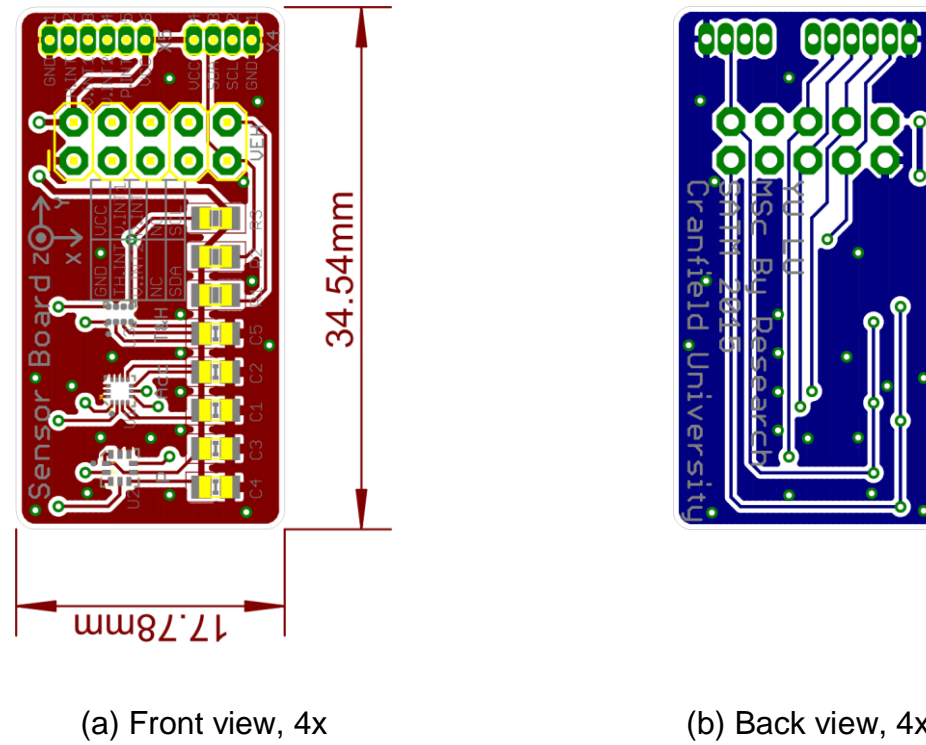


Figure D-2 PCB layout of the sensor board

Appendix E Voltage divider and ADC circuit for storage capacitor

E.1 Schematic of the voltage divider and ADC circuit for storage capacitor

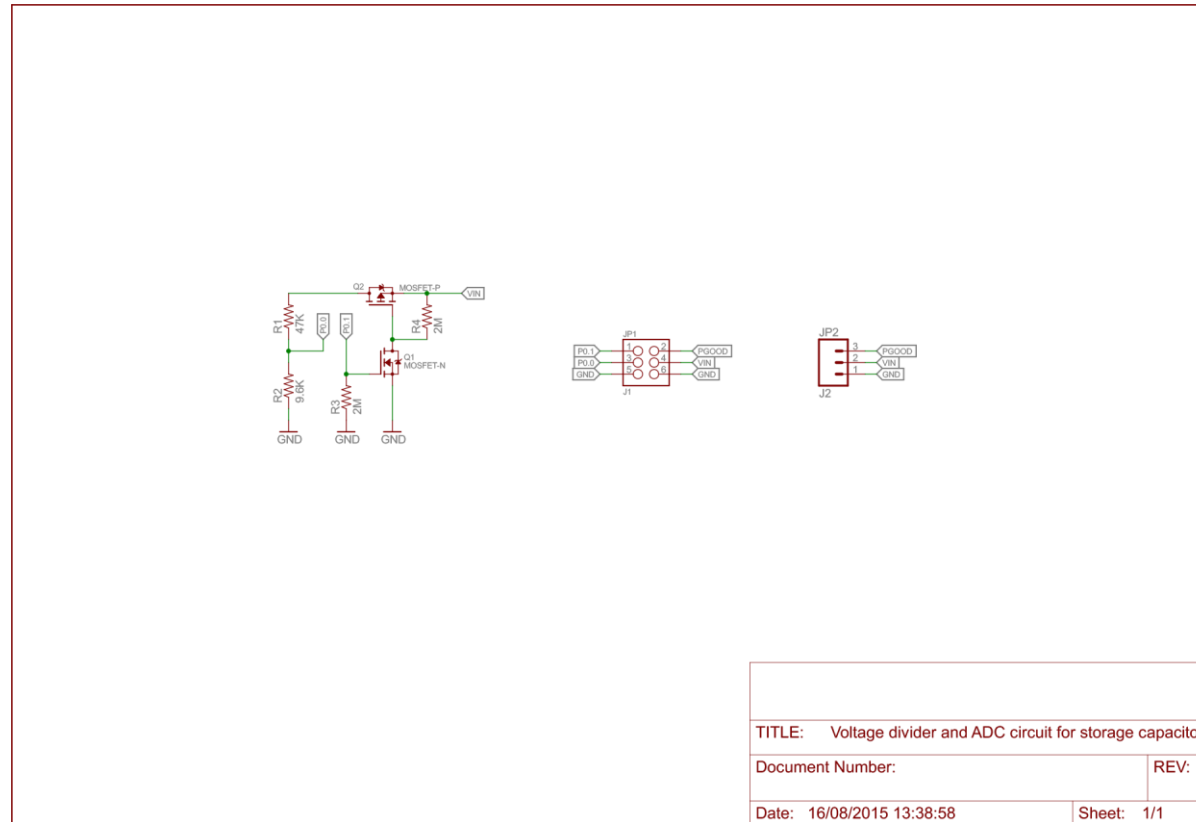


Figure E-1 Schematic of the voltage divider and ADC circuit for storage capacitor

E.2 PCB Layout of the voltage divider and ADC circuit for storage capacitor

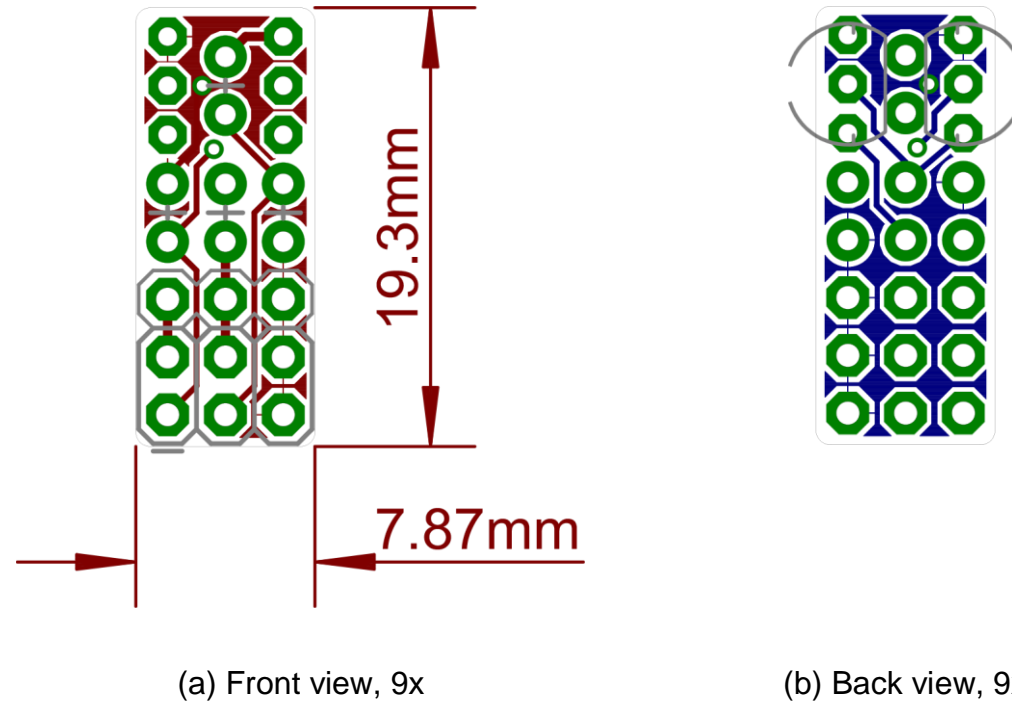


Figure E-2 PCB layout of the voltage divider and ADC circuit for storage capacitor

Appendix F Clamps designed for mounting purpose

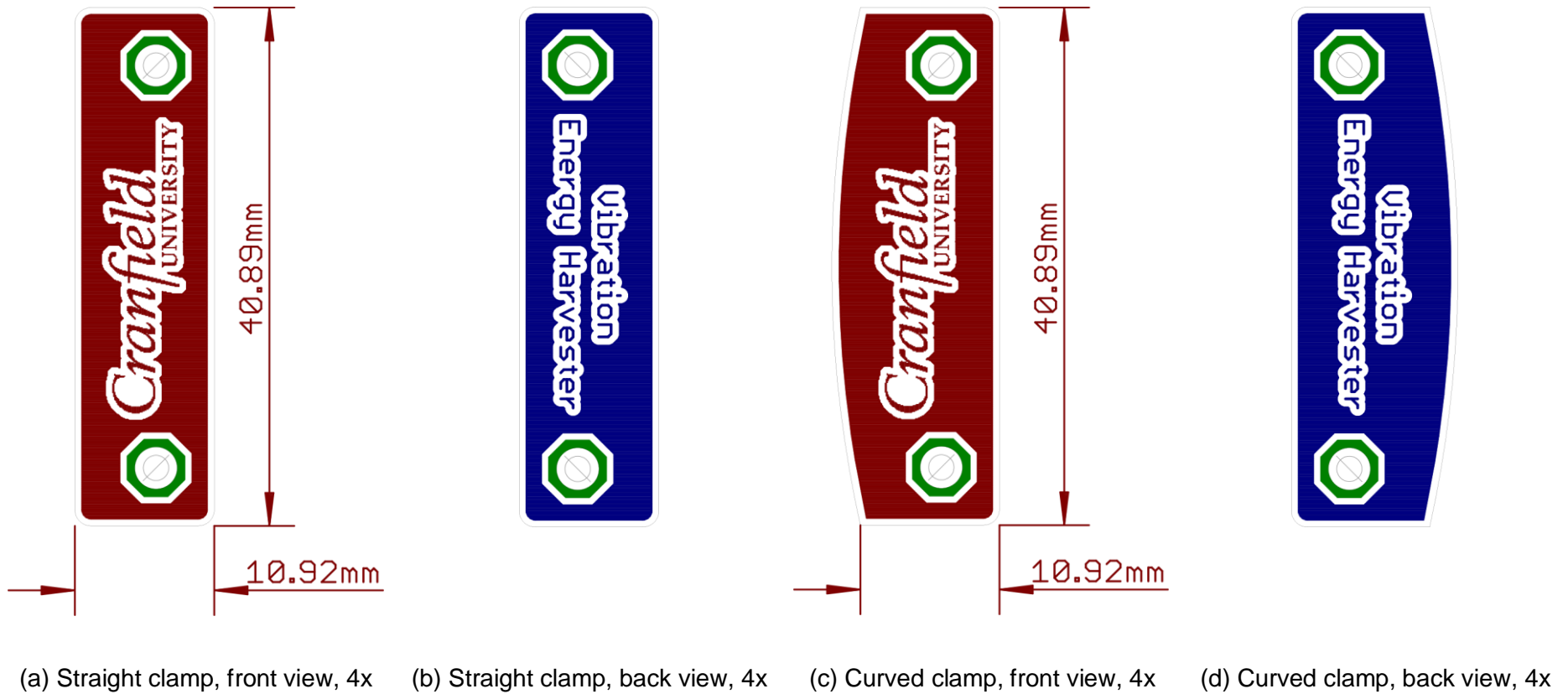


Figure F-1 Straight and curved clamps designed for mounting purpose

Appendix G 2D view of the assembled energy harvesting system

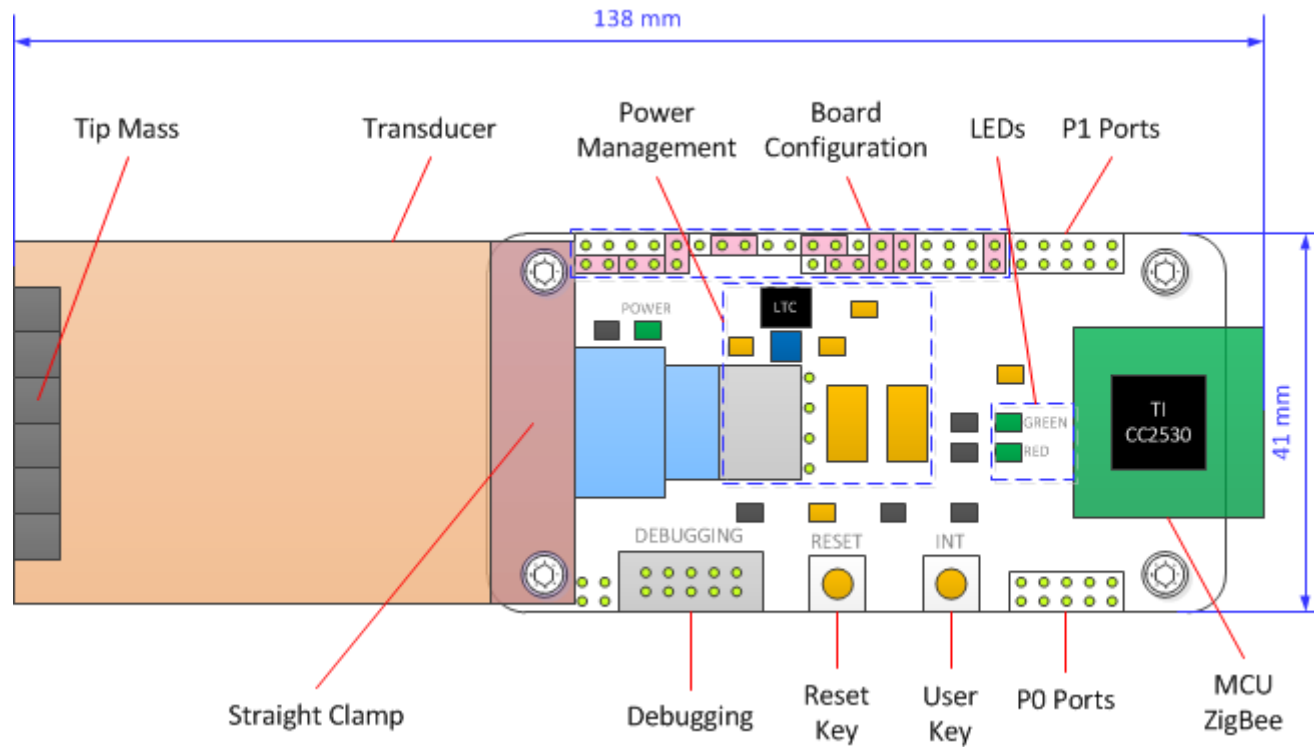


Figure G-1 2D view of the assembled WSN node system based on vibration energy harvesting

Appendix H Assembled energy harvesting system

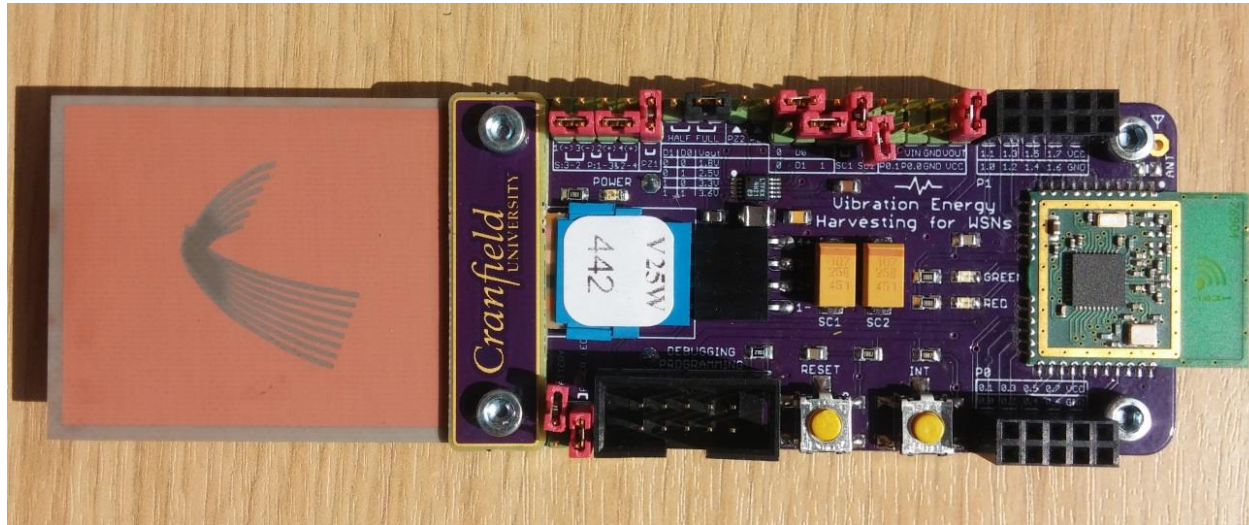


Figure H-1 Assembled energy harvesting system

Appendix I Software used

Table I-1 Software used in this study

Category	Software	Functions
Hardware Design	EAGLE 7.2.0	Schematic capture, PCB layout and traces routing
	Gerbv 2.6A	Gerber files viewer, used for checking Gerber files before manufacturing
Simulation	NI Multisim 13.0	Electronic schematic design and SPICE simulation
	LTspice IV	SPICE simulator, schematic capture and waveform viewer
Software Development	IAR Embedded Workbench for 8051 IDE 9.10.1	IDE tool, used for developing, debugging and compiling the application code and Z-Stack code
	TI Packet Sniffer 2.18.1	Used to sniff and analyse the over-the-air ZigBee packets
	SUDT AccessPort 1.37	Serial monitor, used to log, view, and analyse RS232 communication
Drawing	OriginPro 9.0	Scientific graphing and data analysis
	Microsoft Visio 2010	Process diagram and flowchart graphing